NL 96F4902

INIS-mf--15156

TUDelft
Delft University of Technology

Faculty of Applied Physics
Kramers Laboratorium voor Fysische Technologie

VOL. 27 № 10

KS00197425X
I: FI
DE008376905

Design of gamma radiation equipment for studying a bubbling gas fluidized bed

Determination of a radial void fraction profile and bubble velocities in a 0.40 m column

Graduation report

December, 1993

M.O. Hoogeveen
Faculty of Applied Physics
Delft University of Technology

Professor: Prof.dr.ir. H.E.A. van den Akker
Kramers Laboratory
Department of Transport Phenomena
Faculty of Applied Physics

Supervisors: Ir. Z.I. Kolar
Department of Radiochemistry
Interfaculty Reactor Institute

Dr. R.F. Mudde
Kramers Laboratory
Department of Transport Phenomena
Faculty of Applied Physics

Summary

In this work the possibility of the use of gamma radiation in investigating bubbles in a large three dimensional gas-fluidised bed was examined. A measuring system was designed based upon the absorption of gamma radiation.

As high energy (>100 keV) gamma radiation penetrates deeply into matter, it can be used to scan through a gas-solid fluidised bed. The attenuation of a beam of mono-energetic photons is related to the amount of solid particles in the path of the beam. With the gamma absorption technique two parameters can be determined: the void fraction and the bubble velocity.

With one narrow beam of gamma radiation a chordal void fraction can be measured in the homogeneous part of the bed. An optimalisation procedure for the void fraction determination led to the choice of Cs-137 as radiation source. This optimalisation procedure concerned minimizing of the standard deviation in the determined chordal void fraction as a function of the energy of gamma radiation.

With two narrow parallel beams placed at a distance of 12 cm above each other a bubble velocity can be obtained. A cross-correlation between the two detector responses gives the time shift between the two responses. The system was designed for velocity measurements in the non-homogeneous part of the column. A simulation of the two beam measurement method for an air fluidized bed, 0.40 m in diameter, of polystyrene particles led to the choice of 100 mCi for the source strength for each of the two Cs-137 sources.

For a 100 mCi Cs-137 source a shielding of 8 cm of lead is necessary to comply with safety regulations, concerning the use of radioactive materials. A source holder was designed, containing two encapsulated 100 mCi Cs-137 sources, in accordance with the regulations in the licence of the Delft University of Technology for the use of encapsulated sources.

Contents

1 Introduction

The difficulty in scaling-up fluidized bed reactors results from an incomplete understanding of fluidization hydrodynamics and of hydrodynamic effects on reaction kinetics. Since hydrodynamics are greatly affected by both process conditions (such as gas and particle densities, particle size, gas velocities etc.) and physical aspects of reactor design (such as distributor type and vessel dimensions), it is clear that direct measurement of hydrodynamic properties in operating fluidized-bed chemical reactors is necessary. Various techniques can be used to investigate the fluidization hydrodynamics; optical, electrical, and nuclear techniques. Hetsroni gives an overview of available techniques [Het82]. Experimental techniques which do not disturb the fluidized bed are to be preferred. One such method is that of gamma radiation absorption.

In this work the possibility of applying the gamma absorption method for the investigation of bubbles in a large three-dimensional bed is examined and a design is made for a measuring system based upon this method. As high energy (> 100 keV) gamma radiation penetrates deeply into matter, it is suited to scan through a large gas-solid fluidised bed. The principle of the gamma absorption method is that the thickness of an absorber material can be calculated from the attenuation of a narrow beam of gamma radiation, which is sent through the absorber material, and the properties of the absorber material. The application of gamma radiation absorption to determine fluidized bed properties is not new. Chan and Banerjee [Cha81] described a procedure for designing a gamma densitometer for void fraction measurements. Weimer [Wei85] used a one-beam gamma radiation density gauge to determine hydrodynamic properties of two fluidized beds. The gamma ray technique is attractive because it is quite reliable, accurate and relatively simple. It is versatile because gamma rays of different energies can be applied depending on the size and materials of the fluidized bed that is used. A disadvantage of the use of radiation is the stringent safety requirements when working with radioactive materials and the inherent statistical character of radiation.

By measuring the attenuation of a narrow beam of gamma rays information can be gathered about the amount of gas in the path of the beam; a chordal void fraction can be determined. A radial void fraction profile can be obtained by dividing a cross-section of the column in rings. A measured void fraction is equal to a sum over the path in each of the rings, that the beam intersected, times the radial void fraction in a ring. Mudde [Mud92] used this approach for measurements with a laser beam in a air/water bubble column.

For the determination of a bubble velocity two narrow parallel beams of gamma rays, placed vertically above one another, are necessary. A bubble passes first one beam, and a moment later the other one; the two detector responses will be similar only shifted in time. A cross-correlation between the two detector responses gives the amount of a time a bubble needs to rise from one beam to the other. Combined with the distance between the beams a velocity can be calculated. Mudde [Mud92] also has used this method in his work.

The measuring system was designed for a perspex column, with an outer diameter of 0.40 m, filled with polystyrene particles and fluidised by air. This polystyrene is a Geldart B material. The bubble parameters that can be measured with the system are the void fraction and the bubble velocity. Measurements have to take place in the bubble regime.

At the Kramers Laboratorium voor Fysische Technologie radiation has not been used before in experiments. The necessary experience in working with radiation was found in the Radioisotope Applications Research Group, Department of Radiochemistry, at the Interfaculty Reactor Institute. They provided knowledge about the gamma absorption technique and the SBD (Radiation Protection Service) provided the knowledge about the necessary safety requirements in working with radioactive materials. The measuring system must comply with the regulations in the licence of the Delft University of Technology for the use of encapsulated sources.

In chapter 2 the theory concerning gas-solid fluidised beds is outlined. In chapter 3 the theory about gamma radiation is treated. With one beam of gamma rays a chordal void fraction can be obtained. A radial void fraction profile can be calculated from the measured chordal void fractions with a shell model. In chapter 4 the demands of that technique are given. With two beams of gamma rays and applying a cross-correlation technique a bubble velocity can be determined. A simulation was carried out to get more insight in the two beam technique. In chapter 5 the concept of measuring bubble velocities is treated. A system had to be designed and realised that could be used for both the one-beam measurements and the two-beam measurements. The design of that system is discussed in chapter 6. Chapter 7 contains the conclusions and recommendations for further work.

2 Fluidization

The measuring system was designed for a large three-dimensional gas-solid fluidized bed. In this chapter the principles of fluidization and the characteristic parameters of the fluidized bed will be treated. The system was designed for measurements in the bubbly regime; the characteristic bubble parameters will be given in this chapter.

2.1 The phenomenon of fluidization

Fluidization is the operation by which a powder of solids is transformed into a fluidlike state through suspension in a gas or liquid.

If a fluid or gas is passed upward through a bed of fine particles at a low flow rate, the fluid merely percolates through the void spaces between stationary particles. With an increase in flow rate, particles move apart and a few vibrate and move in restricted regions. At a still higher velocity, a point is reached where all the particles are just suspended by the upward-flowing gas or liquid. At this point the frictional force between particle and fluid just counterbalances the weight of particles; the vertical component of the compressive force between adjacent particles disappears, and the pressure drop through any section of the bed about equals the weight per unit area of fluid and particles in that section. The bed is considered to be just fluidized and is referred to as an incipiently fluidized bed or as a bed at minimum fluidization. With an increase in flow rate beyond minimum fluidization in a gas-solid system, large instabilities with bubbling and channelling of gas can be observed depending on for example the powder characteristics. At higher flow rates agitation becomes more violent and the movement of solids becomes more vigorous. Such a bed is called a heterogeneous fluidized bed or a bubbling fluidized bed.

Both gas and liquid fluidized beds are considered to be dense-phase fluidized as long as there is a fairly clearly defined upper limit or surface to the bed. In gas-solid systems, gas bubbles coalesce and grow as they rise, and in a deep enough bed of small diameter they may eventually become large enough to spread across the vessel. In the case of fine particles, the particles flow smoothly around the rising void of gas. This is called slugging, with axial slugs. For coarse particles, the portion of the bed above the bubble is pushed upward, as by a piston. Particles rain down from the slug, which finally disintegrates. At about this time another slug forms, and this unstable oscillatory motion is repeated. This is a so called flat slug. When fine particles are fluidized at a sufficiently high gas flow rate, the terminal velocity of the solids is exceeded, the upper surface of the bed disappears, entrainment becomes appreciable, and, instead of bubbles, one observes a turbulent motion of solid clusters and voids of gas of various sizes and shapes. With a further increase in gas velocity, solids are carried out of the bed with the gas. In this state we have a disperse- or lean-phase fluidized bed with pneumatic transport of solids. In figure 2.1 the mentioned phenomena are shown.

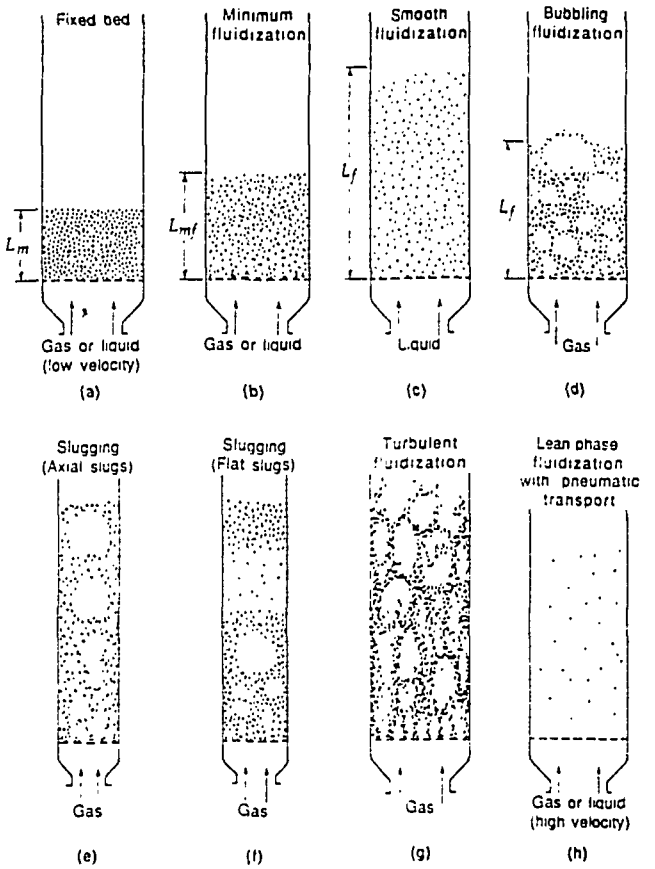

Fig. 2.1 Various forms of contacting of a batch of solids by fluid or gas [Kun91]

From figure 2.1a to 2.1h the velocity of the gas increases from a low to a high velocity. The state of fluidization changes from minimum fluidization to bubbling fluidization to slugging to lean phase fluidization, with the increase of the gas velocity.

A dense-phase gas fluidized bed looks very much like a boiling liquid and in many ways exhibits a liquidlike behaviour. For example, a large, light object is easily pushed into a bed and, on release, will pop up and float on the surface. When the container is tipped, the upper surface of the bed remains horizontal, and when two beds are connected their levels equalize. Also the difference in pressure between any points in a bed is roughly equal to the static head of the bed between these points. The bed also has liquidlike flow properties. Solids will gush in a jet from a hole in the side of a container and can be made to flow like a liquid from vessel to vessel. This fluidlike behaviour of solids with its rapid, easy transport and its intimate gas contacting is often the most important property recommending fluidization for industrial operations.

2.2 Bed characteristics

A fluidized bed filled with polystyrene particles displays a certain behaviour that is characterised by certain parameters. In this chapter it will be tried to give some insight in what can be found about those parameters in literature.

2.2.1 The polystyrene fluidized bed

The fluidized bed that will be worked with contains polystyrene particles. It is fluidized by air; the distributor for the air is a porous plate. The wall of the column used is made of perspex. The following data of the system are available (at a temperature of 293 K and at standard pressure):

ρ_p	$= 1.10\ 10^3$	kg m^{-3}
$\bar{d}_p$	$= 0.56\ 10^{-3}$	m
σ_p	$= 0.16\ 10^{-3}$	m
μ_{gas}	$= 1.84\ 10^{-5}$	kg m^{-1}s^{-1}
ρ_{gas}	$= 1.2$	kg m^{-3}
ρ_w	$= 1.19\ 10^3$	kg m^{-3}
d_w	$= 8.0\ 10^{-3}$	m
D_{outer}	$= 0.40$	m

Here ρ_p is the density of the particles, $\bar{d}_p$ the mean particle diameter, σ_p is the standard deviation in the particle diameter, μ_{gas} is the viscosity of air, ρ_{gas} is the density of air. ρ_w is the density of the wall material (perspex) and d_w is the thickness of the wall. D_{outer} is the outer diameter of the column.

Geldart [Gel78] has defined four types of particles according to their density and particle diameter. In figure 2.2 those types are shown.

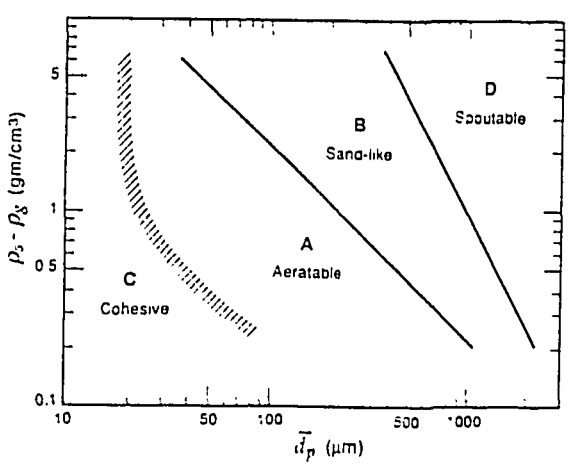

Fig. 2.2 The Geldart classification of particles for air at ambient conditions [Gel78]

In the figure it can be seen that the polystyrene particles are a Geldart B powder; a sandlike material. Geldart B particles have the following characteristics. When the bed is fluidized also the first bubbles appear; the minimum bubble velocity is approximately equal to the minimum fluidization velocity. In addition the bed does not expand much beyond its volume at minimum fluidization. Furthermore the bubble size increases roughly linearly with distance above the distributor and with excess gas velocity, that is the difference between the superficial gas velocity and the minimum fluidization velocity ($= u_0 - u_{mf}$). The bubble size is roughly independent of the mean particle size. The vigorous bubbling at higher flow rates encourages the gross circulation of solids.

2.2.2 Particle diameter

When all the particles are spherical, the size can de measured without ambiguity; however questions arise with non spherical particles. Here one can define the size in several ways. The equivalent spherical diameter is defined as follows:
d_{eq} is the diameter of a sphere having the same volume as the particle. The sphericity ϕ_s of a particle can be defined as:

$$\phi_s = \left[\frac{surface\ of\ sphere}{surface\ of\ particle}\right]_{of\ same\ volume} \tag{2.1}$$

With this definition $\phi_s = 1$ for spheres and $0 < \phi_s < 1$ for all other particle shapes. A bed of non-spherical particles can now be represented by a bed of spheres of diameter d_{eff} such that the two beds have the same total surface area and same fractional voidage α_{pb}. Then by geometry: $d_{eff} = \phi_s\, d_{eq}$

2.2.3 The voidage of a packed bed

Two extreme conditions can be used as reference points for the voidage of a packed bed; 'loose' packing gives the maximum possible voidage, and 'dense' packing the minimum. Obviously the degree to which the bed is vibrated or tapped is very important. Factors influencing the voidage are: particle shape, particle size, size distribution, particle and wall roughness. When the bulk density of the bed ρ_B is known, the voidage of a packed bed can be defined as:

$$\alpha_{pb} = 1 - \rho_B / \rho_p \tag{2.2}$$

In the polystyrene bed the bulk density of the powder in the loosely packed bed ρ_B is equal to 625 kg m^{-3} ; this is an experimental value. The density of polystyrene ρ_p equals 1100 kg m^{-3}. So the voidage of the packed bed is $\alpha_{pb} = 0.433$. Because the expansion of the bed filled with polystyrene particles is very small during fluidization, the minimum fluidization voidage α_{mf} is also equal to 0.433.

2.2.4 Minimum fluidization velocity

The onset of fluidization occurs when the drag force by the upward moving gas is equal to the weight of the particles. At the onset of fluidization the voidage is a little larger than in a packed bed, actually corresponding to the loosest state of a packed bed of hardly any weight. The drag force equals the pressure drop across the bed times the cross-sectional area of the column. The weight of the particles is equal to the volume of the bed multiplied by the fraction of the bed consisting of solids and the specific weight of the solid. The frictional pressure drop through fixed beds containing a single size of isotropic solids of screen size $\bar{d}_p$ has been correlated by Ergun [Erg52]. In general, for isotropic shaped solids this gives a quadratic equation for u_{mf}, the minimum fluidization velocity.

$$\frac{1.75}{\alpha_{mf}^3 \phi_s} Re_p^2 + \frac{150(1-\alpha_{mf})}{\alpha_{mf}^3 \phi_s^2} Re_p = Ar \qquad (2.3)$$

Re_p is defined as :

$$Re_p = \frac{\bar{d}_p \, u_{mf} \, \rho_{gas}}{\mu_{gas}} \qquad (2.4)$$

Ar is a dimensionless parameter, the number of Archimedes. It is defined as:

$$Ar = \frac{\rho_g \, \Delta\rho \, g \, \bar{d}_p^3}{\mu_{gas}^2} \qquad (2.5)$$

with $\Delta\rho = \rho_p - \rho_{gas}$ and g the constant of gravity, 9.8 m s^{-2}. For the polystyrene particles Ar = 6715. Equation (2.3) can be rewritten as :

$$K_1 Re_p^2 + K_2 Re_p = Ar \qquad (2.6)$$

Wen and Yu [Wen66] were the first to note that K_1 and K_2 stayed nearly constant for different kinds of particles over a wide range of conditions ($0.001 < Re_p < 4000$). Wen and Yu found $K_1 = 24.5$ and $K_2 = 1652$. Using those values, u_{mf} and Re_p can be calculated for the polystyrene bed.

$u_{mf} = 0.11$ m s^{-1}

$Re_p = 4.0$

2.3 Bubble characteristics

A bubbling fluidized bed has regions of low solid density, these regions are called gas bubbles, or simply bubbles. The region of higher density are called the suspension or dense phase.

2.3.1 Bubble form

The Davidson model [Dav63] for gas flow at bubbles makes a distinction between clouded and cloudless bubbles.

The cloudless or slow bubble: $u_{bs} < u_f$

u_{bs} is the velocity of a bubble in a swarm of bubbles. u_f is the velocity of the gas at minimum fluidization conditions ($u_f = u_{mf}/\alpha_{mf} = 0.25$ m s^{-1} for the polystyrene case). In the case of a slow bubble the suspension gas rises faster than the bubble; hence it uses the bubble as a convenient shortcut on its way through the bed. It enters at the bottom of the bubble and leaves at the top. However an "annular ring" of gas does circulate within the bubble, moving upward with it. The amount of this accompanying gas increases as the ratio u_f/u_{bs} decreases.

The clouded or fast bubble: $u_{bs} > u_f$

As with the slow bubble, suspension gas enters the lower part of the bubble and leaves at the top. However, the bubble is rising faster than the suspension gas; consequently, the gas leaving the top of the bubble is swept around and returns to the base of the bubble. The region around the bubble penetrated by this circulating gas is called the cloud. The rest of the gas in the bed does not mix with the recirculating gas but moves aside as the fast bubble with its cloud passes by.

The transition from slow to fast bubble is smooth. The cloud is infinite in thickness at $u_{bs} = u_f$, but thins with increasing bubble velocity. Its size for a three-dimensional bed is given by [Dav63] :

$$\frac{R_c^3}{R_b^3} = \frac{u_{bs} + 2u_f}{u_{bs} - u_f} \qquad (2.7)$$

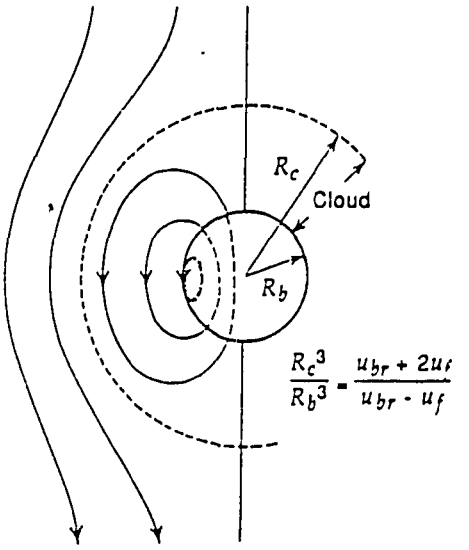

Fig. 2.3 A bubble with its cloud [Dav63]

In figure 2.3 a clouded bubble is shown, with streamlines of the circulating gas. The ratio of cloud to bubble volume is, for three-dimensional bubbles :

$$f_c = \frac{3u_f}{u_{bs} - u_f} \tag{2.8}$$

Solids move aside as a bubble rises. At the front half of the bubble, this movement is well represented by the Davidson model predictions. Typical bubbles are not spherical but have a flattish, or even concave, base; the spherical cap model. The region just below the bubble is the wake region and it most likely forms because the pressure in the lower part of the bubble is less than in the nearby suspension. Thus, gas is drawn into the bubble, causing instability, partial collapse of the bubble, and turbulent mixing. For fast clouded bubbles, this is the reason for the observed leakage of circulating gas into the wake. This turbulence also results in solids being drawn up behind the bubble and forming the wake region. In general bubbles are flatter in small particle beds.

2.3.2 Bubble diameter

The bubbles form just above the distributor, in the present case a porous plate. For a uniform gas flow, $u_0 > u_{mf}$, a highly expanded gas-solid dispersion forms directly above the distributor. This is unstable, and a few millimetres above the plate the dispersion divides into many little bubbles plus a suspension phase. Experiments show that bubble size in fluidized beds increases with gas velocity and with height above the distributor. The flow of gas in bubbles is characterised by the excess gas velocity ($= u_0 - u_{mf}$).

For the growth of bubbles as they rise at least four possible reasons can be given:

- the hydrostatic pressure on the bubbles decreases as they rise up the bed;
- bubbles may coalesce by one bubble catching up with another;
- bubbles which are side by side may coalesce;
- bubbles may grow by depleting the suspension phase locally.

In powders with particles larger than about $150 \cdot 10^{-6}$ m coalescence is the predominant effect occurring in the fluidized bed. Coalescence appears to occur only if a trailing bubble approaches a leading bubble within a critical distance, roughly equal to two times the bubble diameter.

For sand-like solids (Geldart B) there are several correlations published for the bubble diameter as a function of height above the distributor plate, superficial gas velocity and distributor design, though all are derived from data based on air at ambient conditions. The equation of Darton et al. [Dar77] appears to give realistic predictions:

$$d_{bv} = \frac{0.54}{g^{0.2}}(u_0 - u_{mf})^{0.4}(h + 4\sqrt{\frac{1}{N_{dis}}})^{0.8} \qquad (2.9)$$

Where d_{bv} is the diameter of the equivalent volume sphere (in m), h denotes height above distributor (in m), and N_{dis} the number of holes in the distributor per unit area (in m^{-2}). For a porous plate one takes $N_{dis} = 1000\ m^{-2}$. The equation ceases to be applicable when $d_{bv} > D/3$ (slugging). D is the inner diameter of the column. In figure 2.4 the bubble diameter d_{bv} according to this equation is plotted for different superficial gas velocities u_0 as a function of the height above the distributor plate h. For the 0.40 m column filled with the polystyrene particles it can be seen that the higher the gas velocity the larger the bubbles become.

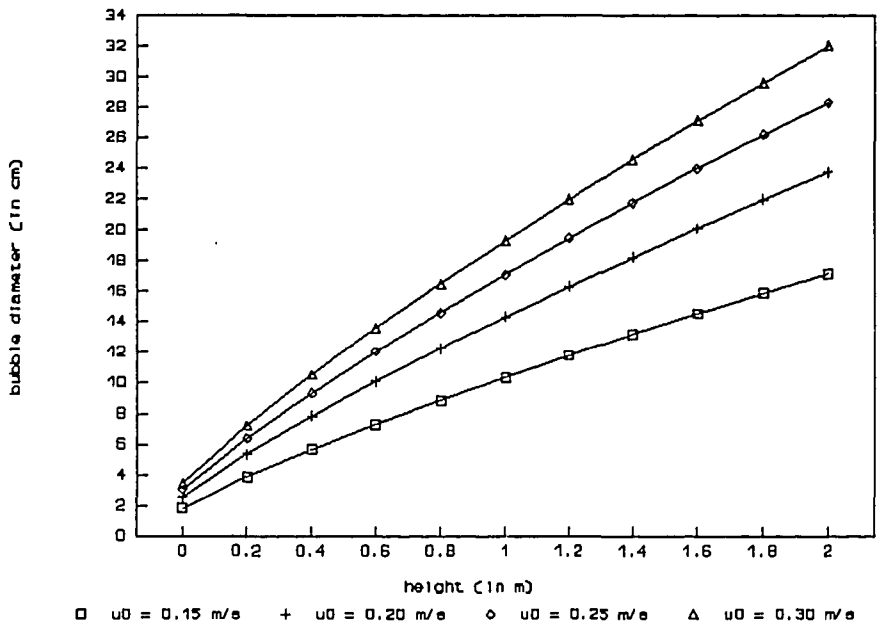

Fig. 2.4 Bubble diameter d_{bv} versus height above distributor plate h for various values of the superficial gas velocity u_0, using the Darton equation.

Slugging is the condition which occurs when the bubbles in the bed grow to a size greater than about ⅓ of the bed diameter. For beds deeper than about 1 m, Stewart's criterion [Ste67] gives the minimum gas velocity at which slugging commences:

$$u_{min,s} = u_{mf} + 0.07\sqrt{gD} \tag{2.10}$$

The last term is equal to 0.14 m s^{-1} for the 0.40 m column, that means slugging commences at a velocity of 0.25 m s^{-1} = 2.3 u_{mf} in the polystyrene case. In practice there are three types of slugging. Axi-symmetric slugs, that are large bubbles in the centre of the column, tend to occur in smooth walled tubes with fine particles at moderate velocities. Solid slugs (sometimes called square-nosed slugs), that are bubbles that cover the entire diameter of the column, occur near the distributor in coarse solids but transform into wall slugs nearer the bed surface. Wall slugs, that are large bubbles situated at the wall of the column, are more likely in most solids when the walls are rough and/or high velocities are used.

As indicated in chapter one, the objective is to gain data on bubble properties such as bubble velocity and void fraction; that means measurements must be done below the height at which slugging commences.

2.3.3 Bubble velocity

In general small bubbles rise slowly and large bubbles rise rapidly. First the rise velocity of a single bubble in fluidized beds will be discussed. Many investigators accept the equation :

$$u_b = 0.7\sqrt{g \cdot d_{bv}} \tag{2.11}$$

The value 0.7 applies for a bubble with a spherical cap form in water. For fluidized beds a value between 0.5 and 0.6 gives better results according to experiments. For the velocity of a bubble in a swarm of bubbles several correlations are available. Kunii and Levenspiel [Kun91] propose the following correlation, which gives realistic predictions. This equation only holds when it is evaluated in SI units.

$$u_{bs} = 1.6[(u_0 - u_{mf}) + 1.13 d_{bv}^{0.5}]D^{1.35} + u_b \tag{2.12}$$

In figure 2.5 the correlation of Kunii and Levenspiel combined with equations (2.9) and (2.11) is used to plot the bubble velocity u_{bs} of a bubble in a swarm as a function of the height above the gas distributor h for different values of the gas velocity u_0, for the 0.40 m column filled with the polystyrene particles.

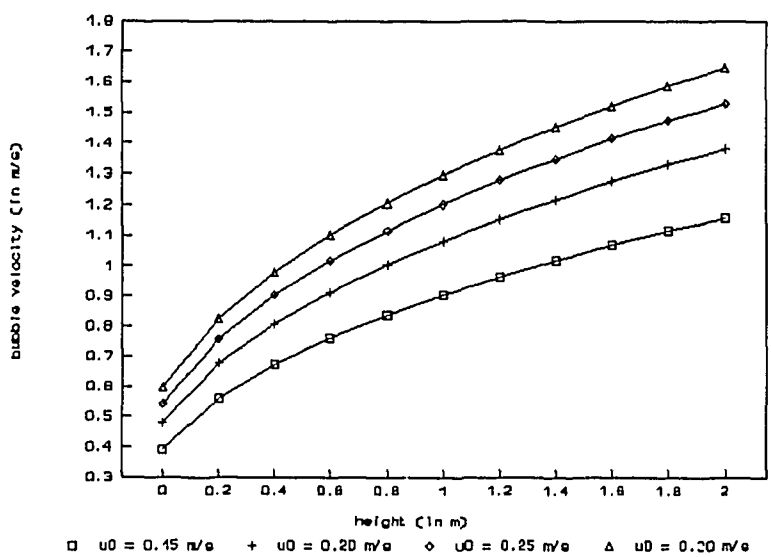

Fig. 2.5 Bubble velocity u_{bs} versus height h above the distributor plate (a porous plate) for a 0.40 m column for various values of the superficial gas velocity u_0 according to the Kunii and Levenspiel equation.

2.3.4 Bubble fraction

The earliest view of the bubbling bed was that all the gas in excess of u_{mf}, thus $u_0 - u_{mf}$, passed through the bed as bubbles while the suspension remained stationary at minimum fluidizing conditions, except when moving aside to let bubbles pass. This is called the simple two-phase model. The many studies of larger beds (D > 0.30 m) indicate that the assumptions of the simple two-phase theory are not well met in that

- the observed bubble flow is not given by $(u_0 - u_{mf})\ A_t$
- the suspension voidage does not stay at α_{mf} as the gas velocity is raised above u_{mf}
- the suspension is not essentially stagnant but develops distinct flow patterns, like gulf streaming, induced by the uneven rise or channelling of gas bubbles.

Simple two-phase theory assumes that the superficial gas velocity u_e through the suspension phase remains at u_{mf} at all gas flow rates u_0. Hildegardt and Werther [Wer86] found for Geldart B particles with a large diameter that u_e did not change appreciably with height in the bed, but that u_e was significantly greater than u_{mf} and dependent on u_0 as follows, for three-dimensional beds :

$$\frac{u_e - u_{mf}}{u_0 - u_{mf}} = 1/3 \tag{2.13}$$

The relationship between the observed bubble flow rate and the excess flow rate can be described with a factor Ψ.

$$\Psi = \left[\frac{\textit{observed bubble flow}}{\textit{excess flow}}\right] = \frac{F_b}{(u_0 - u_{mf})A_t} \tag{2.14}$$

A_t is the cross-sectional area of the bed. Hildegardt and Werther [Hil86] found that for Geldart B solids up to $z/D \approx 2$, $\Psi \approx 0.65$ (for D = 0.1 ~ 1 m). Above $z/D \approx 2$ the rising bubbles seem to progressively deaerate the suspension. Using Ψ one can calculate the bubble fraction δ. The observed bubble flow F_b can be written as :

$$F_b = \delta\ A_t\ u_{bs} \tag{2.15}$$

That gives δ :

$$\delta = \frac{\Psi\ (u_0 - u_{mf})}{u_{bs}} \tag{2.16}$$

In figure 2.6 the bubble fraction δ is plotted as a function of the height h above the distributor plate for various values of the superficial gas velocity u_0, calculated with equations (2.16) and (2.12), for the 0.40 m column filled with the polystyrene particles

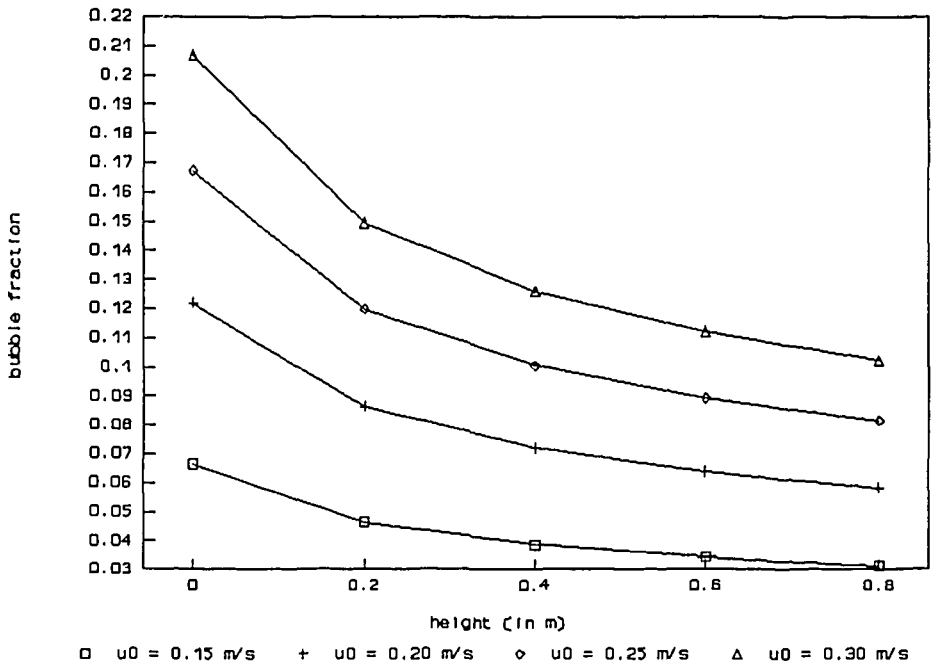

Fig. 2.6 Bubble fraction δ versus height h above the distributor plate according to equation (2.16) for D = 0.40 m, for different values of the superficial gas velocity u_0, up to h = 2D = 0.80 m.

The overall void fraction of the bed α_f consists of two parts, the voidage in the bubbles and the voidage in the suspension and can be calculated with :

$$\alpha_f = \delta + (1 - \delta)\, \alpha_{mf} \qquad (2.17)$$

One may take α_{mf} as the interparticle voidage because the expansion of the bed is small; the interparticle voidage in the suspension phase is approximately equal to the interparticle voidage at minimum fluidization conditions.

The Kunii-Levenspiel [Kun91] model with its Davidson [Dav63] bubbles and wakes model gives a more realistic model for the bubbling bed than the simple two-phase model. Slow cloudless bubbles and fast clouded bubbles give distinctly different flow patterns of gas around bubbles. In addition, by accounting for bubble wakes, solids are dragged up the bed behind bubbles and drift downward in the suspension. This downflow of solids can be so fast that it overcomes the upflow of gas in the suspension, resulting in a net downflow of suspension gas. The fraction of bubbles in the bed is in this model given by different relationships, dependent on the bubble velocity

For slow bubbles, or $u_{bs} < u_f$ ($= u_{mf}/\alpha_{mf} = 0.25$ m s^{-1} for polystyrene)

$$\delta = \frac{u_0 - u_{mf}}{u_{bs} + 2u_{mf}} \tag{2.18}$$

For intermediate bubbles with thick clouds (which may well overlap) or equivalently $u_{mf}/\alpha_{mf} < u_{bs} < 5u_{mf}/\alpha_{mf}$ ($=> 0.25 < u_{bs} < 1.27$), there is a regime that is difficult to represent. Roughly

$$\delta = \frac{u_0 - u_{mf}}{u_{bs} + u_{mf}} \qquad \text{when } u_{bs} \approx u_{mf}/\alpha_{mf} = 0.25 \text{ m s}^{-1} \tag{2.19}$$

$$\delta = \frac{u_0 - u_{mf}}{u_{bs}} \qquad \text{when } u_{bs} \approx 5u_{mf}/\alpha_{mf} = 1.27 \text{ m s}^{-1} \tag{2.20}$$

For fast bubbles, or $u_{bs} > 5u_{mf}/\alpha_{mf}$, clouds are thin and

$$\delta = \frac{u_0 - u_{mf}}{u_{bs} - u_{mf}} \tag{2.21}$$

In vigorously bubbling beds where $u_0 >> u_{mf}$, an approximation is :

$$\delta = \frac{u_0}{u_{bs}} \tag{2.22}$$

With this model δ decreases faster than in the model using the value of Ψ to calculate δ, and at low heights it gives unrealistic high values for δ especially when $u_0/u_{mf} > 2$. But the overall tendency is represented correctly, δ decreases with height above the distributor.

In figure 2.7 the bubble fraction δ is plotted as function of the height h above the distributor using the Kunii-Levenspiel model, for different values of the superficial gas velocity u_0.

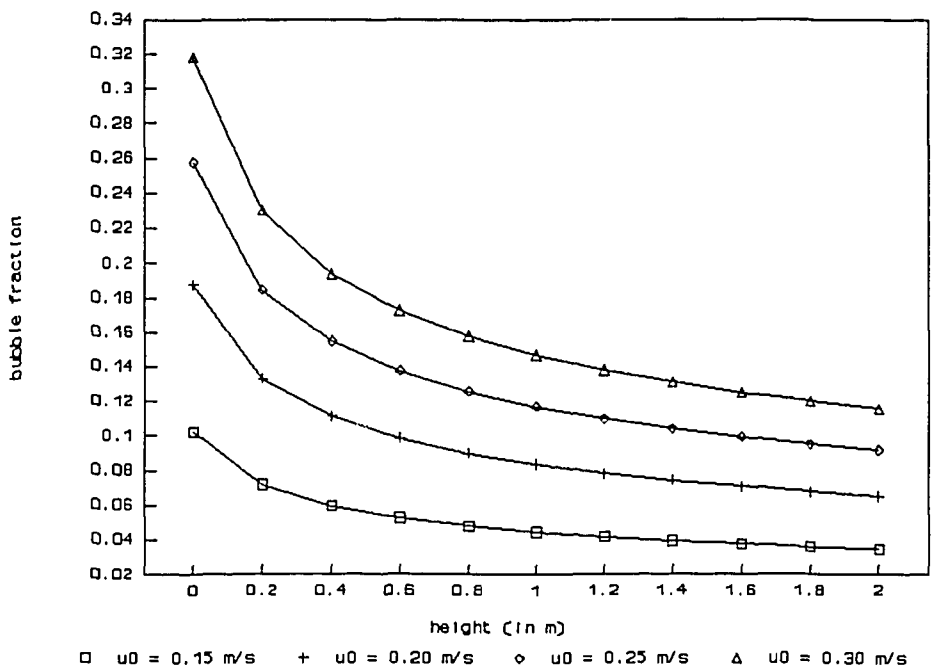

Fig. 2.7 Bubble fraction δ versus height h above the distributor for various values of the superficial gas velocity u_0, according to the Kunii-Levenspiel model. D = 0.40 m.

2.3.5 Bubble frequency

The bubble frequency gives the number of bubbles that pass per second through a cross section. Data found in literature [Hir91] for a 0.40 m bed for a Geldart B powder show that for a height range of 0.50-1.0 m above the distributor the bubble frequency stays fairly constant at a value of 3 bubbles per second. Using the models described in section 2.3.4 for determining the bubble fraction δ, the bubble frequency is calculated. The definition for the bubble frequency f_b is :

$$f_b = \frac{\text{observed bubble flow}}{\text{volume of 1 bubble}} = \frac{F_b}{V_{bubble}} \qquad (2.23)$$

The observed bubble flow F_b is given by formula (2.15). One bubble has a volume of :

$$V_{bubble} = 1/6\ \pi\ d_{bv}^3 \qquad (2.24)$$

Tables 2.1 and 2.2 give bubble frequencies at various heights and gas velocities, calculated with the different models.

Table 2.1 : Bubble frequency (in s^{-1}) for various heights and for various superficial gas velocities. D = 0.40 m. Method using factor Ψ.

height (in m)	u_0= 0.15 m s^{-1}	u_0= 0.20 m s^{-1}	u_0= 0.25 m s^{-1}	u_0= 0.30 m s^{-1}
0	492.6	418.4	383.4	360.7
0.2	52.7	44.8	41.0	38.6
0.4	16.9	14.4	13.1	12.4
0.6	7.8	6.7	6.1	5.7
0.8	4.4	3.7	3.4	3.2

Table 2.2 : Bubble frequency (in s^{-1}) at various heights and for different superficial gas velocities. D = 0.40 m. Kunii-Levenspiel model.

height (in m)	u_0= 0.15 m s^{-1}	u_0= 0.20 m s^{-1}	u_0= 0.25 m s^{-1}	u_0= 0.30 m s^{-1}
0	1555.6	1322.7	1210.8	1139.0
0.2	166.3	141.4	129.4	121.8
0.4	53.3	45.4	41.5	39.1
0.6	24.7	21.0	19.3	18.1
0.8	13.8	11.8	10.8	10.1
1.0	8.7	7.4	6.8	6.3
1.2	5.9	5.0	4.6	4.3
1.4	4.2	3.6	3.3	3.1
1.6	3.1	2.7	2.4	2.3
1.8	2.4	2.0	1.9	1.8
2.0	1.9	1.6	1.5	1.4

As indicated, the Kunii-Levenspiel model overestimates δ in the lower regions, so also the bubble frequency is overestimated in that region. The results in table 1 correspond reasonably well with the values from literature, for a height of 0.80-1.20 m one can expect to find circa 3 bubbles passing per second through a cross section of the bed with a diameter of 0.40 m.

2.3.6 Spatial distribution of the bubbles

The wall region of the column is nearly bubble-free; there is a predominant downward flow of solids close to the wall. The solids are being carried up by bubble wakes; solid circulation patterns are believed to reinforce the preferred bubble paths. About the suspension flow in fluidized beds of Geldart B solids the following remarks can be made:

At low fluidizing velocity in beds of aspect ratio (H/D) close to but less than unity the suspension solids circulate as a vortex ring with upflow at the wall and downflow at the bed axis. As bed aspect ratio approaches unity, suspension solids begin to move down the wall near the bed surface. In deeper beds (aspect ratio > 1), a second vortex ring, with upflow at the centre line of the bed and downflow at the walls starts to exist in the upper part of the bed, see figure 2.8.

At higher gas flows, the solid circulation in the upper vortex ring becomes more vigorous and dominates the overall movement of the suspension.

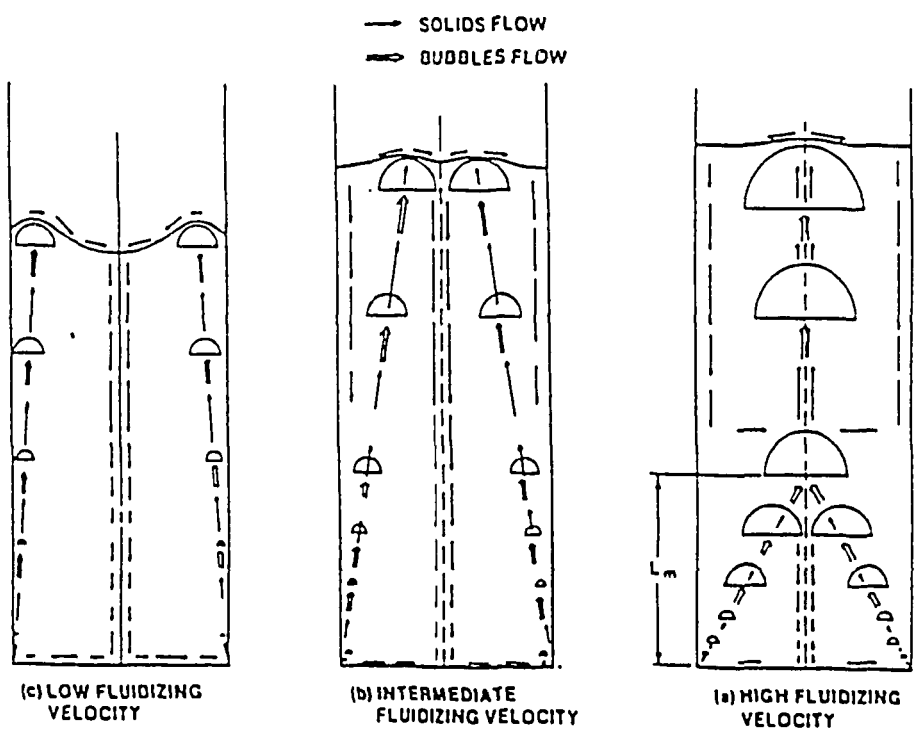

Fig. 2.8 Development of solids circulation versus bubble motion [Gel92]

In this chapter the parameters that characterize a fluidized bed have been treated. The expected values of the parameters that can be determined with the gamma absorption method, the void fraction and the bubble velocity, have been given. Those values can be used in the process of finding design criteria for the measuring system.

3 Gamma radiation

The working principle of the designed measuring system is based on the absorption of gamma radiation, in this chapter the nature of gamma radiation and the principle of the gamma absorption method will be treated.

3.1 What is gamma radiation ?

Following any mode of radioactive decay, the product atom may have some residual excess energy and may be left in an excited state. It can get rid of this energy by emitting one or more characteristic gamma photons of a certain energy. The energy of this gamma ray is equal to the difference in the energy levels of the original excited state and the resulting state (stable or excited) of the nucleus. The nucleus can fall back to a stable state in a number of steps, a step is formed by an intermediary excited state.

As an alternative to gamma ray emission, a nucleus may become de-excited by emitting an extranuclear electron. This process is called internal conversion. The empty shell will generally be filled by an electron from the next highest shell, and this transfer will result in the emission of characteristic X rays and Auger electrons.

3.2 Interaction of gamma radiation with matter

There are several possible interactions of electromagnetic radiation (photons) with matter. Only three of these interactions need to be discussed to cover adequately the interactions in the energy range of 0.01 to 10 MeV. These three interactions are photo-electric effect, Compton effect and pair formation. Each interaction is likely to make a drastic difference in photon direction and energy. Those interactions result in the absorption of gamma radiation; each material has a characteristic absorption coefficient. Instead of the linear absorption coefficient often the mass absorption coefficient $[\mu/\rho]$ (in $m^2\ kg^{-1}$) is used, because energies above 200 keV lead to approximately the same mass absorption coefficients for all absorber materials.

- the photo-electric effect

This is a process in which the total energy of a gamma ray photon is transferred to an atomic electron, preferably from an inner shell. A part E_b (the binding energy of the electron) of the energy of the gamma photon is required to release the electron from its orbit; the remaining energy $E_\gamma - E_b$ is carried over as kinetic energy to the 'photo electron'. The probability for the photo-electric effect strongly depends on the atomic number Z of the absorber material and the energy of the gamma radiation.

- the Compton effect

A photon can interact with a free or loosely bound electron in the absorber material. In this interaction only a part of the photon energy is transferred to the 'Compton electron', and the gamma photon has a different direction and less energy. This is illustrated in the following picture.

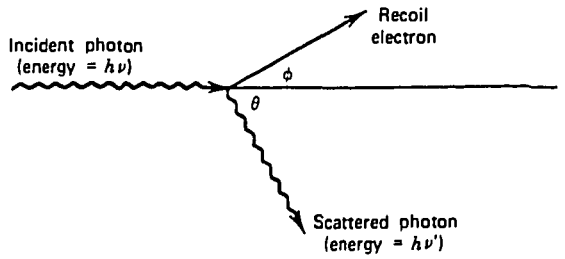

Fig. 3.1 A Compton scattering collision, from Knoll [Kno79]

The partition of E_γ between the Compton electron and the remaining Compton photon γ_c depends on the initial photon energy and the angle between the directions of the primary and the Compton photon.

$$E_{\gamma_c} = \frac{E_\gamma}{1+\alpha(1-\cos\theta)} \tag{3.1}$$

where α is equal to :

$$\alpha = \frac{E_\gamma}{M_0 c^2} \tag{3.2}$$

E_γ is the energy of the incident photon in Joule (1 eV = 1.6 10^{-19} J). M_0 is the mass of an electron (in kg), c is the velocity of light (in m s^{-1}). The probability of the Compton effect is considerably less dependent of absorber material and photon energy than is the case for the photo-electric effect. The scattered Compton photon can on its turn interact with the absorber material, it can collide with an atomic electron and transfer all (photo-electric effect) or a part (Compton effect) of its energy to that electron. If the absorber material is thick enough the original (gamma) photon will transfer all its energy to the absorber material.

- Pair formation

This is a process in which, under influence of the electric field of an atomic nucleus, a high energy photon is transferred into a $ß^+$-$ß^-$ pair. Pair production occurs only when photon energy exceeds 1022 keV (equivalent with twice the rest-mass of the electron). The excess energy E_γ-1022 keV is carried by the 2 particles as kinetic energy. When the positron has lost its energy and has come to rest, it can interact with a loose electron. Annihilation occurs, and two gammas with each an energy of 511 keV are formed.

With low energies (< 0.1 MeV) the photo-electric effect is dominant, with high energies (> 10 Mev) pair formation is dominant; in the intermediate range the Compton effect is dominant. The following figure gives an example of the contribution of each of the three processes to the total attenuation of gamma radiation as a function of the gamma energy for NaI (an often used detector material).

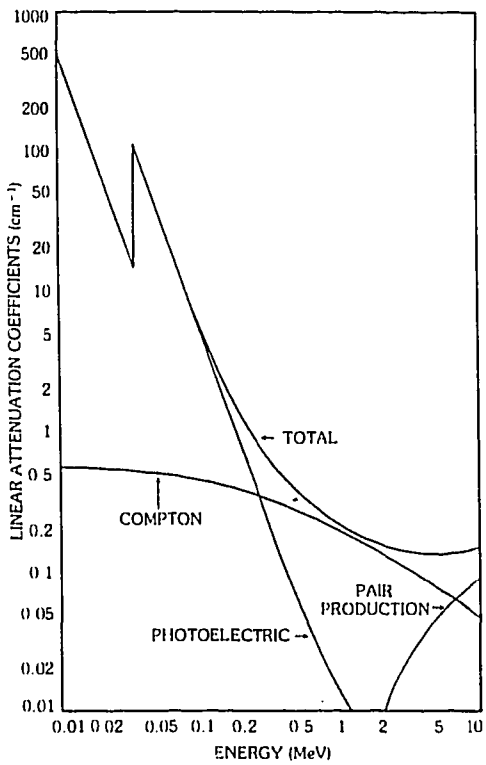

Fig. 3.2 Example of the contribution of each of the three processes to the total attenuation coefficient for NaI as a function of gamma energy, from Harshaw [Har].

If mixtures or chemical compounds are the absorbers of interest, the total mass absorption coefficient can be determined in relation to the weight fraction w of each element and the mass absorption coefficients of each element;

$$[\mu/\rho] = w_1[\mu/\rho]_1 + w_2[\mu/\rho]_2 + w_3[\mu/\rho]_3 + ... \qquad (3.3)$$

3.3 Detection of gamma radiation

In order for a detector to respond at all the incident radiation must undergo interaction through one of the mechanisms discussed in section 3.2. The net result of the radiation interaction in a wide category of detectors is the appearance of a given amount of electric charge, depending on the amount of energy the photon has transferred to the detector material. Compton interaction leads to the appearance of a Compton electron, the photo-electric effect leads to a free electron. For high energy gamma radiation several interactions must take place before the photon has transferred all its energy to the detector material. In most practical situations the interaction times are so short that they can be considered instantaneous. Ideally all photons transfer their total energy to the detector material, but in practice for example some Compton photons will escape from the detector, resulting in the detection of a lower energy.

In figure 3.3 the spectrum of gamma radiation, emitted by a Cs-137 source is shown. The spectrum was obtained with a multi channel analyzer. On the horizontal axis the channel number is shown. Each channel represents a certain energy range. On the vertical axis the number of counts is registered. If a photons with an energy in a certain energy interval is detected a count is added to that energy channel. With a single channel analyzer only one energy channel is chosen, by setting a lower and an upper level, and only photons with an energy in that single channel are counted. Figure 2.3 is obtained from an experiment with no absorber material between Cs-137 source and detector.

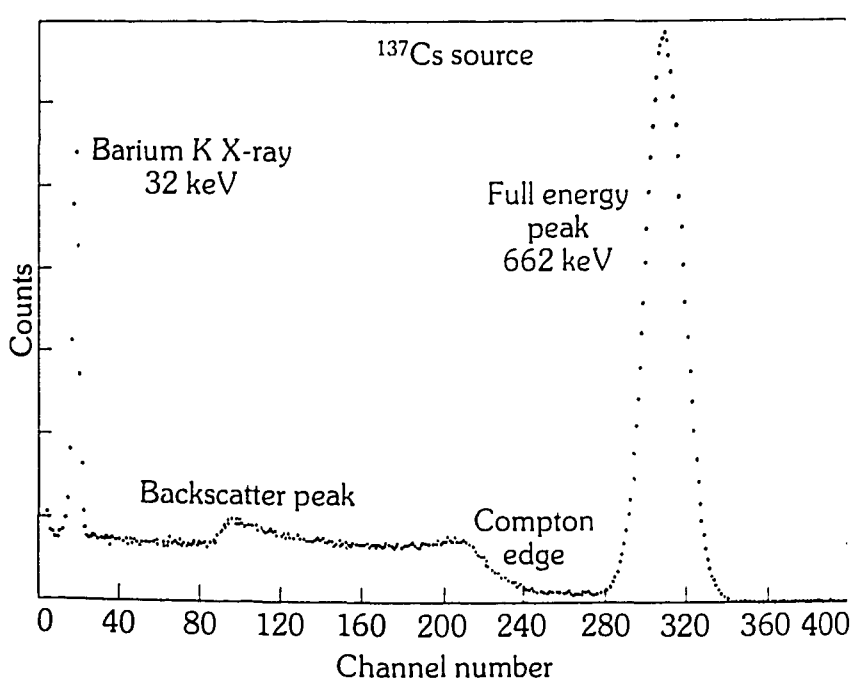

Fig. 3.3 Example of a gamma spectrum obtained with a multichannel analyzer, from Harshaw catalogue [Har]

In this spectrum several characteristic aspects are visible: the photo peak, the Compton edge, the backscatter peak. The prominent peak at 662 keV is the full energy peak indicating events completely absorbed by the detector crystal. This peak is called the photo-peak, because for those events the photo-electric effect has taken place. Compton events in which a scattered gamma travels 180° opposite to the incident radiation produces electrons of 477 keV in the crystal. These events produce the Compton edge noted in the figure. Other scattering events at lesser angles produce the characteristic counts to the lower side of the Compton edge. The back-scatter peak results from Compton scattering from the surroundings, a photon is scattered out of the detector and is rescattered by the housing of the detector for example.

In nearly all counting systems there will be a minimum amount of time that must separate two events in order that they can be recorded as two separate pulses. This minimum time separation is usually called the dead time of the counting system. Because of the random nature of radioactive decay there is always some probability that a true event will be lost because it too quickly follows a preceding event. These dead time losses can become rather severe when high counting rates are encountered.

In this project scintillation detectors will be used. A scintillation counter relies upon the rapid conversion of ionisation energy to light in certain materials. The excited ion falls back to a stable state under emission of a photon, with a wavelength in the visible light range. An ionising event is therefore registered as a small flash off light which is detected and amplified by a photomultiplier. The ideal scintillation material should posses the following properties, according to Knoll [Kno79]:

- high density for greater gamma ray stopping power;
- high scintillation efficiency;
- the light yield should be proportional to deposited energy over as wide a range as possible;
- the medium should be transparent to the wave length of its own emission for good light collection;
- the decay time of the induced luminescence should be short so that fast signal pulses can be generated;
- the material should be of good optical quality and subject to manufacturing in sizes large enough to be of interest as a practical detector. Its index of refraction should be near that of glass($\sim$1.5) to permit efficient coupling of the scintillation light into a photomultiplier tube.

Sodium iodide activated by thallium (NaI(Tl)) gained much if its early popularity as detector material because the relatively high atomic number (Z = 53) of its iodine constituent assures that photoelectric absorption will be a relatively important process. The corresponding high detection efficiency and large photo fraction have contributed to the success of sodium iodide scintillation spectrometers. The photo fraction is the amount of counts in the peak area divided by the total number of counts in the spectrum.

Other materials such as BGO have even higher density (see table 3.1) or effective atomic number and therefore the response function for these materials shows an even greater detection efficiency and photo fraction. The mechanical and chemical properties of BGO make it easy to handle and use, and detectors using BGO can be made more rugged than those employing the more fragile and hygroscopic sodium iodide. However the relative high light output and smaller decay time have led to the dominance of sodium iodide in spectroscopy with scintillators.

Table 3.1 Properties of scintillation materials NaI(Tl) and BGO, from Harshaw catalogue [Har]

Material	Wavelength of maximum emission (nm)	Decay constant (μs)*	Density (kg m^{-3})	Hygroscopic	Scintillation Conversion Efficiency (%)**
NaI(Tl)	410	0.23	3670	yes	100
$Bi_4Ge_3O_{12}$ (BGO)	480	0.30	7130	no	8

* Room temperature, best single decay constant
** Referred to NaI(Tl) with S-11 photo cathode response

3.4 The gamma absorption method

The gamma absorption method relies upon the attenuation of mono-energetic photons by absorber material. For mono-energetic photons the transmission through an absorber of a certain thickness is given by a simple exponential relationship. When the number of transmitted photons per second and the original number of incident photons per second are known, the absorber thickness can be calculated. The transmitted photons of that one energy can be found in the net area underneath the photopeak, because the photo peak is caused by photons that have transferred all their energy to the detector crystal. With a photopeak efficiency the number of counts in the net photopeak area is related to the number of transmitted mono-energetic photons that were incident on the detector crystal.

A problem is that interactions in the absorber lead to the appearance of Compton photons with a lower energy. So instead of mono-energetic photons, photons with different energies are incident on the detector. Each of those energies leads to its own photopeak and Compton edge. To deal with this problem one can make use of the fact that scattered photons move with a different direction after the Compton collision in the absorber material. If the original beam of gamma radiation is very narrow, then all scattered photons will leave the beam. In that narrow beam only the transmitted photons will stay, and a beam of mono-energetic photons will be incident on the detector when an appropriate detector collimator is used. But a Compton photon can be rescattered and still pass the collimator. In the resulting spectrum the net area must be determined under the photopeak, the (re)scattered Compton photons from the absorber give an extra contribution in the spectrum. That contribution in the photopeak area has to be subtracted from the area under the photopeak to give the net area. Only when the net area is used a correct determination of absorber thickness can be made. When a source of gamma radiation emits more than one energy it becomes more difficult to determine the net photopeak area because a photopeak of one energy can lay on top of a Compton edge of another energy, or because the photopeaks of two energies lay very close to each other and give a combined peak in the spectrum.

3.5 Choice of radiation energies

In a gamma ray absorption approach the choice of absorber material has already been made, but the energy of the radiation can still be chosen. It is possible to find an optimal energy; the standard deviation in the parameter to be determined can be minimized. This procedure is described by Gardner [Gar67]. The intensity of a narrow beam of gamma or X rays of a particular energy E, transmitted by a radiation absorbing material of thickness l is given by following equation

$$I(E) = I_0(E)\exp(-[\frac{\mu}{\rho}]x) \tag{3.4}$$

where mass thickness x is equal to the thickness l times the density ρ of the absorber material. I is the transmitted intensity in photons per second, I_0 is the original intensity. Equation (3.4) is only valid for mono-energetic photons. That means for a narrow beam geometry, because in a narrow beam there will be only mono-energetic photons and no scattered photons with a lower energy and a different angle due to scattering.

The intensity of transmitted radiation is measured by means of a counting system typically consisting of a radiation detector and a pulse handling system. The number of counts in the net area under the photo-peak is related to the number of transmitted (mono-energetic) photons that was incident on the detector:

$$R(E) = I(E)\,\eta(E) \tag{3.5}$$

where R(E) is the number of counts in the net photopeak area per unit of time and η(E) is the photo peak efficiency. With this equation the attenuation equation (3.4) can be rewritten in terms of R(E).

$$R(E) = R_0(E)\exp(-[\frac{\mu}{\rho}]x) \tag{3.6}$$

The decay of radioactive nuclei is a Poisson process. The standard deviation in the number of decayed nuclei is equal to the square root of that number. When a nucleus decays radiation is emitted and can be measured as counts. Hence the standard deviation in the number of counts is also equal to the square root of N, the number of counts. The counting rate is equal to

$$R = N/\tau \tag{3.7}$$

τ is the measuring time. Assuming the largest source of uncertainties is the statistic behaviour of the radiation source, so the standard deviation in N is larger than the one in τ, the standard deviation in the counting rate is equal to :

$$\sigma(R) = \frac{\sqrt{N}}{\tau} = \sqrt{\frac{R}{\tau}} \tag{3.8}$$

Alternatively equation (3.6) can be written as:

$$x = \frac{1}{[\frac{\mu}{\rho}]}\ln\frac{R_0(E)}{R(E)} \tag{3.9}$$

the standard deviation in x is equal to

$$\sigma(x) = \frac{\partial x}{\partial R}\sigma(R(E)) \tag{3.10}$$

This is only valid for small values of σ(R(E)), see Gardner [Gar67]. From equations (3.6) it follows that:

$$\frac{\partial x}{\partial R} = - \frac{1}{[\frac{\mu}{\rho}]\ R(E)} \tag{3.11}$$

Using formulas (3.6), (3.8) and (3.11) the relationship for $\sigma(x)$ becomes :

$$\sigma(x) = - \frac{\exp([\frac{\mu}{\rho}]\frac{x}{2})}{[\frac{\mu}{\rho}]\sqrt{R_0(E)\tau}} \tag{3.12}$$

$\sigma(x)$ has a negative value, when calculated from equation (3.12). $\sigma(x)$ is usually expressed as a positive number, so the minus sign in equation (3.12) is omitted.
$\sigma(x)$ is minimized with respect to the mass attenuation coefficient $[\mu/\rho]$ when the first derivative becomes zero and the second derivative is positive. That leads to the following minimizing condition:

$$\frac{d\sigma(x)}{d[\frac{\mu}{\rho}]} = 0 = \frac{\exp([\frac{\mu}{\rho}]\frac{x}{2})}{[\frac{\mu}{\rho}]\sqrt{R_0(E)\tau}} [\frac{x}{2} - \frac{1}{[\frac{\mu}{\rho}]}] \tag{3.13}$$

To satisfy this condition it follows that : $[\mu/\rho] \cdot x = 2$

This means that 13.5 % ($e^{-2} = 0.135$) of the original intensity is transmitted by the absorber, when the minimum standard deviation in x is obtained. In the literature the value of $[\mu/\rho]$ can be found for different absorber materials as a function of the energy, and the optimal energy of the radiation for a specific gamma absorption problem can be found using those tables in literature, see Hubbell [Hub82].

This procedure can also be applied when the attenuation is caused by several absorber materials, as is the case with a column filled with polystyrene particles and fluidized by air. In that case the parameter that has to be determined is the void fraction α. A minimum standard deviation in that parameter is obtained when the sum of mass absorption coefficients times the mass thicknesses of each material is equal to 2.

In this chapter the nature of gamma radiation and the principle of detection of radiation have been treated. The gamma absorption method has been described. With the gamma absorption method the thickness of an absorber material can be determined. Also a method has been given to choose a gamma radiation energy that leads to a minimum standard deviation in the parameter to be determined with the gamma absorption method.

4 Void fraction measurements

In this chapter a method will be described to determine a chordal void fraction with the gamma absorption technique. In literature this method is described by Chan [Cha81] and by Gardner [Gar67]. This method can be used in the lower parts of the column, where a homogeneous situation is expected. From the measured chordal void fractions a radial void fraction profile will be constructed with a shell model [Mud92].

4.1 Choice of radiation source

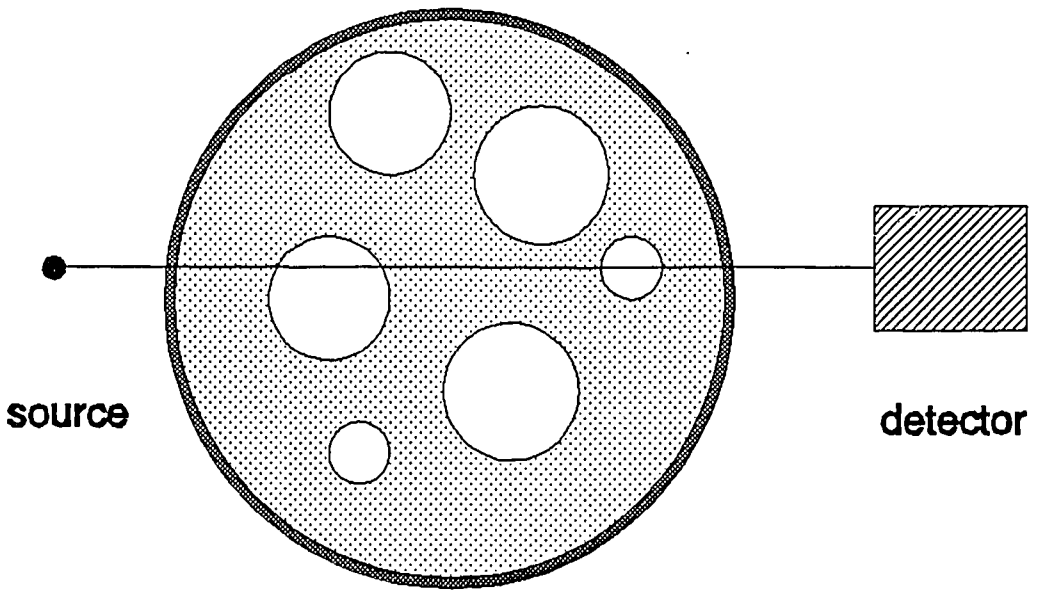

Fig. 4.1 Cross-section of the fluidized bed

The beam intersects the perspex wall and a mixture of bubbles and suspension, as can be seen in figure 4.1. The beam is attenuated by the wall material, by the polystyrene and by the air. In reality around the source and the detector shielding material will be present, and the beam will not be a straight line but diverges.

For the total attenuation of the photon beam the following equation applies:

$$R = R_0 \exp(-[\frac{\mu}{\rho}]_w \rho_w d_w - [\frac{\mu}{\rho}]_{air} \rho_{air} \alpha_f l - [\frac{\mu}{\rho}]_{poly} \rho_{poly} (1-\alpha_f) l) \qquad (4.1)$$

In this equation α_f is the void fraction in a cross-section of the bed; the length of the column in the path of the beam is denoted by l, the thickness of the wall in the path of the beam by d_w. In equation (4.1) the attenuation by the air outside the column is neglected. R_0 is the counting rate when no column is present, in this counting rate the attenuation by the air between source and detector is neglected.

The same procedure as outlined in section 3.4 can be used to find an optimal energy, that is the energy for which the standard deviation in the measured chordal void fraction is minimal. The mass absorption coefficients of wall, polystyrene and air have to satisfy the following equation:

$$[\frac{\mu}{\rho}]_{wall} \rho_{wall} d_{wall} + [\frac{\mu}{\rho}]_{air} \rho_{air} \alpha_f l + [\frac{\mu}{\rho}]_{poly} \rho_{poly} (1-\alpha_f) l = 2 \qquad (4.2)$$

The objective is to construct a radial void fraction profile. The chordal void fraction has to be measured at different positions in a cross-section to be able to calculate the radial void fractions with a shell model [Mud92]. In equation (4.2) l and d_{wall} will have different values depending on the position of the measurement. Also α_f can vary between 0.433 and 0.70. It is clear that it is not possible to satisfy the condition in equation (4.2) for all situations. The energy of the gamma radiation should lead to absorption coefficients for which the value of the sum of absorption terms in equation (4.2) is close to 2.

A spreadsheet was constructed, containing the absorption coefficients for different energies, and the sum of absorption terms was calculated for different void fractions and different measuring positions. The standard deviation in the measured void fraction has a minimum when the sum of absorption terms is equal to 2. In figure 4.2 the standard deviation times a constant is set on the y-axis and the energy of gamma radiation on the x-axis. This constant is determined by the values of the source strength and the measuring time. The measured void fraction has a value of 0.5 in figure 4.2. The different lines correspond with different positions x_b of the beam, x_b is the distance between the beam and the centre of the column. This figure gives an indication of the consequences of choosing a certain energy for the experiments on the standard deviation in the determined void fraction.

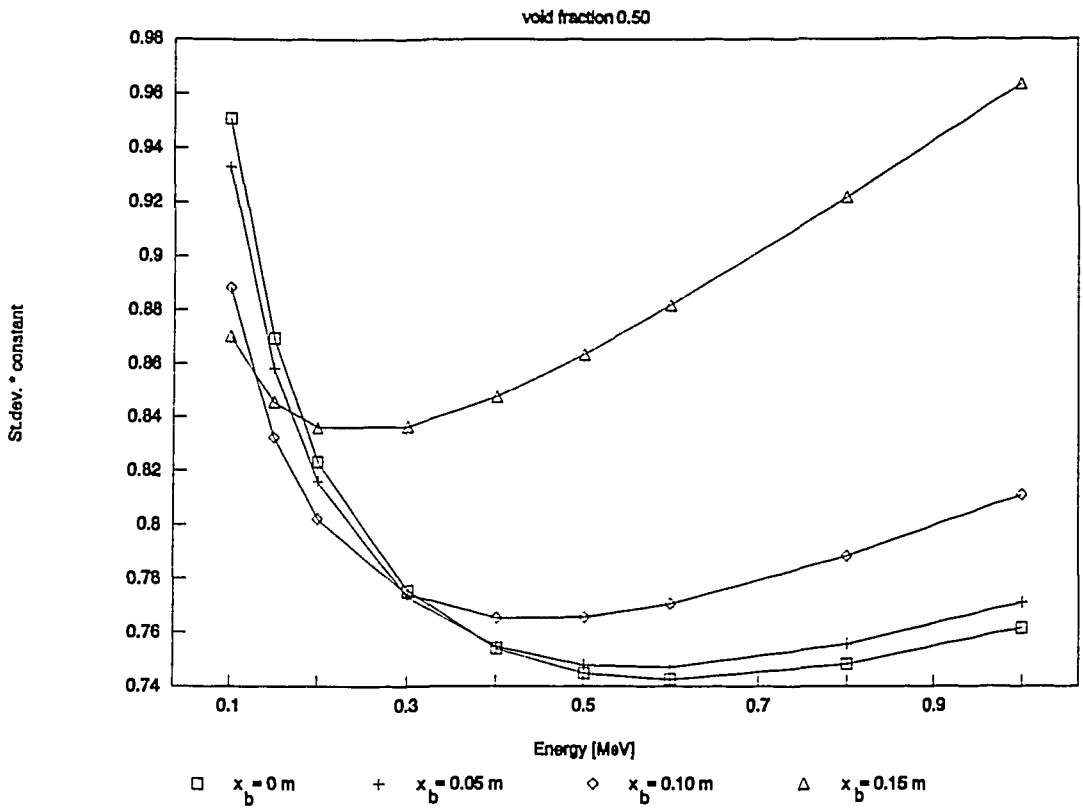

Fig. 4.2 Standard deviation in the void fraction as function of energy of gamma radiation, for a void fraction of 0.5, and for various distances x_b from the centre of the column of the beam for the position of the beam.

Similar figures can be obtained for other values of the void fraction. An energy around 500 keV would give the best results. In practice not all energies are available and there are some restrictions. In figure 4.2 can be seen that the standard deviation rises faster when a lower energy is chosen than when a higher energy is chosen. The source should have a sufficiently long half-life and preferably emit only one gamma energy. If only one gamma energy is emitted the determination of the net photo-peak area is more simple, the net photo-peak area is related to the number of transmitted photons. That leaves only two possibilities around 500 keV : Cs-137 with a 662 keV gamma and Ba-133 with a 356 keV gamma.

Cs-137 has an half-life of 30 year [CRC85]. Cs-137 emits one gamma energy of 662 keV. Cs-137 is available in large source-strengths up to a few curie. Cs-137 is a standard source for gamma radiation gauging applications. Cs-137 leads to the following absorption coefficients, obtained by linear interpolation between known values from literature [Hub82]:

$[\mu/\rho]_{polystyrene} = 0.8345 \cdot 10^{-2}\ m^2kg^{-1}$
$[\mu/\rho]_{air} = 0.7752 \cdot 10^{-2}\ m^2kg^{-1}$
$[\mu/\rho]_{perspex} = 0.8373 \cdot 10^{-2}\ m^2kg^{-1}$

In figure 4.3 the sum of absorption terms is plotted for Cs-137 for different positions in a cross-section of the intersection of the beam and for different void fractions (α_f). Most of the values of the sum of absorption terms are lower than 2, this means that more than 13.5 % (e^{-2}) of the incident radiation is transmitted by the column.

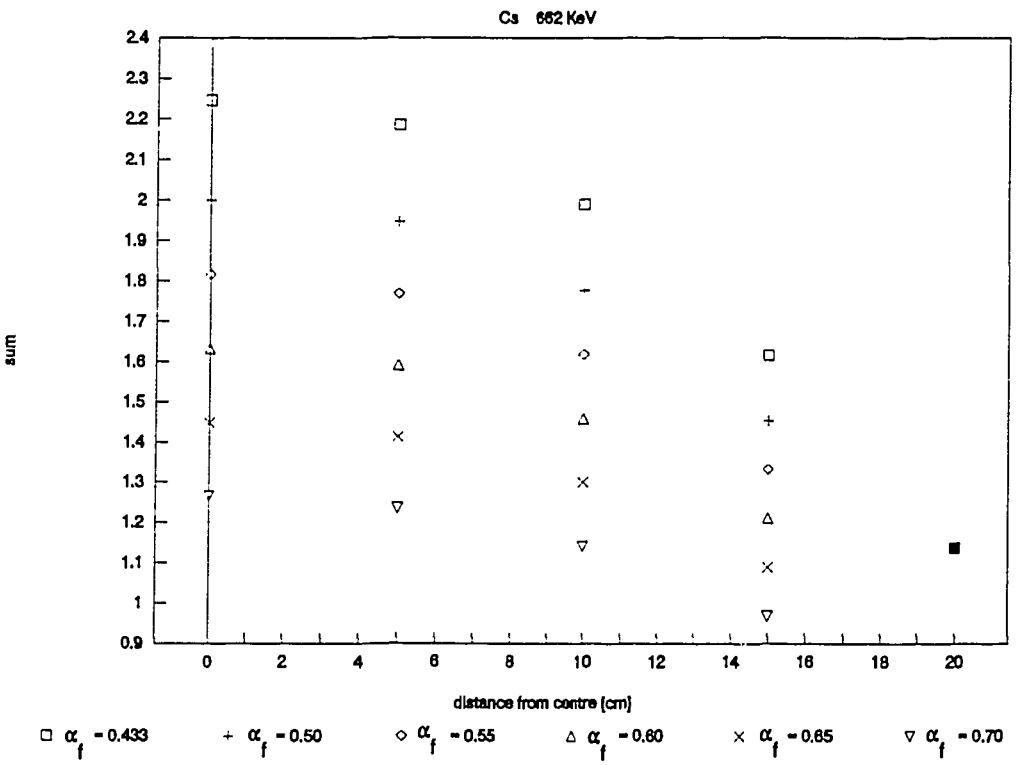

Fig. 4.3 Sum of absorption terms for Cs-137 as function of the distance of the beam from the centre of the column for various values of the void fraction α_f.

Ba-133 emits several gamma energies, the most important ones are 81 keV (33% gamma ray intensity), 303 keV (19%) and 356 keV (62%) [CRC85]. The gamma ray intensity is given in percents of the total decay rate for a given gamma ray transition. The sum of those percentages can be higher than 100% because several photons can be emitted in one transition because there can exist intermediary exited levels. The one of interest is the gamma with an energy of 356 keV. Ba-133 has a half-life of 10.53 years. Ba-133 leads to the following absorption coefficients for the gamma radiation with an energy of 356 keV, obtained by linear interpolation between known values from literature [Hub82]

$[\mu/\rho]_{polystyrene} = 1.080 \cdot 10^{-2}\ m^2kg^{-1}$
$[\mu/\rho]_{air} = 1.005 \cdot 10^{-2}\ m^2kg^{-1}$
$[\mu/\rho]_{perspex} = 1.084 \cdot 10^{-2}\ m^2kg^{-1}$

In figure 4.4 the sum of absorption terms is plotted for the 356 keV gamma of Ba-133 for different position in a cross-section of the intersection of the beam and for different void fractions. Again α_f is the void fraction in a cross-section of the column. Most of the values of the sum of absorption terms are higher than 2, this means that less than 13.5 % (e^{-2}) of the incident radiation is transmitted by the column.

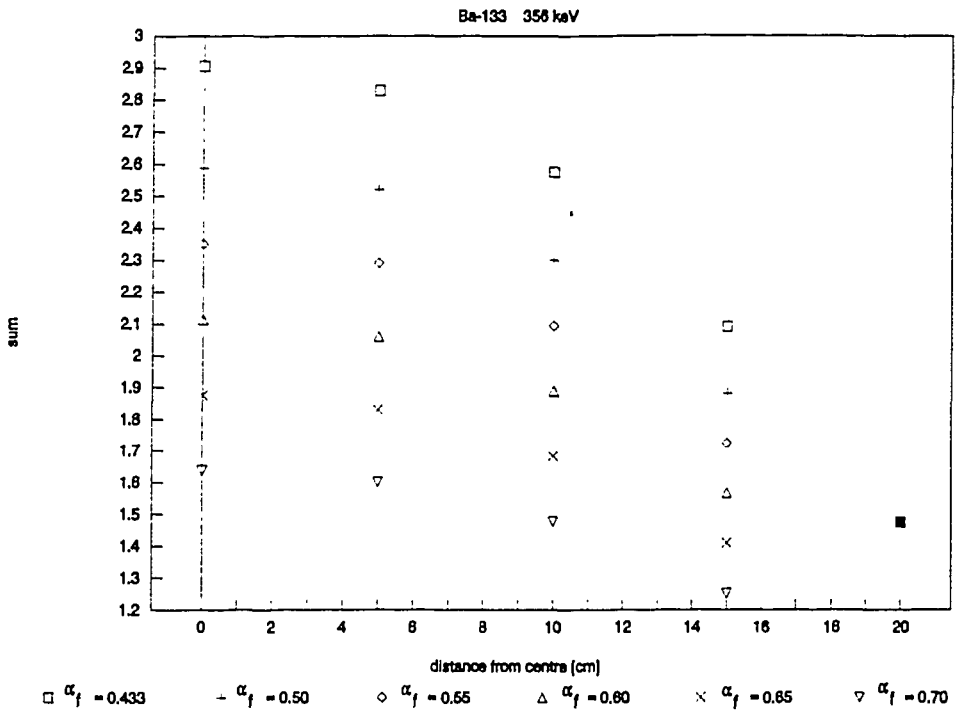

Fig. 4.4 Sum of absorption terms for Ba-133 as function of the distance of the beam from the centre of the column for various values of the void fraction α_f.

Cs-137 has been chosen as source of gamma rays [1], because of the following reasons. The 662 keV photon of Cs-137 has an energy higher than the optimal value of circa 500 keV and the 356 keV photon of Ba-133 a lower value, and as mentioned before for higher energies than the optimum the standard deviation in the void fraction rises slower than for lower values. Hence the 662 keV photon leads to a smaller standard deviation in the chordal void fraction than the 356 keV photon.

[1] At present in the Kramers Laboratorium a large fluidized bed with a diameter of 0.80 m is under construction. So the same procedure as in section 4.1 has also been carried out for a 0.80 m column with a 4 mm steel wall; in that case Co-60 is the source to use. Co-60 has two gamma energies, 1.17 MeV and 1.33 MeV.

Another reason is that Ba-133 emits several energies around 356 keV, the photo-peak of the 356 keV photon cannot be seen separately from those other peaks, and that the photo-peak will on top a Compton edge resulting from an higher gamma energy that Ba-133 also emits. Cs-137 emits only one gamma energy. Furthermore Cs-137 is cheaper and it is standard (out of a catalogue) available in the required source strength.

In figure 4.5 the relative standard deviation in the determined void fraction has been plotted with Cs-137 as source, as a function of the position of the beam for several void fractions, with R_0 equal to 50000 counts s^{-1} and a measuring time of 1 s. The position of the beam is given as a distance from the centre of the column of the beam.

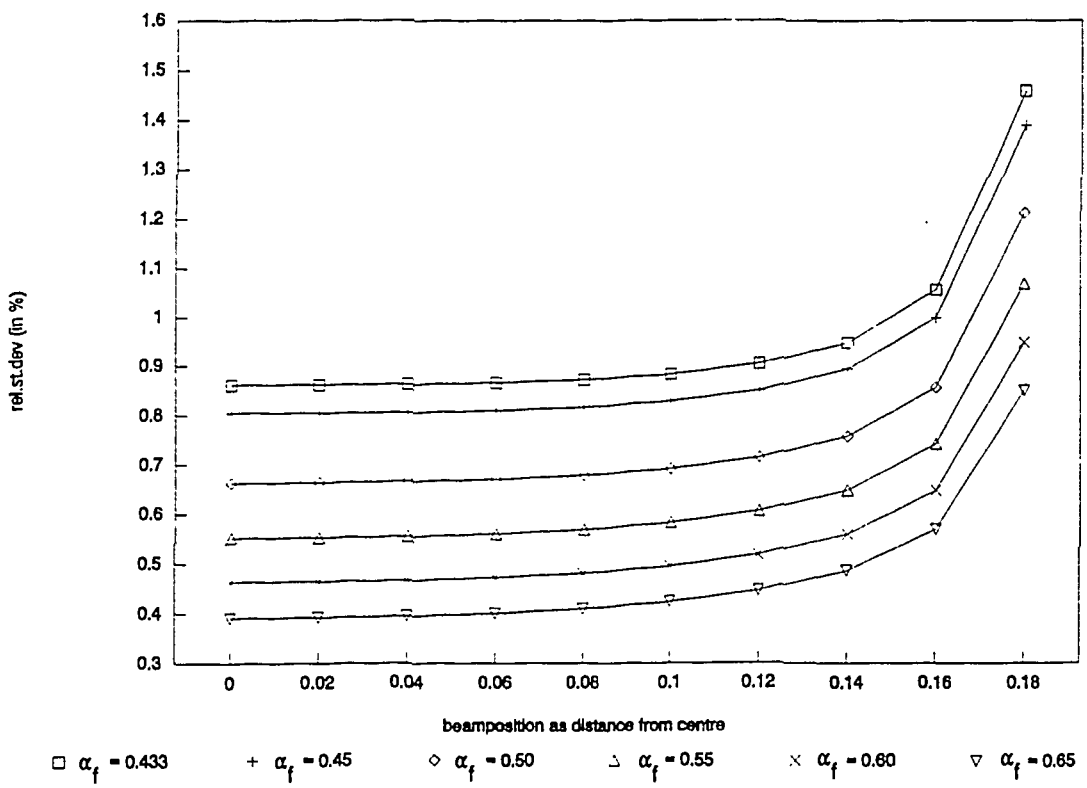

Fig. 4.5 Relative standard deviation in the void fraction as a function of the distance of the beam from the centre of the column with Cs-137 as source, for several void fractions α_f. R_0 = 50000 counts s^{-1}, and measuring time = 1 s.

4.2 Calculation of the chordal void fraction

For the determination of a chordal void fraction more than one measurements is always necessary. First a reference counting rate has to be measured; using that counting rate and the actual measurement the required chordal void fraction can be calculated. That reference counting rate can be the counting rate after the beam has passed the empty column or the counting rate after passing the column, that is filled with polystyrene particles, but not fluidised. Here the counting rate after the beam has passed the empty column (R_{empty}) will be used as reference counting rate.

$$R_{empty} = R_0 \exp(-[\frac{\mu}{\rho}]_w \rho_w d_w - [\frac{\mu}{\rho}]_{air} \rho_{air} l) \tag{4.3}$$

The void fraction measurements will be done with a multi channel analyzer. In that mode a complete spectrum is displayed, in counts per energy channel. A discrete histogram is produced of the energy transferred to the detector material by the incident photons. The net area below the photo peak at 662 keV is related to the number of 662 keV photons that is transmitted through the absorber materials. The number of counts in that area divided by the measuring time gives a measure for the counting rate.

The equation for the determination of α_f is :

$$\alpha_f = 1 - \frac{\ln(R_{empty}/R)}{l\,([\frac{\mu}{\rho}]_{poly} \rho_{poly} - [\frac{\mu}{\rho}]_{air} \rho_{air})} \tag{4.4}$$

Also two reference counting rates can be used in determining α_f to be less dependent of the values of mass absorption coefficients in equation (4.4). Those two counting rates are R_{empty} and R_{mf}, the counting rate after attenuation of a column at minimum fluidization conditions.

$$\alpha_f = 1 - (1-\alpha_{mf}) \frac{\ln(R_{empty}/R)}{\ln(R_{empty}/R_{mf})} \tag{4.5}$$

This equation is only valid in a homogeneous situation, when at each moment the same amount of gas is present in the path of the beam. Due to the exponential relationship between void fraction and measured number of counts errors can come up when this approach is used in a non-homogeneous situation. The following somewhat exaggerated example in figure 4.5 will illustrate this statement.

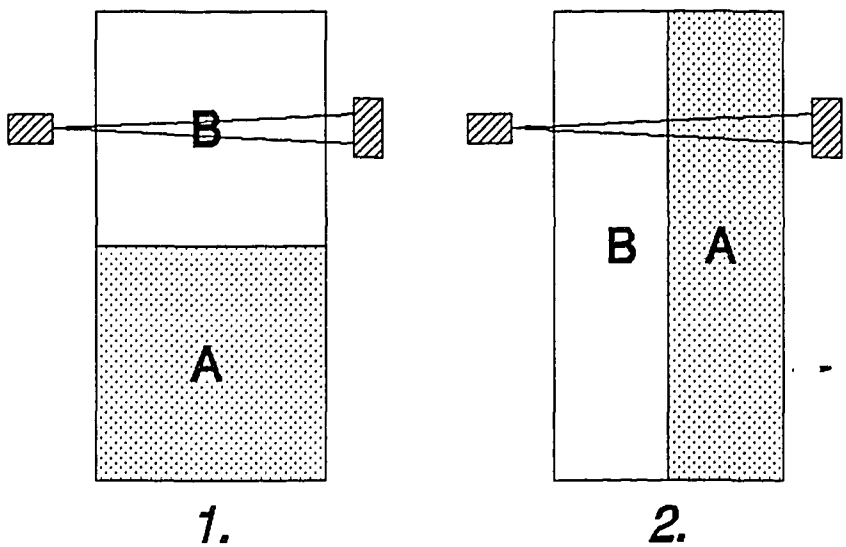

Fig. 4.6 Example of a different non-homogeneity, for a test section with thickness D.

In both situations half of the column is filled with gas, the void fraction is 50%. In situation 1 one period of time $\Delta\tau$ substance A passes the beam and the next $\Delta\tau$ substance B passes the beam. In situation 2 a mixture of A and B passes the beam for a period of 2 $\Delta\tau$, each moment the amount of gas in the path of the beam is constant. Although the total average void fraction is equal, the total number of counts differs in both situations.

$$N_1 = R_0 \Delta\tau \left(\exp(-[\mu/\rho]_A \rho_A D) + \exp(-[\mu/\rho]_B \rho_B D)\right) \quad (4.6)$$

$$N_2 = R_0 \Delta\tau \, 2 \exp(-[\mu/\rho]_A \rho_A D/2 - [\mu/\rho]_B \rho_B D/2) \quad (4.7)$$

In case the polystyrene is material A and gas material B, and D is equal to 0.40 m, those equations become: $N_1 = R_0 \Delta\tau$ 1.02 and $N_2 = R_0 \Delta\tau$ 0.32. This show that the deviations can be substantial depending on the sort of in-homogeneity that occurs.
In literature some calculations have been done by Oyedele [Oye84] and Akintola [Aki91] to correct for that error by assuming a certain form of in-homogeneity in time and space. But in our case that seems not possible because we do not know beforehand the sort of inhomogeneity that occurs. In general can be said that when the amount of gas in the path of the beam is not constant but varies with time an overestimation of the void fraction will occur.

In the lower parts of the column (at a height lower than 0.4 m above the distributor plate) a homogeneous situation is expected. A lot of small bubbles exist there. At those heights the chordal void fraction can be determined correctly with this method. For measurements close to the wall there might be a problem, because the amount of column in the path of the beam is smaller and the number of bubbles in the path of the beam also. The assumption that at each moment the amount of gas in the path of the beam is constant might not be valid for measurements at that position. In experiments the gravity of this problem will have to be examined.

4.3 The diverging beam

In reality the beam of gamma rays is not a straight line but diverges. It was tried to calculate the error that is made when is assumed that the beam is a straight line while in reality the beam diverges. In case of an uniform void fraction, the response obtained with the diverging beam is compared with the response when assuming a straight beam.

The intensity I of photons can be made up of infinitesimal contributions dI corresponding with photons moving at angles between ϕ and $\phi + d\phi$ and between θ and $\theta + d\theta$.

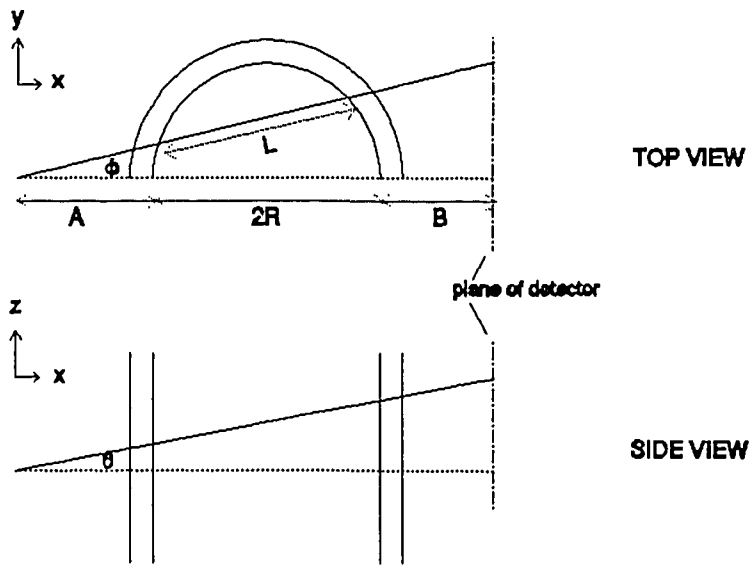

Fig. 4.7 Top and side view of diverging beam.

The total distance between source and detector located at $(\phi,\theta) = (0,0)$ is X;
$X = A + 2R + B$ (see fig 4.6). The source is assumed to be a point source. This distance is increased if the angles becomes (ϕ,θ). The photon flux of contribution dI that is incident on the detector at angle (ϕ,θ) without attenuation will become smaller due to the increase in distance:

$$I_{\phi,\theta} = \frac{I_{0,0}}{(1+\tan^2\phi)(1+\tan^2\theta)} = I_{0,0}\cos^2\phi\cos^2\theta \qquad (4.8)$$

$I_{0,0}$ is the photon flux (photons m^{-2} s^{-1}) without attenuation for $(\phi,\theta) = (0,0)$
Also the distances travelled in the wall material and in the two-phase mixture are changed. L is the distance in the mixture, d_w is the distance in the wall.

$$L = 2R\sqrt{1+\tan^2\theta}\sqrt{1-\sin^2\phi\,[\frac{A+R}{R}]^2} \qquad (4.9)$$

$$d_w = 2(R_u-R)\sqrt{1+\tan^2\theta}\sqrt{1-\sin^2\phi\,[\frac{A+R}{R}]^2} \qquad (4.10)$$

The total intensity can be written as a surface integral over the contributions dI with angles (ϕ,θ) incident on the detector, the extra attenuation by the air outside the column is neglected. A uniform void fraction α_f is assumed.

$$I = \int_\phi \int_\theta \frac{I_{0,0}\,X^2}{\sqrt{1+\tan^2\theta}} \exp[(-\mu_{poly}(1-\alpha_f)-\mu_{gas}\alpha_f)L]\exp[-\mu_w d_w]d\phi d\theta \qquad (4.11)$$

This integral was integrated numerically, assuming a distance of 0.60 m between source and detector (X), and a beam diameter of 0.02 m at the detector, R = 0.192 m, A = 0.158 m ,B = 0.058 m. The boundaries for ϕ and θ are -0.0167 and + 0.0167 (in radials), they follow from the beam diameter at the detector and the source detector distance.

The change in distance due to divergence is very small. L was 0.394 m for a straight line through the centre of the column and when an angle (ϕ,θ) equal to the boundary values is introduced L becomes with equation (4.8) equal to 0.39387 m. At the same position d_w was 1.6 mm and becomes equal to 1.5995 mm with equation (4.9). Both distances L and d_w become smaller.

For a uniform void fraction and for a empty column the intensities at the detector were calculated and using equation (4.4) the detected void fraction was calculated. The ratio of the two counting rates (R_{empty}/R) can be replaced by the ratio of the two intensities (see equation (3.5)). Equation (4.4) was valid for a straight non-diverging beam.

The difference between the uniform void fraction and the calculated void fraction was of order 0.1 % for values of the void fraction between 0.433 and 0.70. In this position the beam radiates through the centre of the column, for other positions a similar result is expected. Hence the beam can be assumed to be non-diverging if the beam has a diameter of 2 cm at a distance of 0.60 m from the source.

4.4 Obtaining a radial void fraction profile

Chordal void fractions, determined with the gamma absorption method have to be converted into a radial void fraction profile. That can be done by applying a model of shells. A similar approach has been followed by Bakker [Mud92] and by Corten [Cor92]. A cross-section of the column is divided in a number of rings and in each ring the radial void fraction is assumed to be constant. The profile is assumed to be rather flat. The number of rings depends on the number of positions where the chordal void fraction is measured, see figure 4.7.

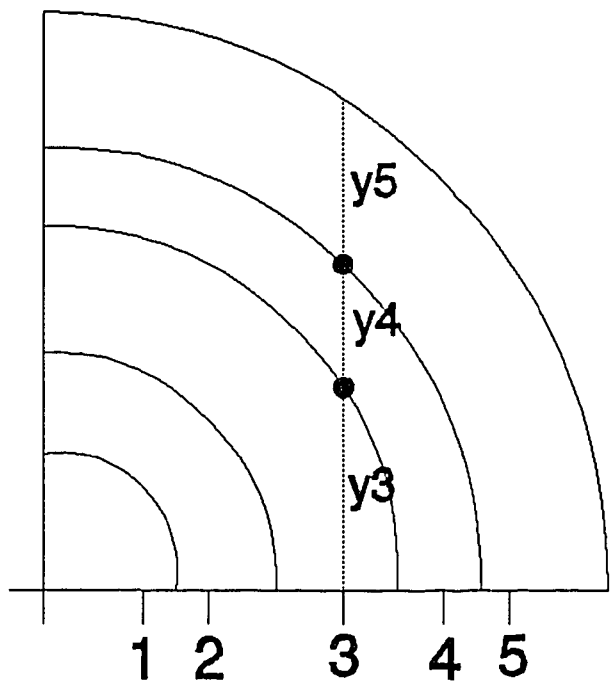

Fig. 4.8 Model with five shells

The boundary of each shell is laid just in between two adjacent intersections of the beam with the column, this can be seen in figure 4.7. In each shell the radial void fraction is assumed to have a constant value. So a measured chordal void fraction can be written as a sum over those shells which the beam intersected.

$$\alpha_{ch,j} \sum_i y_{j,i} = \sum_i \alpha_{r,i}\, y_{j,i} \qquad (4.12)$$

In this formula $\alpha_{ch,j}$ is the measured void fraction at position j. Vertcal length $y_{j,i}$ is the distance in shell i of the beam for a measurement at position j. $\alpha_{r,i}$ is the radial void fraction in shell i.

The innermost shell is shell 1 and the shell around shell 1 is called shell 2, according to this procedure all shells are numbered. Going from outside to inside the radial void fraction in each shell can be calculated from measured chordal void fractions. In the following example that is illustrated with a three shell model.

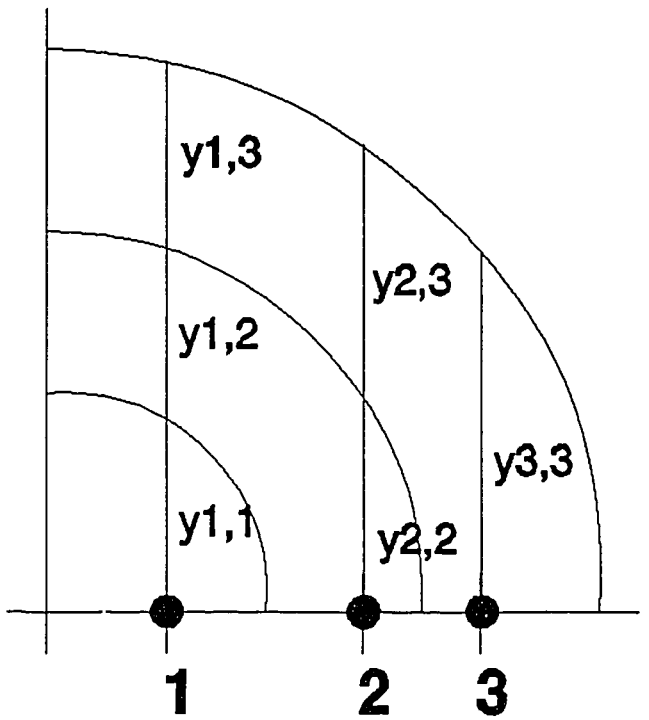

Fig. 4.9 A three shell model

In figure 4.8 a part of the cross-section is shown with three paths of intersection. Each path consists of a number of $y_{j,i}$, depending on the number of shells intersected by the path. From equation (4.11) three equations can be derived for the three shell example:

$$\alpha_{ch,3}\, y_{3,3} = \alpha_{r,3}\, y_{3,3} \tag{4.13}$$

$$\alpha_{ch,2}\, (y_{2,2} + y_{2,3}) = \alpha_{r,2}\, y_{2,2} + \alpha_{r,3}\, y_{2,3} \tag{4.14}$$

$$\alpha_{ch,1}\, (y_{1,1} + y_{1,2} + y_{1,3}) = \alpha_{r,1}\, y_{1,1} + \alpha_{r,2}\, y_{1,2} + \alpha_{r,3}\, y_{1,3} \tag{4.15}$$

This is a system of 3 equations and 3 unknown variables. The first equation gives $\alpha_{r,3}$. Substituting that value in equation 2 leads to an equation for the calculation of $\alpha_{r,2}$. Substituting the two found values in the third equation leads to an equation for the determination of $\alpha_{r,1}$.

A problem is the error propagation, the outer chordal void fractions have to be measured with sufficient accuracy (order 0.1%) to achieve a good accuracy in the radial void fraction of the first shell (order 5 %). This problems results from the manner of calculating of each $\alpha_{r,i}$; the void fractions of all shells around the shell of which the radial void fraction is calculated are needed to calculate that value.

Since the measurements are done in the homogeneous part of the fluidised bed the measuring can be chosen as long as necessary, depending on the used source strength. If R_{empty} = 50000 counts s^{-1}, a measuring time of 60 s would be sufficient in case of a five shell model and a uniform void fraction of 0.50. So the criterion for the necessary source strength has to come from demands in the determination of bubble velocities.

In this chapter the reasons for the choice of Cs-137 as gamma radiation source have been given, and the consequences of assuming a straight photon beam have been examined. A method has been described to convert the measured chordal void fractions into a radial void fraction profile.

5 Bubble velocity measurements

In this chapter a method will be described to determine a bubble velocity with a two beam gamma absorption technique. The two parallel beams are located above each other and a bubble passing the two beams is expected to give a similar response at the two detectors only shifted in time. The method is designed for the case when one bubble at a time passes the beam. That situation is expected at a height of 1 m above the distributor plate and higher. A relative short sample period will have to be used because the bubbles at that height have a velocity of around 1 m s^{-1}. A measurement will consist of a discrete series of number of counts per sample period. A cross-correlation technique can give the time shift between the two responses, combined with the distance between the beams a bubble velocity can be calculated. The resolution of this measurement method will depend on the sample time used and on the source strength used, because sufficient counts per sample time have to be assembled.

5.1 Cross correlation method

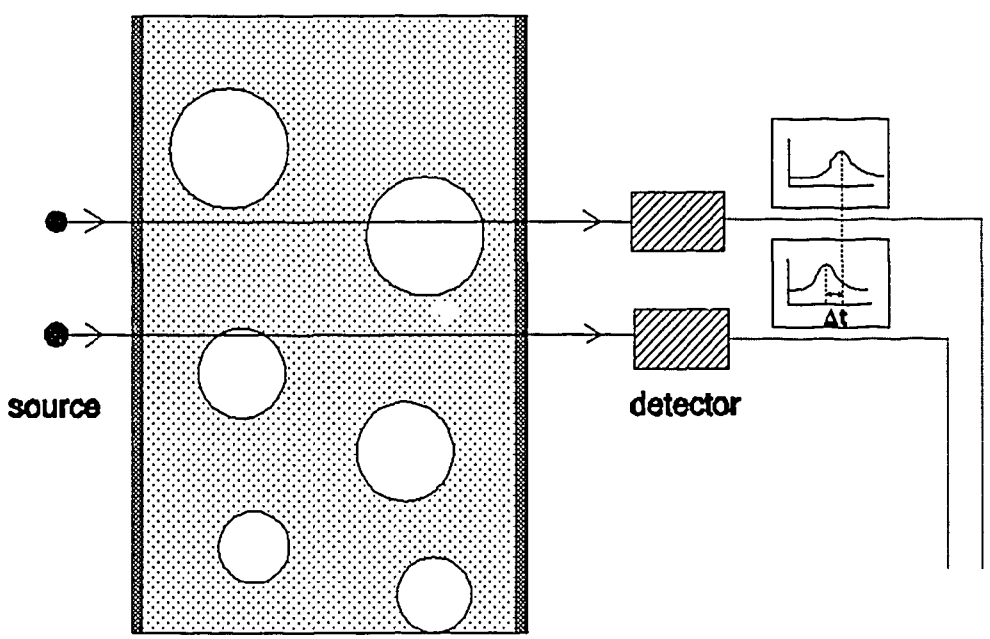

Fig. 5.1 A two beam source detector system.

In figure 5.1 the set-up for the velocity measurements is given; two sources and two detectors are necessary. The system is designed to measure velocities of large isolated bubbles. One rising bubble will give two similar responses only shifted in time.

A cross correlation between two signals gives a peak at that time shift for which correlation exists. Not so much the accuracy in the measurements is important but the presence of preserved characteristic peaks in both responses. The measurements have to be performed in the upper non-homogeneous part of the column, because the passage of single bubbles has to be detected. In that regime there exist large bubbles with a diameter of around 0.15 m, which rise with a high velocity of around 1 m s^{-1}. The measured response is not a continuous signal but a discrete signal due to the statistical character of radiation. A certain amount of time is needed to assemble enough counts (the standard deviation is equal to the square root of the measured number of counts). The sample time used has to be shorter than the passage time of a bubble to get enough (sample) points per bubble passage. Priestly [Pri89] gives as estimation for the cross-covariance between two discrete signals with a finite number of samples M :

$$R_{21}(s) = \frac{1}{M}\sum_t (N_{1,t}-\overline{N_1})(N_{2,t+s}-\overline{N_2}) \qquad (5.1)$$

For $s \geq 0$ the summation goes from 1 to (M-s). For $s < 0$ the summation goes from (1-s) to M. $N_{1,t}$ is the number of counts in signal 1 in sample period number t. $N_{2,t+s}$ is the number of counts in signal 2 in sample period number (t+s). The overlined N denotes the average number of counts per sample period of signal 1 or signal 2. The total measuring time is equal to the number of samples M times the time of one sample period. The cross-correlation function is a normalized cross-covariance function and is defined as [Pri89]

$$\rho_{21}(s) = \frac{R_{21}(s)}{\sqrt{R_{11}(0)R_{22}(0)}} \qquad (5.2)$$

$R_{11}(0)$ is equal to the standard deviation of signal 1, $R_{22}(0)$ to the standard deviation of signal 2. The cross-correlation function has a value between 0 and 1. All simulations are done with the cross-covariance function because it requires less calculation time and gives a similar picture. In figure 5.2 an example is given of an expected response when one bubble passes the beams, and an example of the according cross-covariance function. The expected responses are calculated with a computer simulation that is treated in section 5.4.

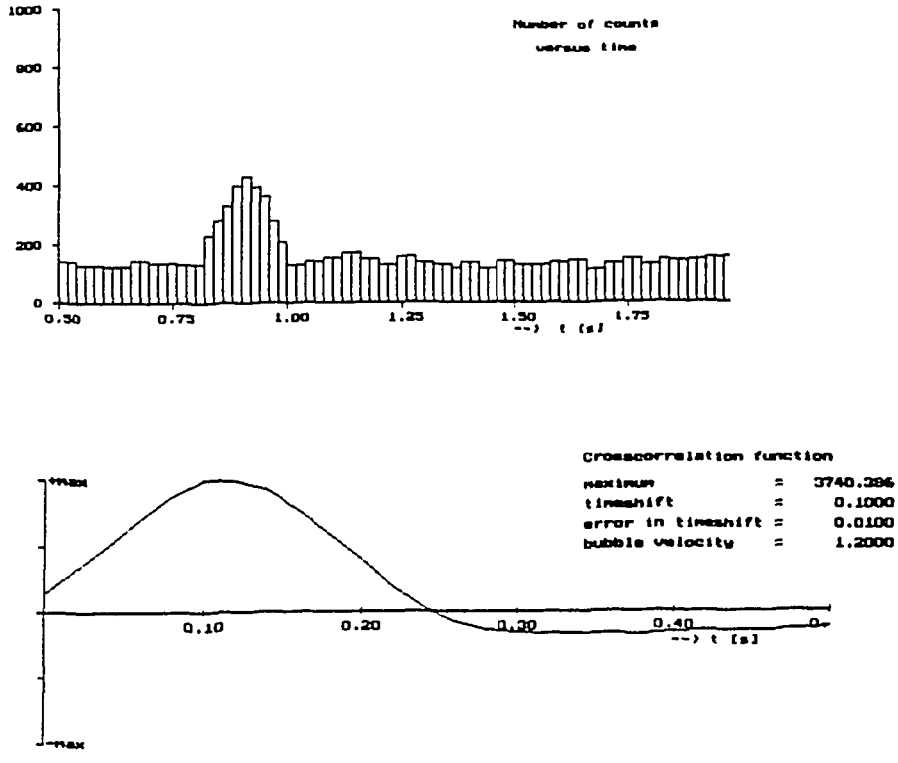

Fig 5.2 Simulated detector response for a bubble with diameter of 20 cm and velocity of 1.1 m s^{-1} and the according cross-covariance function when the second beam is located 12 cm above the first one.

The cross-correlation method gives a time shift between the two signals; combined with the distance between the two beams a bubble velocity can be calculated. When one bubble at a time passes the beams of gamma rays (that is to be expected at a height above the distributor plate of 1 m and higher) the best results can be achieved because the peak in the cross-covariance function will be more clearly visible than in the case more bubbles at the same time pass the beam.

A single channel analyzer will be used in the velocity measurements. On a single channel analyzer a dwell-time (equivalent with sample time) can be adjusted. For a single channel analyzer the processing time of a pulse, generated by the detector material, is shorter than for a multichannel analyzer because energy discrimination only has to be carried out for one energy channel. The width of the channel is determined by setting a lower and a upper boundary for the photopeak of Cs-137; the net photopeak area is a measure for the number of transmitted 662 keV Cs-137 photons. If a photon with an energy in that energy range is detected, a count is registered.

5.2 Sample frequency

The sample frequency is determined by the characteristic size and velocity of a bubble in the upper part of the polystyrene fluidised bed. There is an upper and a lower limit for the sample time. It has to be shorter than the passage time of a bubble and it has to be long enough to get sufficient increase in counts on the detector when the bubble is in the beam. If there are not enough counts the passage of a bubble cannot be discerned from a statistical fluctuation in the response when there is no bubble in the beam. In that case the attenuation of the photon beam is caused by the suspension phase and due to the source statistics the number of measured counts per sample period will vary.

Characteristic values for bubble diameter and bubble velocity at a height of 1 m above the distributor plate are (see chapter 3):

bubble diameter: 0.15 m
bubble velocity: 1.1 m s^{-1}

The total time in view when a characteristic bubble is hit in the centre by the beam of gamma rays can be found by dividing the bubble diameter by the bubble velocity.

time in beam: 0.14 s

A sample time of 20 ms will lead to 7 measured points per bubble passage and is considered to be a good compromise. A sample time of 20 ms corresponds with a sample frequency of 50 Hz. A shorter sample time would require a stronger source to still get enough counts per sample time and a stronger source more shielding. More shielding material around the sources makes the handling of the measuring system more difficult.

The discrete character of the obtained response leads to the introduction of a discretization error in the determined time shift. The peak position in the cross-correlation function is given as a multiple of the sample period. With a sample time of 20 ms a peak in the cross-correlation function may be found at say 120 ms. That means that the actual time shift lays between 110 ms and 130 ms. The discretization error is equal to half the sample time; in case of a sample time of 20 ms an discretization error of 10 s will always be present in the determined timeshift. In practice the time shift is determined by dividing the total measured response of both beams in smaller pieces, each containing one bubble passage, and calculating the cross-correlation for each of the pieces. The resulting time shift is an average over the time shifts determined from each of the pieces. The measurements only have to be accurate enough to get a standard deviation of 10 ms in that average because a discretization error of 10 ms will be the limiting factor.

5.3 Distance between the beams

Several aspects play a role when choosing the distance between the beams. The distance can not be too large, because when a bubble does not rise vertically it may hit one beam and miss the other one. From that point of view the distance should be chosen as small as is possible. The closer the two beams are the more preserved is the response signal. When they are too close to each other a problem might arise in determining the distance between the two diverging beams.

There is the practical aspect, the detectors have a certain volume and shielding around the detectors may be necessary. The shielding is needed against background radiation, against scattered radiation from the column and against scattered radiation coming from the other detector. Hence there is a certain minimum distance needed between the detectors. It is clear that the distance between the sources has to be equal to the distance between the two detectors.

The distance between the beams is used to determine a bubble velocity. For the error in that determination the following equation can be derived.

$$\delta v = \frac{1}{\Delta t}\sqrt{(\delta x)^2+(v\,\delta t)^2} \tag{5.3}$$

A larger distance between the beams leads to a larger Δt and a better velocity resolution, if δt does not increase likewise due to peak broadening in the cross-correlation function.

The detectors that will be used are enclosed in a protection cylinder. For the (2"*2") [1] NaI(Tl) detectors that will be used in the first test experiments (see section 5.6) the outer diameter of that cylinder is 7 cm. In the future a leaden cylinder may be placed around the protection cylinder to provide more shielding against scattered- and background radiation. Enough room must be left between the detectors to be able to place a cylinder with a thickness of 2 cm around the protection cylinders of the detectors. That leads to the choice of 12 cm as distance between the Cs-137 sources.

5.4 Simulations

Computer simulations were carried out to get more insight in the important parameters in determining a bubble velocity with a cross-correlation technique. The objective of the simulations is to get a criterion for the source strength of the two Cs-137 sources, and to find a relationship between the required source strength and the detection limit for bubble velocity measurements.

[1] a cilindrical NaI crystal with a diameter of 2 inch and a height of 2 inch.

A detection limit exists because a too small bubble that passes the beams will not give enough increase in the detector response to be able to determine an accurate bubble velocity. In the simulations an isolated bubble is considered that passes the two beams, the detected void fraction will be a time-varying function. The detector response will also be a time varying function, from the two detector responses a cross-correlation function can be calculated. In the simulations for different source strengths the bubble diameter is decreased until the statistical fluctuations form higher peaks in the cross-correlation function than the bubble passage peak and errors come up in the velocity measurements.

5.4.1 Simulation of the time varying chordal void fractions for the passage of an isolated bubble

In the lower part of the column there is a homogeneous mixture of bubbles and suspension so the measured chordal void fraction is stationary. Higher in the column there are much less bubbles, it is a non-homogeneous mixture of bubbles and suspension; the chordal void fraction will vary with time. In this section a simulation of the time varying chordal void fraction for an isolated rising bubble is described.

In figure 5.3 a cross section of the bed is shown, with a beam of gamma-rays radiating through the column. The beam intersects the bed and the bubble at certain points. When those points are known the bubble fraction δ at the chord can be calculated.

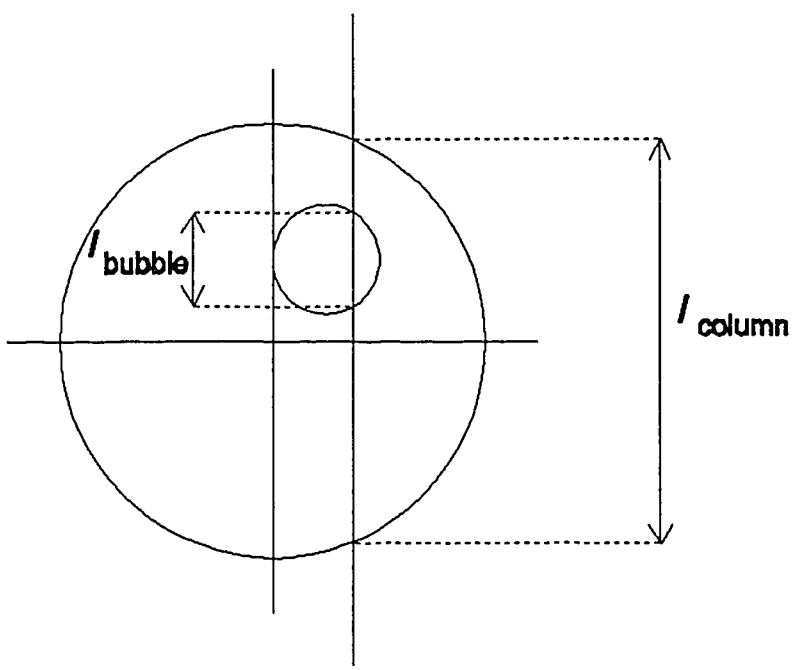

Fig. 5.3 A cross section of the fluidized bed

For the calculation of the chordal bubble fraction δ applies:

$$\delta = \frac{l_{bubble}}{l_{column}} \tag{5.4}$$

l_{bubble} is the length the beam travels in the bubble. l_{column} is the length the beam travels through the column. A chordal void fraction α_l can be obtained using equation (2.17). This is a fraction of a line instead of a fraction of a whole cross section. The centre of a bubble has coordinates (r,θ,z), see figure 5.4.

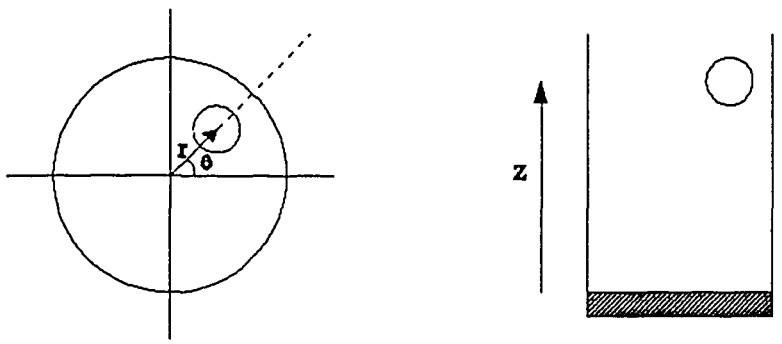

Fig. 5.4 Bubble coordinates

The beam of gamma-rays is situated at height z_s, and at a distance s from the centre of the column, see figure 5.5.

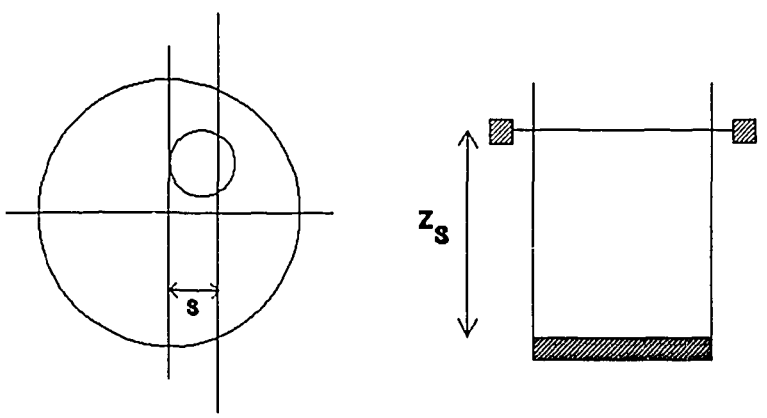

Fig. 5.5 Place of the gamma beam

l_{column} is equal to :

$$l_{column} = 2\sqrt{(\frac{D}{2})^2 - s^2)} \tag{5.5}$$

The bubble has velocity u_{bs} and a diameter d_{bv}. In the simulation a bubble moves upwards (hence r,θ are constant, but z = z(t)), and the overall void fraction at the chord is displayed as a function of time. Different contours are drawn, each contour corresponds with a certain place of intersection. When the place of intersection lays more at the centre of the bubble, a higher contour is drawn. A contour gives the void fraction as a function of time during the bubble passage. First only a slight part of the bubble is in the beam; when the centre of the bubble is at the same height as the beam l_{bubble} reaches its maximum. Than l_{bubble} decreases until the bubble is out of the beam.

The bubble sphere has the following equation :

$$(x-r\cos\theta)^2 + (y-r\sin\theta)^2 + (z-u_{bs}t)^2 = (\frac{d_{bv}}{2})^2 \tag{5.6}$$

The beam is situated at (x,z) = (s,z_s), at $t=t_0$ the bubble enters the beam. At $t=t_0$ only one point of the bubble touches the beam, so t_0 is equal to :

$$t_0 = \frac{z_s - \sqrt{(\frac{d_{bv}}{2})^2 - (s - r\cos\theta)^2}}{u_{bs}} \tag{5.7}$$

The total time a bubble stays in the beam is :

$$t_{total} = \frac{2\sqrt{(\frac{d_{bv}}{2})^2 - (s - r\cos\theta)^2}}{u_b} \tag{5.8}$$

For the bubble fraction δ the following equation is derived from equations (5.4), (5.5) and (5.6), on the condition that $t_0 < t < t_0 + t_{total}$:

$$\delta = \frac{2\sqrt{(\frac{d_{bv}}{2})^2 - (s - r\cos\theta)^2 - (z_s - u_b t)^2}}{2\sqrt{(D/2)^2 - s^2}} \qquad (5.10)$$

From the bubble fraction a chordal void fraction can be calculated. The minimum value of the void fraction is equal to the void fraction at minimum fluidization conditions. In a pascal program the time varying void fraction during a bubble passage is calculated and a figure is plotted on the screen; in figure 5.6 a typical example is shown.

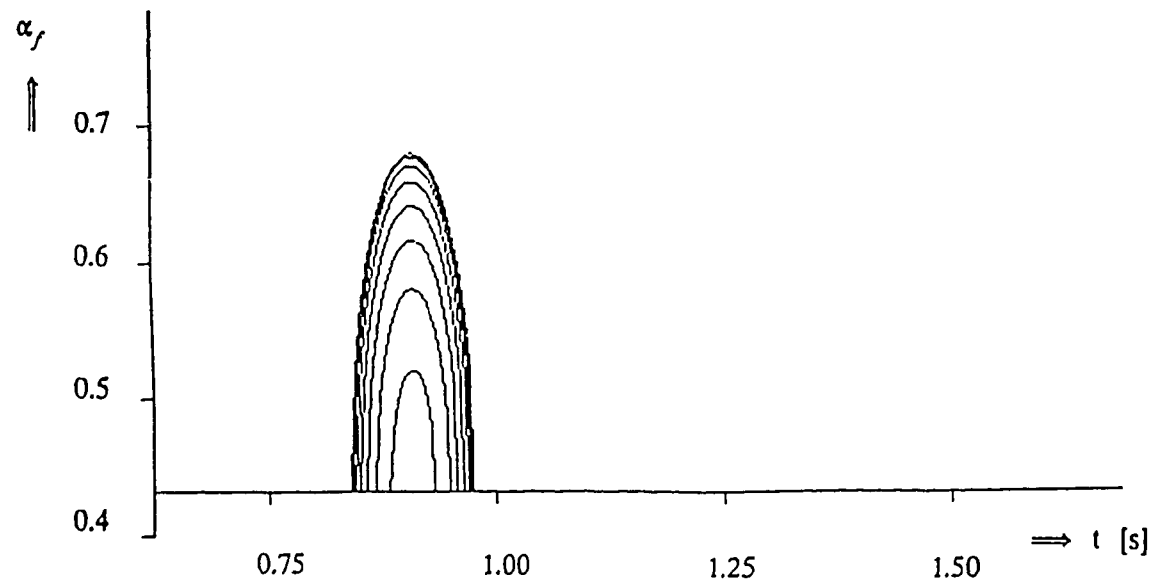

Fig. 5.6 Example of a simulation of the 0.40 m bed. d_{bv} = 0.15 m; u_{bs} = 1.1 m·s^{-1}; s = 0.1 m. The time varying chordal void fraction is shown during a bubble passage.

The occurring time-varying chordal void fraction when a bubble passes the beam is shown in the picture 5.6, obtained from the computer simulation. In this simulation the beam is positioned at one place, and the same bubble rises through that beam each time starting at a different position. The lowest contour is valid when only the outer part of the bubble comes in the beam. The next contour is formed when the centre of the bubble is shifted more towards the position of the beam and the beam intersects a larger part of the bubble. Each time the centre of the bubble is shifted over a constant distance of 1 cm towards the place of the beam and a new contour is drawn, until the centre of the bubble lays at the position of the beam. The bubble diameter is 0.15 m, the bubble velocity is 1.1 m s^{-1}, and the beam is situated 0.10 m from the centre of the column.

In figure 5.6 there are two characteristic scales, the first one is the width of the peak, that corresponds with the time a bubble is in the beam. The time in the beam is equivalent to the length of intersection of the bubble by the beam in vertical direction divided by the bubble velocity. The second one is the peak height, that is determined by the maximum thickness of the bubble as detected by the beam. The thickness corresponds with the length of intersection of the bubble by the beam in horizontal direction.

A slower bubble will lead to the same peak height but to a larger peak width. A larger bubble will lead to a higher and broader peak. The question arises to what is more important in determining a bubble velocity: the passage peak height or the passage peak width?

In reality there are always two difficulties:

- Where was a bubble hit by the beam, in the centre or more to the side of a bubble? A large bubble hit at the side will give the same response as a smaller bubble hit in the centre, provided the velocities of both bubbles are the same.

- How much bubbles were hit by the beam? When one bubble at a time passes the beam, a clear passage peak is obtained. With two or more bubbles at a time the passage peaks are superimposed on each other, so the form of the signal variations will differ depending on the number of superimposed passage peaks. Furthermore the shape of the response is less well preserved when several bubbles are in view.

There will be a detection limit: bubbles, that are too small or are hit at the far outer side, do not stay long enough in the beam or will not give enough counts for a correct velocity measurement. In the simulations it was tried to get an idea of the detection limits in the bubble velocity measurements, depending on the source strength used and distance between the beams.

5.4.2 Determination of the detection limit by means of a computer simulation

The following simulation was carried out. Only one isolated bubble passes the beams. This means that the behaviour of the upper part of the bed is simulated (i.e. at a minimum height of 1 m above the gas distributor). The beam was situated at the centre of the column, because at that position the attenuation of the photon beam when no bubble is present is the highest. Since a larger bubble hit in the side behaves like a smaller bubble hit in the centre, all simulated bubbles are hit in the centre.

One bubble rises vertically with a velocity of 1.1 m s^{-1} and passes the two beams. A sample time of 20 ms is used. In that 20 ms enough counts have to be registered, to be able to distinguish the passage peak from a statistical fluctuation in the detected response. Due to the statistics of the source the number of counts per sample period when no bubble is present will vary. Using the two detector signals a cross-covariance function can be calculated. As measure for the source strength R_{empty} is used (the counting rate caused by a certain source strength with attenuation from the empty column). To be able to simulate a real situation the correct statistic character of radiation has to be incorporated in the simulation. In the next section the implementation of the statistical fluctuations of the source by means of a Poisson distribution is outlined.

5.4.2.1 Poisson distribution

The number of counts per sample period is distributed according to a discrete Poisson distribution. That is a result of the statistical character of radioactive decay in the source. In the simulations the average number of counts is calculated per sample period, the standard deviation in that number is equal to the square root of the number of counts. With that calculated mean and standard deviation the Poisson probability density function is completely known. A method must be found to get an outcome for the number of counts per sample time according to that probability density function. The probability density function of a Poisson distribution with parameter a is [Pri89]:

$$p_i = e^{-a} \frac{a^i}{i!} \tag{5.11}$$

For parameter a applies $(\mu,\sigma^2) = (a,a)$; μ is the mean of the outcome of a variable with a Poisson distribution, σ is the standard deviation. p_i is the probability that the outcome of the phenomenon, that can be described with a Poisson distribution with parameter a, is equal to i. In figure 5.7 a Poisson distribution is plotted with parameter a equal to 49. It describes the probability that a certain outcome occurs of a variable that has a mean of 49 and a standard deviation of 7.

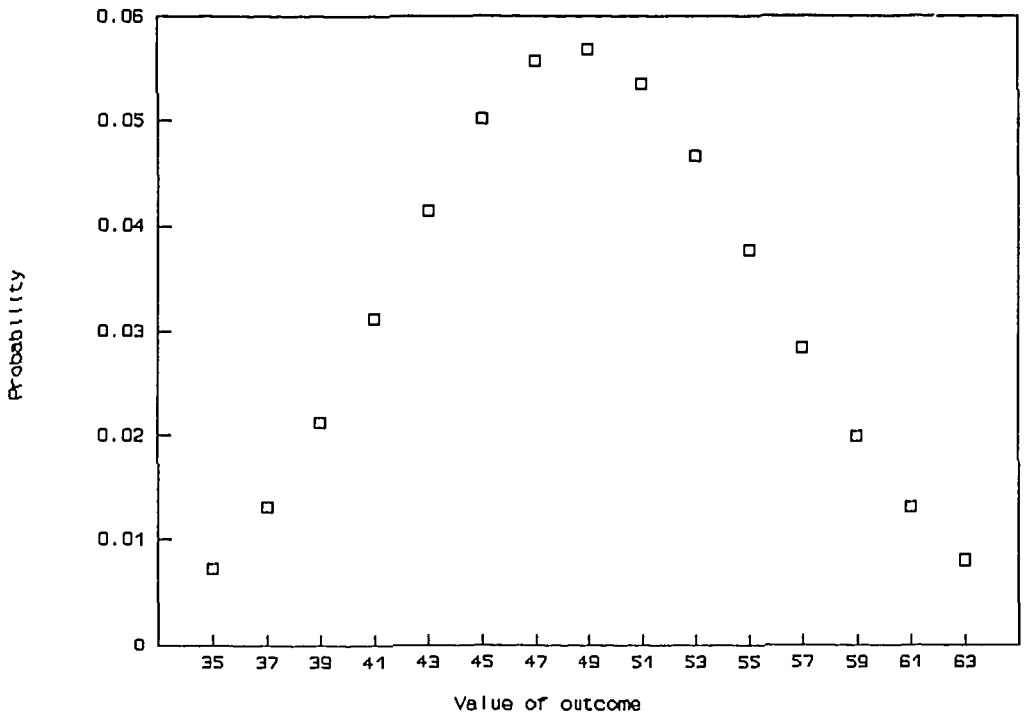

Fig. 5.7 Poisson distribution with parameter a = 49. The probability that a certain outcome occurs is plotted as a function of the value of the outcome.

To get an outcome according to a Poisson function the following approach has been followed. All modern computer languages offer a uniform probability density function between 0 and 1 (the so called random generator). By summation of a number of outcomes of a uniform random generator an outcome of a normally distributed function can be formed. A Poisson distributed function is the discrete equivalent of a continuous normally distributed function. In figure 5.8 both a Poisson probability function and a Gaussian (normal) probability function are drawn. Both describe the probability for an outcome of a variable with mean 49 and standard deviation 7.

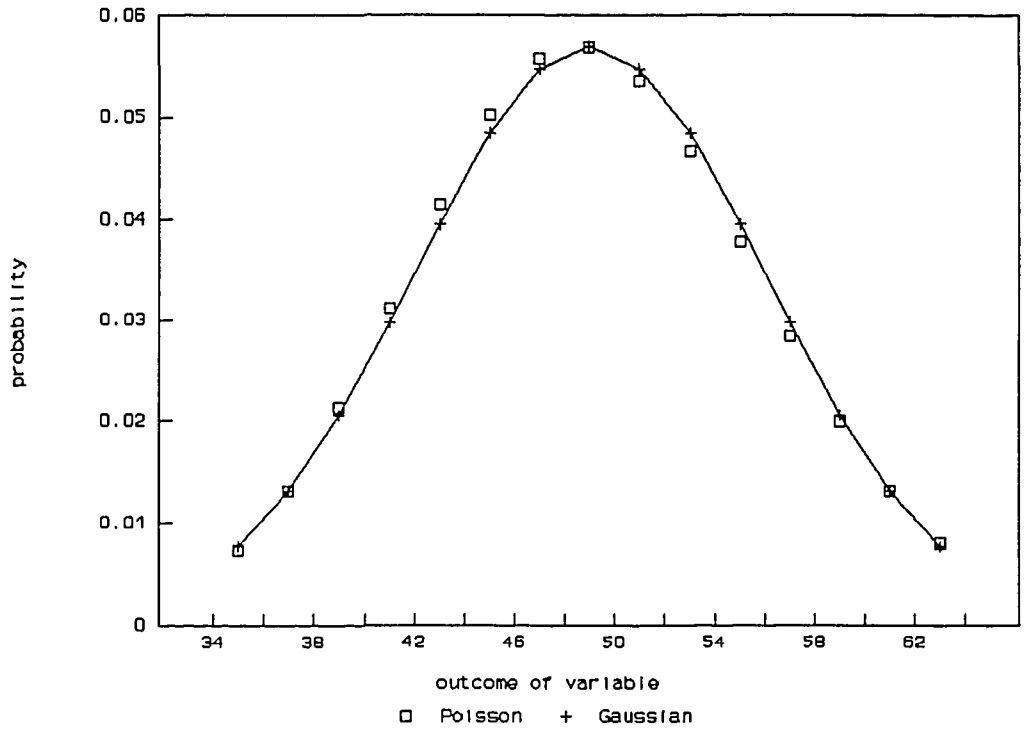

Fig. 5.8 Comparison of a Gauss and a Poisson distribution. The probability for an outcome is given. The outcome has a mean μ equal to 49 and standard deviation σ equal to 7.

The summation is carried out with the following formula [Vro84]:

$$y = \frac{\{ \sum_{i=1}^{N} X_u \} - \frac{N}{2}}{\sqrt{\frac{N}{12}}} \qquad (5.12)$$

X_u is uniform distributed between 0 and 1. y is an outcome of a normal (gaussian) distribution function; for y is valid $(\mu,\sigma^2) = (0,1)$. N is the number of outcomes of X_u that are summed. In theory equation (5.6) is valid for $N \to \infty$, it follows out of the central limit theorem.

With a simple transformation an outcome of a normally distributed function with any mean μ and standard deviation σ can be obtained.

$$X_N = \sigma.y + \mu \tag{5.13}$$

X_N is an outcome of a normally distributed function, N indicates that N values of a uniform distributed function were summed in the process of obtaining X_N. Tests have been done to find a number of summation N in equation (5.12) to give a satisfactory Poisson distribution. A large number of outcomes was generated and a histogram was made. A value of 300 for N seemed sufficient because higher N lead to no visible change in the distribution of the obtained values X_N.

This approach has been used in the simulation program for generating the correct statistics in the measured number of counts. An average number of counts for each sample period is calculated with a standard deviation equal to the square root of the number of counts, and by following the approach described above an outcome of a Poisson distributed function (the number of counts per sample period) is obtained.

5.4.2.2 Simulation results

When one bubble passes the beam of gamma rays the simulation gives the following result.

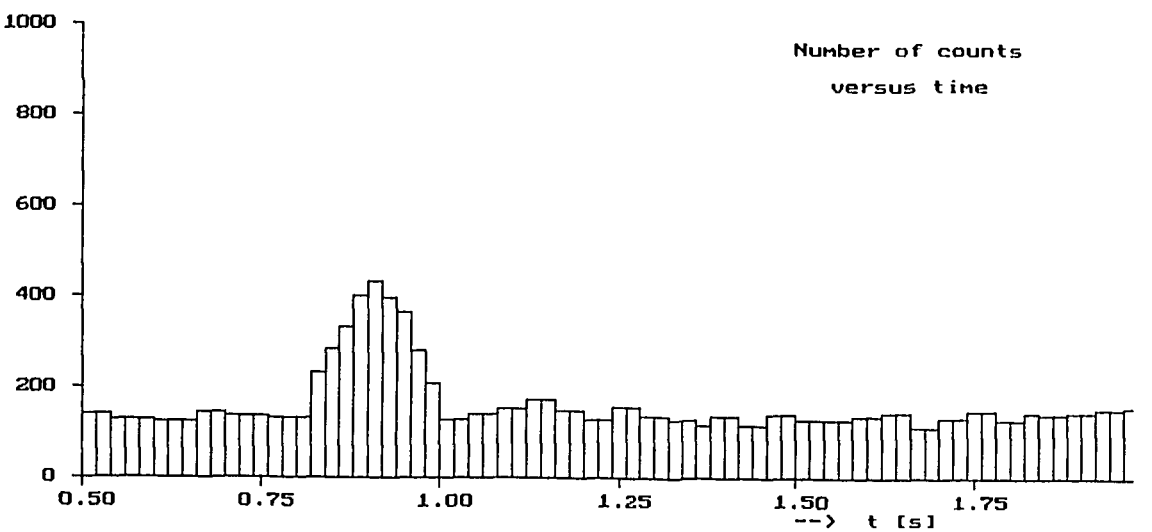

Fig. 5.9 A bubble passage. d_{bv} = 0.20 m. u_{bs} = 1.1 m s^{-1}. R_{empty} = 50000 counts s^{-1}. sample period = 20 ms.

The statistical character of radiation can be seen in figure 5.9; the signal is not constant when there is no bubble in the beam. The number of counts per sample period is an outcome of a Poisson distributed function.

The other beam gives a similar result only shifted on the time axis. That time shift can be determined by calculating a cross-covariance function. The simulation program calculates that function. In figure 5.10 an example is shown. The maximum value of the cross-covariance function can vary from case to case, and to be able to draw each function on the same axis the function is normalized with respect to its maximum.

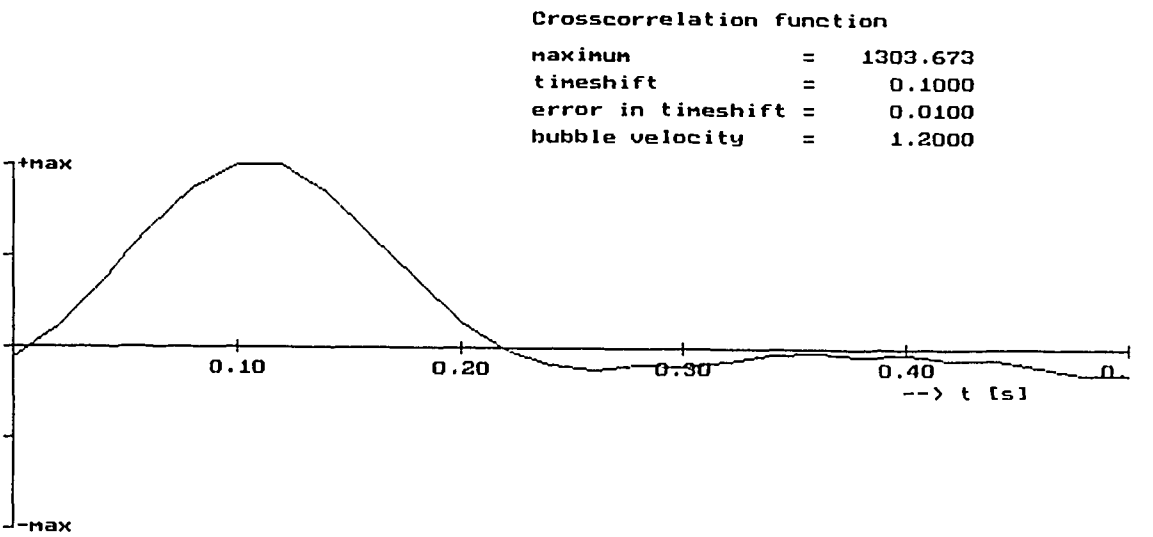

Fig. 5.10 Example of an obtained cross-correlation function. It is a discrete function, but to guide the eye the points have been connected. Each point lays at a multiple of the sample time (here 20 ms).

This picture is from a large bubble, so the time shift can easily be determined, because there is only one large peak in the cross-correlation spectrum. In determining the time shift there is always a discretization error of 10 ms, equal to half the sample time.

If the simulated bubbles become smaller the peak height will decrease in the cross-covariance function, and other statistical peaks will become apparent. The peak height is equal to the plotted maximum value. The program determines the position of the highest peak. The position of that peak on the time axis gives the time shift from which the bubble velocity is calculated. So if a statistical peak is higher than the time shift peak, an error is made because the wrong peak is picked. In appendix B, figures B.4a to B.4d some examples of this phenomenon are shown.

In repeated simulations the time shift was determined and from those outcomes an average time shift with a certain standard deviation was calculated. If the bubble is large enough the peak will always be at the same place, but with smaller bubbles a statistical fluctuation may give a higher peak than the bubble passage. In Appendix B the simulation results are given, in tables B.1, B.2 and B.3, in the form of an average time shift with a standard deviation as function of distance between the beams and as function of the source strength.

For each source strength in the simulation there is a certain minimum bubble diameter needed for a bubble with a certain velocity to give a reliable velocity measurement. The detection limit given in the following table is the diameter of a bubble, with a velocity of 1.1 m s^{-1}, from which the velocity can no longer be detected with enough accuracy, because the relative standard deviation in the determined time shift becomes larger than 25%.

Table 5.1 Detection limits as function of the source strength, for a bubble velocity of 1.1 m s^{-1}

R_{empty} (in counts s^{-1})	Bubble diameter
25000	7 cm
40000	6 cm
50000	5 cm
60000	5 cm
75000	5 cm
100000	5 cm

From these data it can be concluded that a source strength larger than R_{empty} = 50000 counts s^{-1} leads to no improvement in resolution, the detection limit stays 5 cm. Therefore a R_{empty} of 50000 counts per second is chosen, this gives a measure for the source strength to be used in the measuring system.

It is concluded that for a velocity determination the width of a passage peak is more important than the height of a passage peak. If the height would be more important, than a larger source strength, which leads to higher peaks, would lead to a lower detection limit. Since the width of a passage peak in the detector response is more important (that is the time a bubble has been in the beam) the velocity of a bubble with a certain bubble diameter can no more be detected, independent of the source strength used. The latter is the case according to the presented data. The width of a bubble passage peak determines the number of sample points in a bubble passage. A bubble with a diameter of 5 cm, a velocity of 1.1 m s^{-1} and hit in the centre gives 2 to 3 sample periods in a bubble passage, that is simply not enough for a velocity determination with a cross-correlation technique.

In the simulations the bubble is a sphere but in reality a bubble has a different shape. The model of a spherical cap is widely accepted. To give an idea of the consequences a spherical cap bubble can be thought of as half a sphere. Figure 5.11 illustrates when a bubble velocity can be detected, depending on the position of intersection of the gamma beam. If the point of intersection is too far to the side the vertical intersected length will be smaller 5 cm or smaller, and no longer a reliable velocity can be determined.

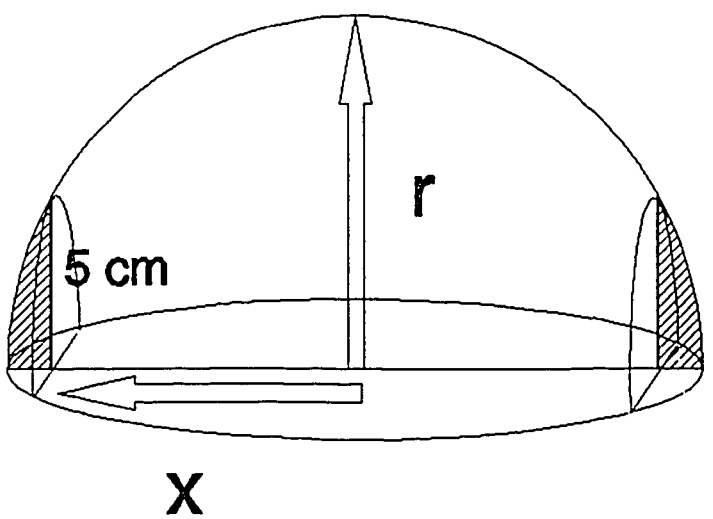

Fig. 5.11 Illustration of the meaning of the detection limit.

In figure 5.11 r is the radius of the half sphere, x is the horizontal distance from the centre that leads to a vertical intersection length of 5 cm. In table 5.2 the values of x are calculated for various values of r. This gives an idea where a bubble still can be intersected by the beams and still a reliable bubble velocity can be determined.

Table 5.2 : Values of r and x, as defined in figure 5.11						
r (in m)	0.10	0.12	0.14	0.16	0.18	0.20
x (in m)	0.087	0.109	0.131	0.152	0.173	0.194

For a half sphere a vertical intersected length of 5 cm means that the horizontal intersected length at the bottom of the sphere is 10 cm. So a larger bubble diameter is needed to get the same vertical intersected length when the bubble is not spherical but has a spherical cap form. Compared to spherical bubble form in the simulations, the horizontal intersected length is increased and more counts per sample period during bubble passage can be expected due to the increased amount of gas in the path of the beam. The influence of this fact will not be large because the time in the beam is the same as in the case of the spherical bubble in the simulation.

It can be concluded that the velocity of a spherical cap bubble will be accurately measurable when a length of more than 5 cm of a bubble, that has a velocity of 1.1 m s^{-1}, has been in view, if a R_{empty} of 50000 counts per second is chosen.

5.5 Practical considerations

In the simulation the signal length of a bubble passage is only 1.5 seconds, so only 75 sample points are obtained. In reality a longer measuring time will be used, and the detector responses will contain more than one bubble passage. The signal can be divided in pieces and per piece a correlation can be calculated and those correlation can be summed to give the resulting cross-correlation. That technique is to be preferred above calculating the resulting cross-correlation over the whole measured response. In that longer measuring period more than one bubble passage will be detected, and those bubble passages may be caused by a bubbles with a different velocity. Perhaps that aspect can be covered by the calculation of the cross-correlation per piece of the total response.

In a practical situation one must be able to tell from a peak in the cross-correlation or cross-variance function whether it will give a reliable velocity or not. That can be done by looking at its height compared to the height of a statistical peak. After some testing the maximum level of a statistical peak can be estimated and if a peak rises above that level a reliable velocity can be determined.

In a regime where more smaller bubbles at the same time may be in the beam, a more varying signal with smaller variations will be obtained compared to the regime where one bubble at a time passes the beams. That might lead to lower peaks in the cross-correlation spectrum. Also coalescence may occur, that leads to a less definite peak in the cross-correlation because there are more velocities involved, the velocities of each bubble before coalescence and the velocity of the resulting bubble after coalescence.

Perhaps it is possible to determine a bubble frequency by applying a auto-correlation on one of the two detector responses.

5.6 Source strength

As measure for the source strength R_{empty} has been used. Here the usable strength will be calculated from R_{empty}. The original source strength is reduced by several factors; the following formula describes the source strength corresponding with a measured counting rate.

$$A = \frac{R}{f_y f_g f_a \eta_f} \tag{5.14}$$

A is the source strength, given in becquerel. One becquerel (Bq) is equivalent with one disintegrations per second in the source. f_y is the number of photons per disintegration. Cs-137 gives f_y = 0.85 for the 662 keV gamma [CRC85]. Thus 100 disintegrations of source material will lead to the appearance of 85 photons with an energy of 662 keV.

f_g is the geometry factor, a source radiates in all directions in this case the narrow beam contains only a small part of the total angles of emitted radiation. If the distance between source and detector (l) is much larger than the detector diameter (2r), the following equation applies.

$$f_g = \frac{\pi r^2}{4\pi l^2} \tag{5.15}$$

The surface of a circular part of a sphere is approximated by the surface of a flat circle. The beam diameter at the detector is set at 2 cm, that will be achieved with a detector collimator with an aperture of 2 cm, so r = 1 cm. The source-detector distance is set at 60 cm to leave enough room for the source shielding and the detector shielding around the 0.40 m column, hence l = 60 cm. That leads to a value for f_g of $6.94\ 10^{-5}$. The absorption factor f_a describes the attenuation of the empty column. The 0.40 m perspex column with a wall of 8 mm thickness leads to f_a = 0.85. η_f is the photo-peak efficiency of the detector used, it gives the percentage of incident photons of 662 keV that is counted in the photo-peak at 662 keV. In the test experiments a NaI detector will be used, later on BGO will be use as detection material. For NaI applies η_f = 0.15, for BGO η_f = 0.50 those values were found in Knoll [Kno79] for a crystal with dimensions 38mm*38mm. For a 2"*2" crystal the efficiencies will be somewhat larger.

Those factors lead to the following source strengths, corresponding with a R_{empty} of 50000 counts s^{-1}. If the NaI detector is used the source strength should be 180 mCi, if the BGO detector is used 50 mCi is sufficient (1 Ci is $3.7\ 10^{10}$ becquerel).

The chosen sources must be usable for both the test experiments and for the experiments later on with the BGO detectors. Therefore a source strength of 100 mCi is chosen, it is good enough for testing and will give an even better performance if BGO is used. When the BGO detectors will be used it might be possible to choose a shorter sample time, because the source strength is larger than was required for a sample time of 20 ms. A shorter sample time leads to a decrease of the discretization error and the resolution in the velocity measurements will increase. For the same bubble a shorter sample time means that more sample points per bubble passage can be obtained. Hence a smaller time in the beam is needed for a bubble to give an accurate velocity determination, and the resolution increases.

In this chapter a method has been described to determine bubble velocities with two beams of gamma radiation and the application of a cross-correlation technique. A sample time and a distance between the two beams have been chosen. Simulations have been presented for the expected response when an isolated bubble passes the two beams. A relationship between the source strength and the detection limit has been found. When the bubble is longer in the beam than the value of the detection limit an increase in source strength leads to an improvement in the accuracy of the velocity measurements. A discretization error equal to half of the sample time is always present. When the bubble is shorter in the beam than the detection limit an increase in source strength leads to no improvement in the accuracy, because the number of samples per bubble passage is too small for an reliable velocity determination. A source strength characterized by R_{empty} = 50000 counts s^{-1} leads to a detection limit in the form of a vertical intersected length of 5 cm for a bubble with a velocity of 1.1. m s^{-1}. From this value of R_{empty} the according source strength has been calculated.

6 Final design

The requirements that followed from demands in the one and two beam absorption technique lead to a design of a source holder, containing two sources. The source holder can be adjusted to either emit one narrow beam or emit two narrow parallel beams of gamma radiation. An set-up was made for the first test experiments in compliance with the regulations for the use of radioactive materials.

6.1 Necessary source shielding

Stringent shielding requirements had to be applied for the source holder containing two Cs-137 sources with each a source strength of 100 mCi. For the received dose of radiation the regulations for the storage of radioactive materials were applied. At 10 cm from the surface of the source holder the exposure rate has to be lower than 1 μSv per hour. The following equation applies for the exposure rate X of a (point) source of gamma radiation

$$X = \Gamma \frac{A}{r^2} \tag{6.1}$$

The exposure rate constant Γ for Cs-137 is equal to 8.73 10^{-12} R m^2 Bq^{-1} h^{-1} [Web85]. The source strength A for each of the Cs-137 sources is equal to 3.7 10^9 Bq. r is the distance from the source (in m). For gamma radiation an exposure of 1 R (röntgen) is equivalent with a dose equivalent of 0.01 Sv (sievert).

Lead is used as shielding material. The source radiates in all directions, in a observation point not only transmitted photons, that moved with a direction towards the observation point are found but also scattered photons, that originally had a different direction. This contribution is calculated with a build-up factor B. The build-up factor depends on the geometry of the source and the shielding, the thickness and kind of shielding material, and on the energy of gamma radiation. The attenuation by the lead can be described by:

$$X = X_0 B \exp(-\mu d) \tag{6.2}$$

The build-up factor B is equal to circa 2.75 for a thickness d of lead of around 10 cm, lead as shielding material and for an energy of 662 keV. The mass absorption coefficient $[\mu/\rho]$ of lead for the 662 keV gamma equals 1.136 10^{-2} m^2 kg^{-1}, the density ρ of lead equals 11350 kg m^{-3}. A shielding of 8 cm of lead gives an dose equivalent of 9.1 10^{-7} Sv h^{-1} at a distance of 10 cm from the surface of the lead shielding around the source. In this case the source holder contains two sources of Cs-137. The second source is placed at a distance of 12 cm above the first one, this is shown in figure 6.1.

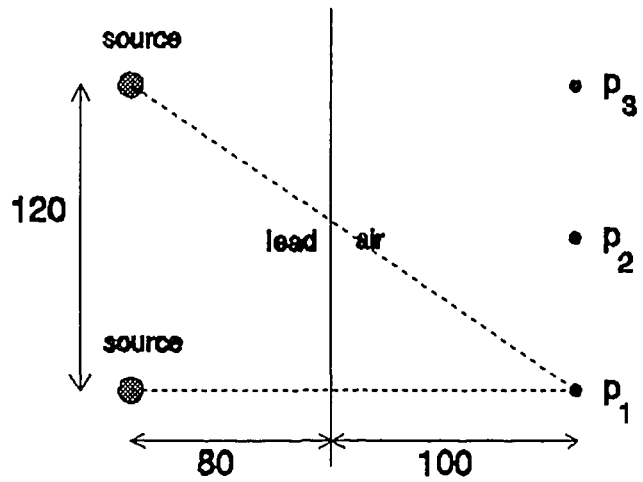

Fig. 6.1 Contribution of second source to exposure rate a point 10 cm from the surface of the source shielding, distances are given in mm.

The contribution of the second source to the dose equivalent at a point with a distance of 10 cm from the shielding, but closest to the first source (points p_1 and p_3) is equal to 8.1 10^{-8} Sv h^{-1}, that leads to a total dose equivalent at points p_1 and p_3 of 9.9 10^{-7} Sv h^{-1} (< 1 μSv h^{-1}). The points closest to one of the sources will give the maximum exposure rate, all points in between give lower exposure rates. At point p_2 the dose equivalent is equal to 8.5 10^{-7} Sv h^{-1}. A shielding of 8 cm lead is sufficient, and both sources will be stored in a leaden cylinder with a radius of 8 cm.

6.2 Additional safety requirements

The SBD (radiation protection service) formulated some additional demands, in order to comply with the licence for encapsulated radiation sources of the Delft University of Technology. In appendix D a copy is present of the licence of the DUT. For the source holder the storage regulations apply. The source holder must be fire-resistant for at least 1 hour. On the outside of the source holder a well readable and ineffaceable superscription, reading "Radioactive Materials" together with the warning sign for radioactivity has to be put. The source holder must have a lock, when the system is left unattended the source holder must be locked and the key given to an authorised person.

When the experimental set-up is changed or not used the sources must be in a non-radiating or shielded position. From the outside it must be clearly visible whether the sources are in shielded or in radiating position, for example by means of a green and red light. In case of a calamity the sources have to fall back in the shielded position automatically. If the amount of radiation, scattered by the polystyrene particles, is too high additional shielding may be necessary, this will be judged by the SBD when the system is put into use.

6.3 Final design of source holder

Von Gahlen B.V. in Didam was asked to make an offer for the manufacturing of the source holder. Their design is shown in the figure 6.1.

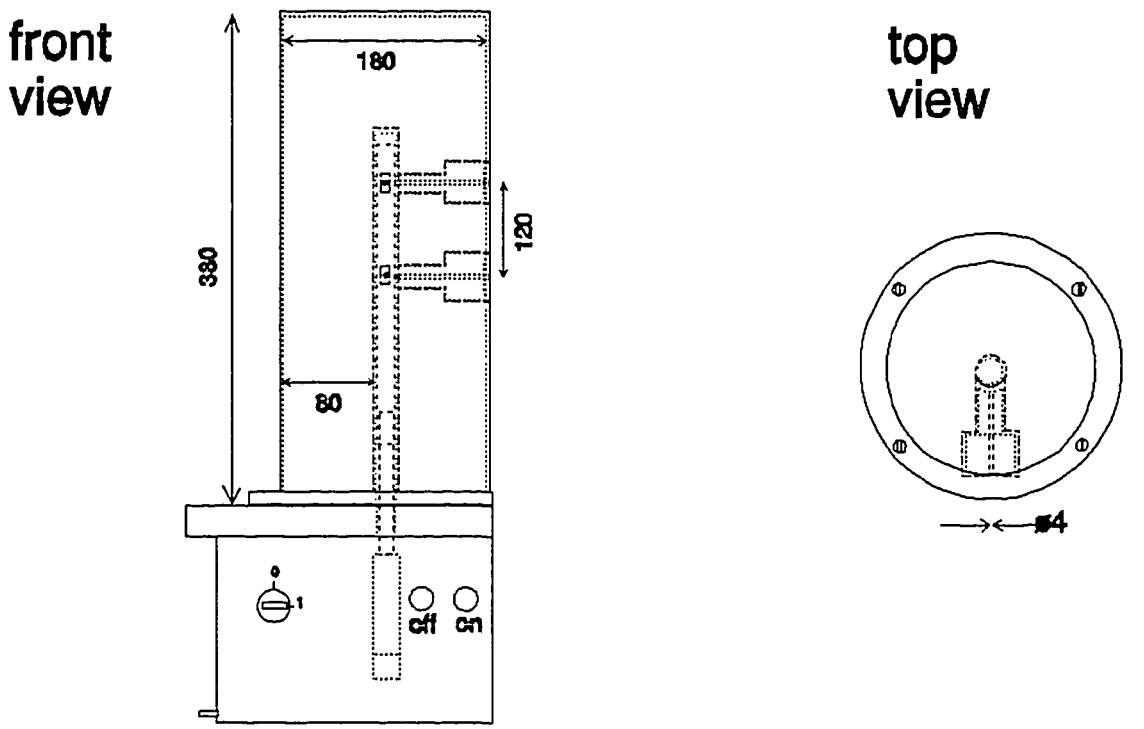

Fig. 6.2 Design of the source holder, measures are given in mm.

The axis, made of stainless steel, contains two encapsulated sources of 100 mCi Cs-137. The sources are placed at a distance of 12 cm from each other. Each encapsulated source is a cylinder, having a diameter of 6 mm and a height of 8 mm containing an active pellet of 3 mm (diameter) * 3 mm (height), described in the Amersham catalogue, code CDC.809 [Ame]. The axis can be moved between two positions; the low position is the shielded position, the high position is the radiating position.

With the use of pressurized air the axis can be lifted to the radiating position. When the pressurized air falls out, the sources will fall back in the shielded position. The diameter of the collimation hole is 4 mm. To comply with the fire-resistance regulations the lead is packed in a stainless steel housing with a thickness of 4 mm. Four collimation plugs will be delivered, two blind plugs and two plugs with a collimation hole of 4 mm. That means the measuring system can serve both as a one beam and as a two beam measuring system. The plugs can be safeguarded against dropping out of the source holder. Around the on/off switch a cap with a lock is placed. At the top of the source holder an eye is attached to be able to lift the source holder, which has a weight of around 150 kg.

6.4 Detector shielding

In the calculations the beam diameter at the detector was 2 cm. With the collimator hole of 4 mm in the source holder the total beam diameter at the detector will be 6 cm, if the source-detector distance is 0.60 m. So collimation and shielding is necessary at the detector side. For the first test experiments standard leadstones will be used to make collimators. A hole of 2 cm diameter will be drilled in two of those stones. A standard leadstone measures 10*10*5 cm^3, contains 0.5 l lead and has a weight of 5.7 kg. With other leadstones a leadcastle will be build around the detectors to shield against scattered radiation and background radiation. In figure 6.2 the detector shielding and collimation is shown. In total 29 leadstones are used.

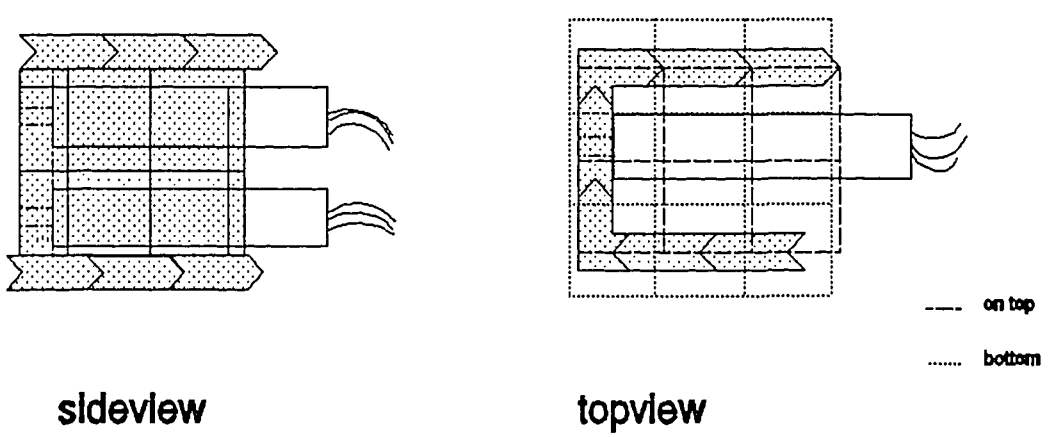

Fig. 6.3 Detector shielding

6.5 Positioning of the measuring system

In figure 6.3 the experimental set-up is shown. On both sides of the column a pallet carrier is placed. On one side the detectors are placed and on the other side the source holder. The detectors are connected with signal processing electronics and a computer will be used to analyze the signals.

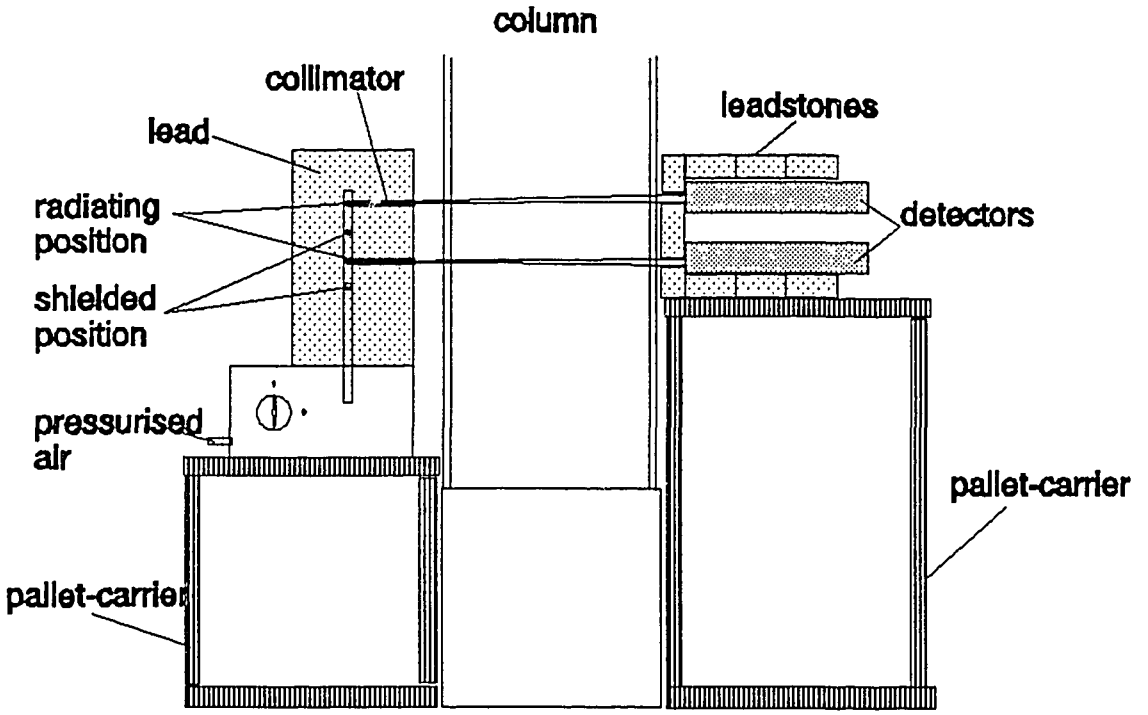

Fig. 6.4 Experimental set-up

The height of both the source holder and the detectors has to be variable. In the first test experiments pallet-carriers will be used to adjust the height of the source holder and the detectors. In the first tests traversing is not possible, at one place in the cross-section will be measured. Later a positioning system has to be build, in order to measure at each height and at each position in a cross-section. A thick solid plates underneath both the source holder and the detectors will be used to ensure a horizontal positioning of both source and detectors. The beams of gamma rays must be aimed at the middle of the detectors, the fine adjustments that are necessary to reach that optimal position must be done manually. The use of a laser beam may be handy for the alignment. A laser beam can be placed at the position of a detector and the beam is aimed through the collimation hole in front of the detector at the collimation hole in the source holder.

7 Conclusions and recommendations

A system was designed specifically for a bubbling gas-solid fluidized bed with a diameter of 0.40 m to measure void fractions and bubble velocities. The bed contains polystyrene particles (Geldart B) and is fluidized by air. The measuring system consists of a source holder, containing two gamma sources, two NaI(Tl) detectors and the necessary electronic analyzing equipment. The measuring principle is the absorption of gamma radiation.

With one beam of gamma radiation a chordal void fraction can be determined in the lower part of the bed. With two parallel beams of gamma radiation and the application of a cross-correlation technique between the two detector responses a bubble velocity can be obtained in the upper part of the bed. For the bubble velocity measurements a sample time of 20 ms is chosen to deal adequately with both the inherent statistical character of the decay of the gamma radiation source and with the high bubble velocities.

The criteria for the choice of a gamma radiation source were:

- the gamma energy used must lead to a minimisation of the standard deviation in the chordal void fraction to be determined
- for the application of the gamma absorption method the source should preferably emit one gamma energy
- the source has to have a sufficiently long half life.

These requirements led to the choice of Cs-137 as source for gamma radiation.
Cs-137 emits one photon with an energy of 662 keV, and has a half life of 30 year.

A computer simulation of the two beam technique for determining bubble velocities was performed to find a relationship between the source strength of the two Cs-137 sources and the minimum time a bubble has to remain in the beam for an reliable velocity determination. A vertical intersected length of 5 cm of a bubble with a velocity 1.1 m s^{-1} has been chosen as the detection limit. That led to the choice of 100 mCi as the source strength for each of the Cs-137 sources.

An increase of the source strength only leads to significant improvement of the results of the bubble velocity measurements if a bubble remains in the beam for a longer time than the time equivalent with the detection limit. A discretization error equal to half the sample time will always be present in the determined time shift.

The designed and manufactured source holder, containing two Cs-137 sources of each 100 mCi complies with all regulations in the licence of the Delft University of Technology for the use of encapsulated radioactive sources.

Since there was not sufficient time to do the first test experiments, carrying out of those test experiments is strongly recommended.

It can be possible to choose a shorter sample time when BGO detectors with a higher detection efficiency are used. A shorter sample time leads to a smaller discretization error and a lower detection limit for bubble velocity measurements.

References

Aki91 J.A. Oyedele and T.A. Akintola, *Appl. Radiat. Isot.*, **42**, 4, 341-346 (1991)

Ame *Industrial gauging and analytical instrumentation sources*, Amersham Nederland BV, Den Bosch

Cha81 A.M.C Chan and S. Banerjee, *Nucl. Instr. and Meth.*, **190**, 135 (1981)

CRC85 *CRC Handbook of chemistry and physics*, 66th edition, 1985-1986, CRC Press inc., Boca Raton, Florida

Cor92 G.P. Corten, *Radiogauging to investigate two-phase flow*, graduation report, Department of Reactor Physics, Interfaculty Reactor Institute, Delft University of Technology, november 1992.

Dar77 R.C. Darton et al., *Trans. Inst. Chem. Engrs.*, **55**, 274 (1977)

Dav63 J.F. Davidson and D. Harrison, *Fluidized Particles*, Cambridge Univ. Press, New York, 1963

Erg52 S. Ergun, *Chem. Eng. Prog.*, **48**, 89 (1952)

Gar67 R.P. Gardner, and R.L. Ely, *Radioisotope measurement applications in engineering*, Reinhold Publishing Corporation, 1967

Gel73 D. Geldart, *Powder Techn.*, **7**, 285 (1973)

Gel78 D. Geldart, *Powder Techn.*, **19**, 133 (1978)

Gel92 D. Geldart, *Gas Fluidization Technology*, the centre for professional advancement, Amsterdam, 10-13 feb. 1992

Har *Harshaw radiation detectors*, Harshaw scintillation phosphor catalogue, Harshaw Chemie BV, The Netherlands

Het82 G. Hetsroni, *Handbook of Multiphase Systems*, Hemisphere Publishing Corporation, Washington, 1982

Hil86 K. Hilligardt and J. Werther, *German Chem. Eng.*, **9**, 215 (1986)

Hir91 Hiraki et al., from D. Kunii and O. Levenspiel, *Fluidization Engineering*, p. 128, Butterworth-Heinemann, 1991

Hub82 J.H. Hubbell, *Int. J. Appl. Radiat. Isot.*, **33**, 1269-1290 (1982)

Kno79 G.F. Knoll, *Radiation detection and measurement*, John Wilsey and Sons, Inc, 1979

Kun91 D. Kunii and O. Levenspiel, *Fluidization Engineering*, Butterworth-Heinemann, 1991

Mud92 R.F. Mudde, R.A. Bakker, H.E.A. van den Akker, *Chem. Eng. Sci.*, **47**, 3631-3638 (1992)

Oye84 J.A. Oyedele, *Int. J. Appl. Radiat. Isot.*, **35**, 9, 865-873 (1984)

Pri89 M.B. Priestly, *Spectral analysis and time series*, Academic Press, 1989

Ste67 P.S.B. Stewart and J.F. Davidson, *Powder Techn.*, **1**, 61 (1967)

Vro84 A.C.W.M. Vrouwenvelder and J.K. Vrijling, *Probabilistisch Ontwerpen*, diktaat b3, Fcaulteit der Civiele Techniek, TU Delft, 1984

Web85 J. Weber and C.E. Rasmussen, *Stralingsbescherming*, Delftse Uitgevers Maatschappij b.v., 1985

Wei85 A.W. Weimer, and D.C. Gyure, D.E. Clough, *Powder Techn.*, **44**, 179-194 (1985)

Wen66 C.Y. Wen and Y.H. Yu, *AiChE J.*, **12**, 610 (1966)

Wer86 K. Hilligardt and J. Werther, in *Proc. 3rd World Cong. of Chem. Eng.*, 429-432, Tokyo, 1986

Appendix A : List of used symbols

A	source strength, in Bq or in Ci (1 Ci = 3.7 10^{10} Bq)
A_t	cross sectional area of bed, in m^2
Ar	number of Archimedes
B	build-up factor
c	light velocity, in m s^{-1}
d_p	particle diameter, in m
d_w	wall thickness, in m
d_{eq}	diameter of sphere with same volume as particle, in m
d_{eff}	ϕ_s d_{sph}, in m
d_{bv}	diameter of equivalent volume sphere of a bubble, in m
D	inner diameter of column, in m
D_{outer}	outer diameter of column, in m
E_b	binding energy of photon, in eV
E_γ	gamma energy, in eV
$E_{\gamma c}$	energy of compton photon, in eV
f_a	absorption factor
f_b	bubble frequency, in s^{-1}
f_c	ratio of cloud to bubble volume
f_g	geometry factor
f_y	number of photons per disintegration
F_b	observed bubble flow, in m^3 s^{-1}
g	gravity constant, in m s^{-2}
h	height above air distributor, in m
I(E)	photon intensity, in photons s^{-1}
l	($=l_{column}$), column length in path of the beam, in m
l_{bubble}	bubble length in path of the beam, in m
l_{column}	column length in path of the beam, in m
M_0	electron mass, in kg
N	number of counts
N_{dis}	number of holes in air distributor plate per unit area
p_i	probability
r	r-coordinate
R(E)	counting rate, in counts s^{-1}
R_b	radius of bubble, in m
R_c	radius of cloud, in m
$R_{21}(s)$	cross-covariance function
Re_p	Reynolds number for a particle
s	distance between beam and centre of column, in m
t	time, in s
t_{total}	total time a bubble is in the beam, in s
t_0	time a bubble enters the beam, in s

u_b	rise velocity of single bubble, in m s^{-1}
u_{bs}	bubble velocity in a swarm of bubbles, in m s^{-1}
u_e	superficial gas velocity through suspension phase, in m s^{-1}
u_f	u_{mf}/ϵ_{mf}, gas velocity at minimum fluidization conditions, in m s^{-1}
u_{mf}	minimum fluidisation gas velocity (superficial), in m s^{-1}
$u_{min,s}$	superficial gas velocity at which slugging commences, in m s^{-1}
u_0	superficial gas velocity, in m s^{-1}
V_{bubble}	volume of one bubble, in m^3
w_i	weight fraction of element i
x	l ρ, mass thickness, in kg m^{-2}
x_b	distance of beam from the centre of the column, in m
X	exposure rate, in R h^{-1} (1 R = 2.58 10^{-4} C kg^{-1})
X_u	outcome of a uniform probability function
z	z-coordinate
z_s	z-coordinate of position of the gamma beam
Z	atomic number

Greek symbols

α_{ch}	chordal void fraction
α_f	total void fraction in a cross-section of the bed
α_{mf}	voidage of a bed at minimum fluidisation
α_{pb}	voidage of a packed bed
α_r	radial void fraction
Γ	gamma exposure rate constant, in R m^2 h^{-1} Ci^{-1}.
δ	bubble fraction
$\Delta\rho$	$\rho_p - \rho_{gas}$, in kg m^{-3}
$\Delta\tau$	measuring interval, in s
$\eta(E)$	photo peak counting efficiency
θ	θ-coordinate
μ	linear absorption coefficient, in m^{-1}
μ_{gas}	gas viscosity, in kg m^{-2}
$[\mu/\rho]$	mass absorption coefficient, in m^2 kg^{-1}
ρ_B	bulk density of bed, in kg m^{-3}
ρ_{gas}	gas density, in kg m^{-3}
ρ_p	particle density, in kg m^{-3}
ρ_w	wall density, in kg m^{-3}
$\rho_{12}(s)$	cross-correlation function
$\sigma(x)$	standard deviation in x
σ_p	standard deviation in d_p, in m
τ	measuring time, in s
ϕ	ϕ-coordinate
ϕ_s	sphericity of a particle
Ψ	ratio of observed bubble flow to excess flow

Appendix B : Simulation results

In the figures B.1a to B.1d results from the program counts2.pas are presented. The bubble velocity is 0.9 m s^{-1}. The beam and the bubble are at the centre of the column. R_{empty} = 50000 counts s-1. Sample time = 20 ms. The bubble diameter varies per figure.

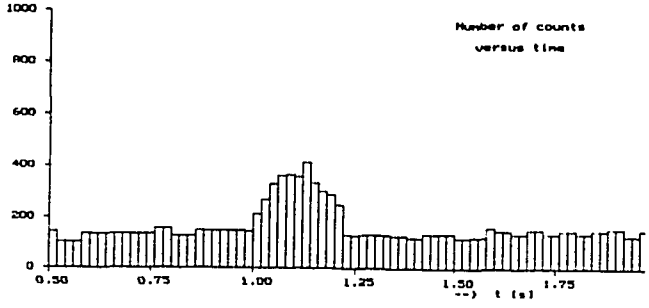

Fig. B.1a bubble diameter = 20 cm.

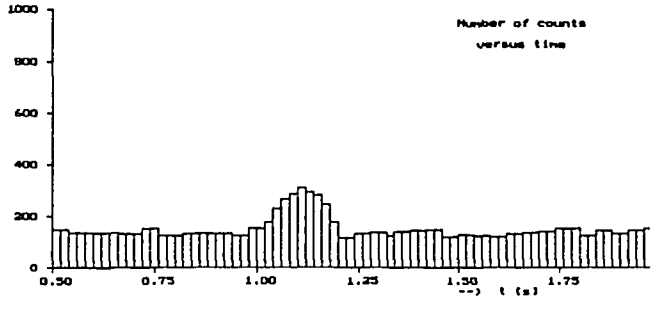

Fig. B.1b bubble diameter is 15 cm.

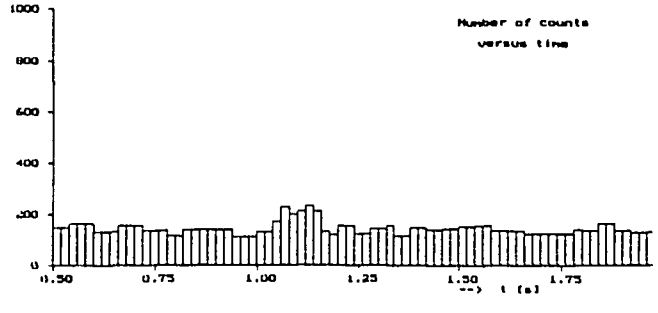

Fig. B.1c bubble diameter is 10 cm.

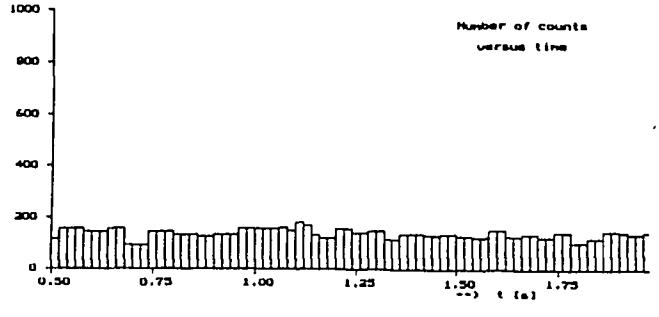

Fig. B.1d bubble diameter is 6 cm.

In figures B.2a to B.2d more results are shown from the program counts2.pas. The same conditions apply as in figures B.1a to B.1d, only the bubble velocity is now 1.1 m s^{-1}. The peak width diminishes, the peak height is the same.

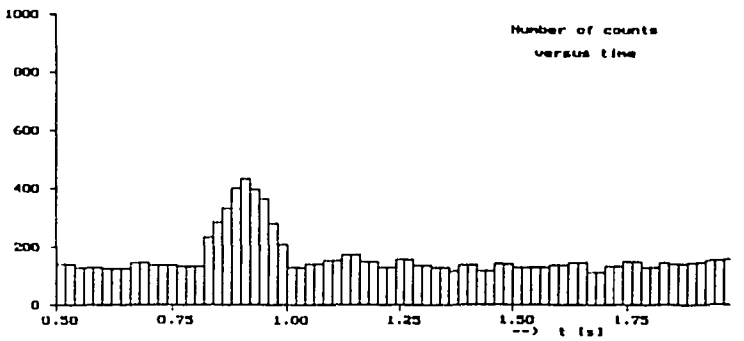

Fig. B.2a bubble diameter is 20 cm.

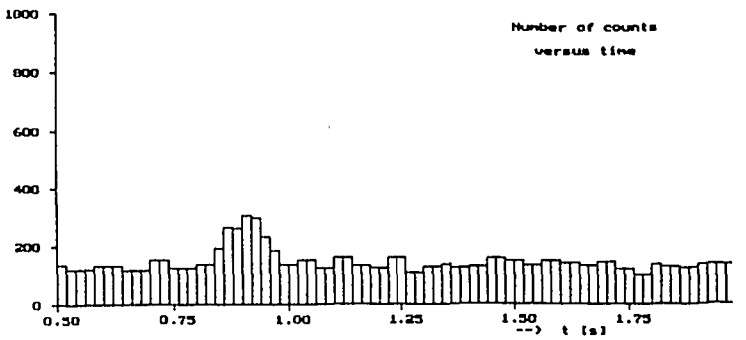

Fig. B.2b bubble diameter is 15 cm.

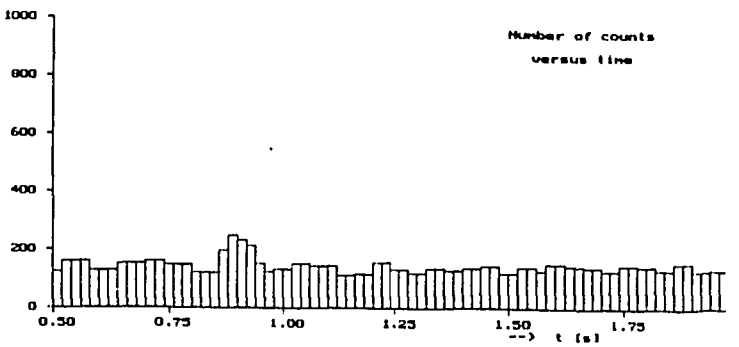

Fig. B.2c bubble diameter is 10 cm.

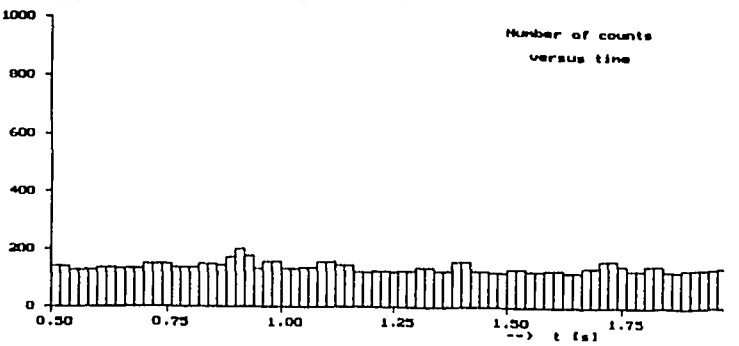

Fig. B.2d bubble diameter is 6 cm.

In figures B.3a to B.3d results are shown from the program correl.pas. A cross-correlation function is calculated. Beams and bubble are at the centre of the column. The distance between the beams is 12 cm. Bubble velocity is 1.1 m s^{-1}. R_{empty} is 50000 counts s^{-1}. The sample frequency is 50 Hz.

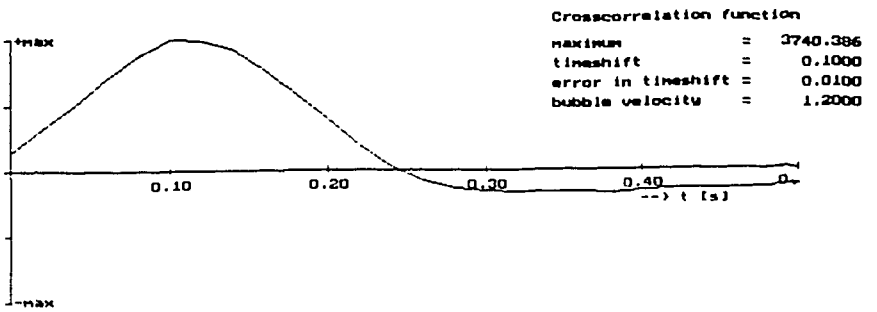

Fig. B.3a Bubble diameter is 20 cm.

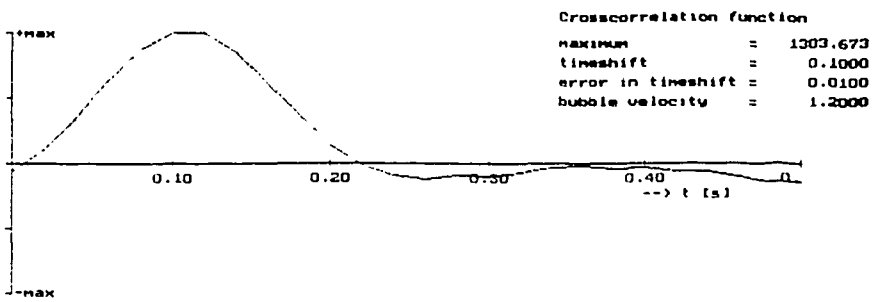

Fig. B.3b Bubble diameter is 15 cm.

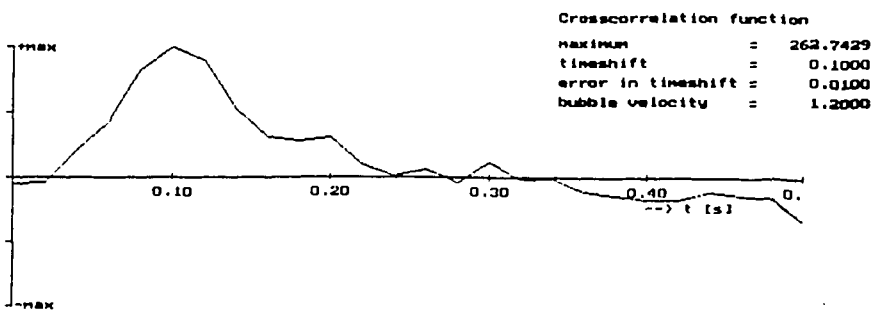

Fig. B.3c Bubble diameter is 10 cm.

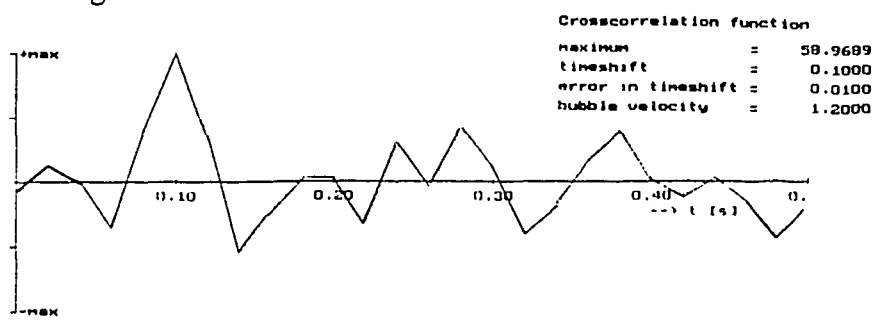

Fig. B.3d Bubble diameter is 6 cm.

Figures B.4a to B.4d also show results from correl.pas. With a bubble diameter of 6 cm and the same conditions as in figures B.3a to B.3d. The cross-correlation the peak heigth can vary, most of the times the highest peak is the cross-correlation peak but sometimes a staistical peak is higher and a wrong timeshift is the result.

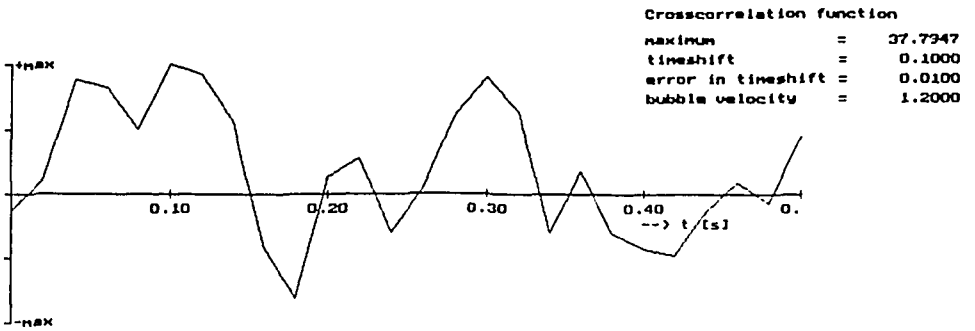

Fig. B.4a Simulated cross-correlation function

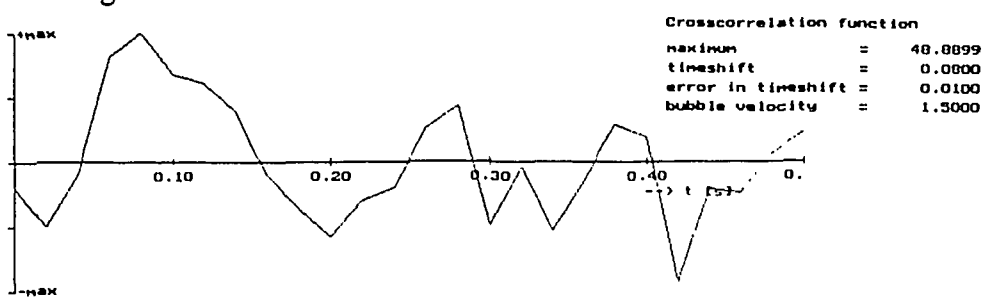

Fig. B.4b Simulated cross-correlation function

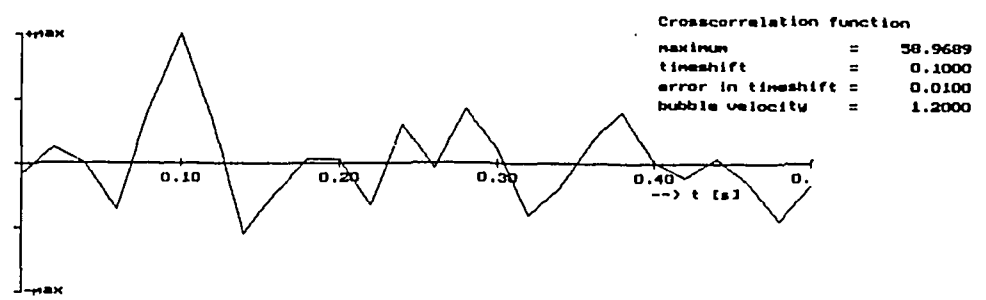

Fig. B.4c Simulated cross-correlation function

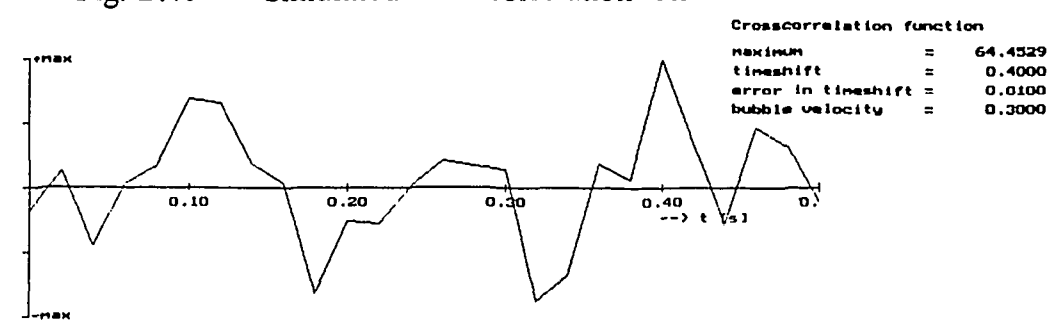

Fig. B.4d Simulated cross-correlation function

Δt_{exact} is obtained by dividing the Δx by the bubble velocity.

Table B.1 Velocity of bubble: 1.1 m/s; bubble diameter 0.05 m; all averages are over 10 samples except R=50000, those averages are over 100 samples.

		$R_{empty\ column}$ (in counts per s) :	100000	75000	60000	50000	40000
distance between beams	Δt_{exact}	simulation results (in s)					
Δx = 0.10 m	0.091 s	mean Δt	0.112	0.182	0.136	0.151	0.092
		st.dev.	0.070	0.138	0.034	0.117	0.041
Δx = 0.11 m	0.100 s	mean Δt	0.116	0.186	0.168	0.165	0.136
		st.dev.	0.062	0.132	0.105	0.116	0.088
Δx = 0.12 m	0.109 s	mean Δt	0.158	0.110	0.198	0.177	0.110
		st.dev.	0.096	0.010	0.124	0.125	0.073
Δx = 0.13 m	0.118 s	mean Δt	0.150	0.146	0.166	0.166	0.198
		st.dev.	0.071	0.112	0.124	0.115	0.119
Δx = 0.14 m	0.127 s	mean Δt	0.122	0.122	0.210	0.167	0.216
		st.dev.	0.011	0.019	0.123	0.114	0.122
Δx = 0.15 m	0.136 s	mean Δt	0.144	0.146	0.172	0.166	0.154
		st.dev.	0.078	0.110	0.084	0.113	0.047
Δx = 0.16 m	0.145 s	mean Δt	0.152	0.172	0.176	0.186	0.158
		st.dev.	0.016	0.100	0.092	0.113	0.136
Δx = 0.17 m	0.155 s	mean Δt	0.162	0.146	0.164	0.170	0.264
		st.dev.	0.032	0.046	0.056	0.096	0.125
Δx = 0.18 m	0.164 s	mean Δt	0.190	0.196	0.176	0.186	0.164
		st.dev.	0.097	0.108	0.135	0.098	0.128
Δx = 0.19 m	0.173 s	mean Δt	0.204	0.198	0.170	0.203	0.186
		st.dev.	0.092	0.111	0.065	0.108	0.109
Δx = 0.20 m	0.182 s	mean Δt	0.206	0.184	0.156	0.206	0.286
		st.dev.	0.105	0.145	0.076	0.114	0.137

Table B.2 Velocity 1.1 m/s; bubble diameter 0.06 m; all averages are over 10 samples except R=50000, those averages are over 100 samples.

		$R_{empty\ column}$ (in counts per s):	100000	75000	50000	40000	25000
distance between beams	Δt_{exact}	simulation results (in s)					
Δx = 0.10 m	0.091 s	mean Δt	0.094	0.094	0.113	0.120	0.156
		st.dev.	0.009	0.016	0.079	0.103	0.131
Δx = 0.11 m	0.100 s	mean Δt	0.102	0.102	0.123	0.090	0.098
		st.dev.	0.006	0.011	0.086	0.033	0.048
Δx = 0.12 m	0.109 s	mean Δt	0.110	0.112	0.129	0.110	0.164
		st.dev.	0.010	0.024	0.082	0.010	0.108
Δx = 0.13 m	0.118 s	mean Δt	0.122	0.108	0.134	0.164	0.146
		st.dev.	0.006	0.013	0.082	0.122	0.105
Δx = 0.14 m	0.127 s	mean Δt	0.128	0.128	0.151	0.144	0.090
		st.dev.	0.010	0.010	0.086	0.086	0.036
Δx = 0.15 m	0.136 s	mean Δt	0.136	0.138	0.144	0.184	0.174
		st.dev.	0.012	0.011	0.061	0.096	0.067
Δx = 0.16 m	0.145 s	mean Δt	0.152	0.140	0.167	0.156	0.128
		st.dev.	0.010	0.009	0.078	0.031	0.110
Δx = 0.17 m	0.155 s	mean Δt	0.154	0.158	0.174	0.170	0.180
		st.dev.	0.009	0.014	0.085	0.105	0.092
Δx = 0.18 m	0.164 s	mean Δt	0.164	0.166	0.172	0.116	0.184
		st.dev.	0.012	0.009	0.059	0.073	0.136
Δx = 0.19 m	0.173 s	mean Δt	0.172	0.146	0.190	0.170	0.158
		st.dev.	0.013	0.044	0.081	0.010	0.039
Δx = 0.20 m	0.182 s	mean Δt	0.182	0.182	0.177	0.170	0.196
		st.dev.	0.014	0.006	0.050	0.060	0.095

Table B.3 Velocity 1.1 m/s; bubble diameter 0.07 m; the bubble is hit in the centre by the beam; the statistics are calculated over 100 determinations of the time shift for R=50000, the others are over 10 samples.

		$R_{empty\ column}$ (in counts per s):	100000	75000	50000	40000	25000
distance between beams	Δt_{exact}	simulation results (in s)					
Δx = 0.10 m	0.091 s	mean Δt	0.092	0.086	0.090	0.092	0.084
		st.dev.	0.010	0.009	0.015	0.022	0.037
Δx = 0.11 m	0.100 s	mean Δt	0.100	0.102	0.104	0.142	0.122
		st.dev.	0	0.006	0.030	0.120	0.108
Δx = 0.12 m	0.109 s	mean Δt	0.106	0.106	0.111	0.112	0.118
		st.dev.	0.009	0.009	0.021	0.010	0.021
Δx = 0.13 m	0.118 s	mean Δt	0.120	0.120	0.116	0.112	0.146
		st.dev.	0	0	0.010	0.013	0.088
Δx = 0.14 m	0.127 s	mean Δt	0.126	0.128	0.129	0.132	0.146
		st.dev.	0.013	0.010	0.011	0.013	0.112
Δx = 0.15 m	0.136 s	mean Δt	0.138	0.140	0.140	0.134	0.126
		st.dev.	0.006	0.009	0.030	0.013	0.040
Δx = 0.16 m	0.145 s	mean Δt	0.144	0.148	0.146	0.150	0.184
		st.dev.	0.008	0.010	0.020	0.013	0.107
Δx = 0.17 m	0.155 s	mean Δt	0.160	0.154	0.157	0.208	0.204
		st.dev.	0	0.009	0.032	0.094	0.094
Δx = 0.18 m	0.164 s	mean Δt	0.162	0.162	0.161	0.166	0.172
		st.dev.	0.006	0.006	0.020	0.009	0.039
Δx = 0.19 m	0.173 s	mean Δt	0.168	0.178	0.172	0.166	0.208
		st.dev.	0.010	0.011	0.018	0.013	0.076
Δx = 0.20 m	0.182 s	mean Δt	0.180	0.186	0.184	0.204	0.174
		st.dev.	0.009	0.009	0.019	0.053	0.090

Appendix C : Software

In the process of designing the measuring system a number of computer programs have been written. The most important programs, written in turbo pascal, are described.

The program bubble.pas describes the time varying void fraction when one spherical bubble rises past two narrow beams of gamma radiation. The bubble diameter, velocity and position can be altered, also the position of the gamma beam can be changed. It gives a number of lines in the resulting figure, each line correspond with the same bubble but with a different place of intersection of the beams. A higher peak corresponds with a place of intersection more towards the centre of the bubble.

The program counts2.pas describes the response of one detector when a bubble passes a narrow beam of gamma radiation. The sampling frequency can be chosen, and R_{empty}, the counting rate with attenuation from the empty column. The programs asks for the same bubble parameters as the bubble.pas program.

The program correl.pas gives a cross-correlation function, calculated from two detector responses. Included is the correct statistical description of radioactive decay. The number of counts measured at the detectors can be described with a Poisson process. The height and position of the cross-correlation peak are determined.

The program handig.pas has been used to determine the detection limit. It repeats a simulation with a certain bubble diameter a chosen number of times, determines each time the time-shift and the peak height, and writes those results in a file. After 10 or 100 repetitions an average time shift and a standard deviation are calculated, those data are put in the same file.

Appendix D : Licence of DUT

This appendix contains a copy of the licence of the Delft University of Technology for the use of encapsulated radioactive sources. Connected with this licence there are a number of regulations concerning each radioactive source.

DE MINISTER VAN VOLKSHUISVESTING, RUIMTELIJKE ORDENING EN MILIEUBEHEER,

Mede namens de Staatssecretaris van Sociale Zaken en Werkgelegenheid en de Staatssecretaris van Welzijn, Volksgezondheid en Cultuur;

Gezien de aanvraag d.d. 11 januari 1988 van de Technische Universiteit Delft te Delft, om wijziging van een vergunning als bedoeld in artikel 29 van de Kernenergiewet (Stb. 1963, 82);

Gelet op de artikelen 29-31 van de Kernenergiewet (Stb. 1963, 82) en het bepaalde in hoofdstuk II van het Besluit stralenbescherming Kernenergiewet (Stb. 1986, 465);

Gelet op de d.d. 23 april 1986, onder nr. 2436008, MHS, verleende vergunning.

B E S L U I T :

De d.d. 23 april 1986, onder nr. 2436008, MHS, verleende vergunning wordt gewijzigd, zodat deze thans luidt als volgt:

Aan de Technische Universiteit Delft, Julianalaan 134 te Delft, wordt vergunning verleend voor het voorhanden hebben en het toepassen van:

- ingekapselde radioactieve bronnen uit groep a met een gezamenlijke activiteit van maximaal 370 megabecquerel (10 millicurie);
- ingekapselde radioactieve bronnen uit groep b met een gezamenlijke acitviteit van maximaal 28,49 gigabecquerel (770 millicurie),
- ingekapselde radioactieve bronnen uit groep c met een gezamenlijke acitviteit van maximaal 37 gigabecquerel (1 curie), en
- ingekapselde radioactieve bronnen uit groep d met een gezamenlijke activiteit van maximaal 37 gigabecquerel (1 curie),

in gebouwen van voornoemde technische universiteit, met uitzondering van radioactieve bronnen in rookmelders.

Onder de groepen a, b, c en d worden hier verstaan de groepen als bedoeld in de Classificatieregeling radiotoxiciteit 1986 (Stcrt. 1987, 60).

Tevens wordt ontheffing verleend van het bepaalde in artikel 70 van het Besluit stralenbescherming Kernenergiewet (Stb. 1986, 465).

Aan deze vergunning en ontheffing worden, met betrekking tot elke radioactieve bron, de hierna volgende voorschriften verbonden:

I. De radioactieve bron

a. de constructie van de radioactieve bron moet voldoen aan de eisen daaraan gesteld in de International Standard ISO 2919/1980;

b. de radioactieve bron moet, hetzij in een snel afneembare bronhouder dan wel in een bronhouder, waarvan de constructie een brandwerendheid van tenminste ½ uur dient te waarborgen, zijn aangebracht in het apparaat waarvan de bron deel uitmaakt, hetzij zijn opgeborgen in een uitsluitend voor dit doel bestemde bergplaats;

c. de uitwendige omhulling van het gedeelte van het apparaat, waarin de radioactieve bron zich bevindt, moet zijn voorzien van een duidelijk leesbaar en onuitwisbaar opschrift, luidende: "RADIOACTIEVE STOFFEN", benevens een waarschuwingsteken voor radioactiviteit, waarvan de uitvoering voldoet aan het gestelde in de Regeling waarschuwingssignalering radioactieve stoffen (Stcrt. 1987, 25) en aan de normvoorschriften volgens NEN-3011.

II. De bergplaats

a. de onder I. bedoelde bergplaats moet aan de volgende eisen voldoen:
- de constructie dient een brandwerendheid van tenminste 1 uur te waarborgen, en
- de bergplaats moet zijn goedgekeurd door de plaatselijke brandweer;

b. de radioactieve bron moet op zodanige wijze zijn opgeslagen, dat op 10 cm afstand van enig punt van het oppervlak van de bergplaats geen uitwendige bestraling van enig deel van het lichaam kan worden veroorzaakt die een dosisequivalent van meer dan 1 microsievert in een uur tot gevolg heeft;

c. de buitenzijde van de bergplaats dient te zijn voorzien van een duidelijk leesbaar en onuitwisbaar opschrift, luidende: "RADIOACTIEVE STOFFEN", benevens een waarschuwingsteken voor radioactiviteit, waarvan de uitvoering voldoet aan het gestelde in de Regeling waarschuwingssignalering radioactieve stoffen (Stcrt. 1987, 25) en aan de normvoorschriften volgens NEN-3011;

d. de bergplaats moet met slot en sleutel zijn afgesloten indien het apparaat zich erin bevindt. De sleutel(s) van de bergplaats moet(en) berusten bij de vergunninghouder of zijn gemachtigde.

III. Deskundigheid

a. de Algemeen Stralingsdeskundige, Dr. C.E. Rasmussen, is belast met het toezicht op en de controle van alle werkzaamheden met de radioactieve bron;

b. de dagelijkse werkzaamheden met de radioactieve bron mogen uitsluitend geschieden volgens aanwijzingen van de Algemeen Stralingsdeskundige en door of onder verantwoordelijkheid van een door hem aan te wijzen ter zake kundige.

IV. De werkzaamheden

a. gedurende montage of demontage, alsmede tijdens het bewaren van de radioactieve bron met haar bronhouder in de bergplaats, moet het venster van de bronhouder zijn gesloten, respectievelijk de bron zich in de zogenaamde

niet-stralingspositie bevinden. Het al of niet gesloten zijn van het venster, respectievelijk de positie waarin de bron zich bevindt dient aan de buitenzijde van de bronhouder duidelijk waarneembaar te zijn;
(indien van toepassing)

b. in de nabijheid van de radioactieve bron mogen geen brandbare, brandbevorderende of explosieve stoffen aanwezig zijn, tenzij hun aanwezigheid voor de bedrijfsvoering noodzakelijk is;

c. indien de werkzaamheden met het apparaat, waarvan de radioactieve bron uit groep a of b van de Classificatieregeling radiotoxiciteit 1986 (1987, 60) deel uitmaakt, gedurende meer dan 72 uur worden onderbroken, moet de bron worden opgeborgen in de onder II. genoemde bergplaats.

V. Controle en registratie

a. ten minste eenmaal per 6 opeenvolgende maanden, voor zover het alpha straling uitzendende nucliden betreft, en ten minste eenmaal per 12 opeenvolgende maanden, voor zover het, met uitzondering van tritium en radioactieve edelgassen, de overige nucliden betreft, dient de radioactieve bron, of indien dit niet mogelijk is de bronhouder, op radioactieve besmetting en mechanische defecten te worden gecontroleerd (onder radioactieve besmetting van de bron wordt verstaan een alpha of bèta/gamma besmetting van 185 becquerel (5 nanocurie); onder radioactieve besmetting van de bronhouder wordt verstaan een alpha besmetting van 0,37 becquerel (10 picocurie) of meer per cm^2 en een bèta/gamma besmetting van 3,7 becquerel (100 picocurie) of meer per cm^2). Uitgezonderd hiervan zijn bronnen, welke geen alpha straling uitzenden en waarvan de activiteit minder bedraagt dan 3,7 megabecquerel (100 microcurie). In een register, dat zich op het kantoor van het Bureau Veiligheid van de vergunninghouder dient te bevinden, moet aantekening worden gehouden van elke controle, onder vermelding van:
- de datum waarop het onderzoek plaatsvond,
- de wijze waarop het onderzoek werd uitgevoerd,
- de naam van degene die het onderzoek verrichtte, en
- de resultaten van het onderzoek.
Deze aantekeningen dienen gedurende twee jaren te worden bewaard;

b. indien bij de onder V. a. genoemde controle blijkt dat besmetting is opgetreden, moet de radioactieve bron in de onder II. genoemde bergplaats worden opgeborgen; hierbij dienen zodanige maatregelen te worden genomen, dat (verdere) besmetting van de bergplaats of van de omgeving wordt voorkomen. Bovendien moet het onder VI. a. genoemde districtshoofd der Arbeidsinspectie zo spoedig mogelijk worden gewaarschuwd;

c. de controle op radioactieve besmetting mag uitsluitend worden uitgevoerd door of onder verantwoordelijkheid van een ter zake kundige, die het diploma Ioniserende Straling C, of een gelijkwaardig diploma, heeft behaald;

d. in een speciaal daarvoor bestemd register, dat zich in of nabij de bergplaats moet bevinden, moet, indien de bergplaats is bestemd voor opslag van meer dan 1 radioactieve bron, aantekening worden gehouden van de inhoud van de bergplaats, en wel zo volledig mogelijk gespecificeerd naar nuclide en activiteit;

e. in een speciaal daarvoor bestemd register, dat zich op het kantoor van het Bureau Veiligheid van de vergunninghouder dient te bevinden, moet van elke radioactieve bron zo volledig mogelijk aantekening worden gehouden, onder vermelding van:
- nuclide,
- activiteit,
- plaats van gebruik, en
- plaatselijke deskundige;

f. éénmaal per jaar, en wel in de maand januari, dient een overzicht van alle aanwezige radioactieve bronnen, gespecificeerd naar:
- aantal,
- nuclide,
- activiteit,
- toepassing,
- plaats van gebruik, en
- plaatselijke deskundige,

te worden gezonden aan:
- de regionaal Inspecteur van de Volksgezondheid voor de Milieuhygiëne te Rijswijk (Z.H.),
- het districtshoofd der Arbeidsinspectie te Zoetermeer,
- het hoofd van de afdeling Stralingshygiëne van het Directoraat-Generaal van de Arbeid te Voorburg, en
- de Hoofdinspecteur van de Volksgezondheid voor de Milieuhygiëne te Leidschendam.

VI. Defecten

a. indien het onderdeel van het apparaat, waarin de radioactieve bron zich bevindt, is beschadigd, mag dit apparaat niet worden verwijderd, voordat het districtshoofd der Arbeidsinspectie te Zoetermeer (tel. 079-511611) hiervoor zijn toestemming heeft verleend;

b. na elke beschadiging als bedoeld onder VI. a. dient het onder V. genoemde onderzoek eveneens plaats te vinden.

VII. Vermissing of ongeval

a. in geval van brand of andere calamiteiten moet het venster van de bronhouder met de radioactieve bron zo snel mogelijk worden gesloten respectievelijk de bron in de zogenaamde niet-stralingspositie worden gebracht of dient de radioactieve bron, voor zover deze zich in een snel afneembare bronhouder bevindt, zo spoedig mogelijk in de onder II. genoemde bergplaats te worden opgeborgen;

b. bij vermissing van of een ongeval (zoals mechanisch defect) met de radioactieve bron moeten zo spoedig mogelijk worden gewaarschuwd:
- de regionaal inspecteur van de Volksgezondheid voor de Milieuhygiëne te Rijswijk (Z.H.) (tel. 070-985811),
- het districtshoofd der Arbeidsinspectie te Zoetermeer (tel. 079-511611),
- de directeur van de Keuringsdienst van Waren te 's-Gravenhage (tel. 070-631928), en
- buiten kantooruren het alarmincidentennummer (tel. 070-272800).

VIII. Overdracht

a. iedere overdracht (waaronder ook begrepen tijdelijke overdracht) van de radioactieve bron mag uitsluitend geschieden aan andere vergunninghouders, mits de aan hen verleende vergunning voor de onderhavige bron geldig is;

b. indien definitief niet meer met de radioactieve bron zal worden gewerkt, dient hiervan tijdig mededeling te worden gedaan aan de Minister van Volkshuisvesting, Ruimtelijke Ordening en Milieubeheer. In dat geval moet de bron worden afgevoerd, waarbij door of namens voornoemde Minister gegeven aanwijzingen in acht zullen moeten worden genomen. Na afvoer van de bron zal de vergunning worden ingetrokken. Tot dat tijdstip dient een afschrift van de vergunning ter plaatse waar de radioactieve bron zich bevindt aanwezig te zijn.

Van het verlenen van deze vergunning wordt mededeling gedaan in de Staatscourant.

Afschrift van deze beschikking zal worden gezonden aan Dr. C.E. Rasmussen.

's-Gravenhage, 21 juni 1988
De Minister voornoemd,
voor deze:
de Directeur-Generaal Milieubeheer,
o.l. de Directeur Stralenbescherming,

Appendix E : Safety report

For all experimental set-ups of the Faculty of Chemical Engineering a safety report has to made before the actual experiments start. That report has to be approved first by the safety committee. In this appendix the safety report is presented that was written to get permission to do the experiments with gamma radiation.

Veiligheidsrapportnummer:662

1. ALGEMEEN

Naam van het project: Met behulp van twee smalle bundels gammastraling meten aan een gas-vast gefluïdiseerd bed.

Korte omschrijving van het project:

Een kolom wordt gevuld met polystyreen deeltjes tot een hoogte van 1 m boven de luchtverdeelplaat. Tegen de kolom aan wordt een bronhouder geplaatst, met daarin 2 radioactieve bronnen Cs-137 met elk een sterkte van 100 mCi ($3.7\ 10^9$ Bq). Aan de andere kant staan 2 detectoren tegen de kolom aan, omgeven door lood afscherming. Met behulp van de twee smalle bundels gamma straling kan onderzoek gedaan worden naar de hydrodynamica van het gas-vast gefluidiseerde bed.

Indien voorheen al een veiligheidsrapport
voor dit project werd ingevuld, dan hier
gaarne het desbetreffende rapportnummer invullen:

Opgesteld door : M.O. Hoogeveen
Datum : 30 september 1993
Functie : Afstudeerder

Werkzaam aan het project sinds: 1 november 1992
Naam promovendus: Begeleiders Dr. R.F. Mudde (tst. 2834)
Ir. Z.I. Kolar (IRI tst 6619)
Zaalnummer:
Naam zaalbeheerder: A.W. Gerritsen

Opmerkingen van de zaalbeheerder:

Handtekening voor akkoord zaalbeheerder:

Veiligheidsrapportnummer:662

Opmerkingen van de Veiligheidscommissie:

	Datum	Handtekening Secr. V.C.
Opstelling en rapport goedgekeurd		
rapport niet geaccepteerd		
Opstelling en rapport afgekeurd		
Noodzakelijke voorzieningen aangebracht door opsteller rapport	Datum	Handtekening opsteller:

Veiligheidsrapportnummer:662

2. OPGAVE VAN DE TOEGEPASTE EXPERIMENTELE APPARATUUR

2.1 Wanneer wilt u beginnen met het bouwen van de opstelling?

eind oktober 1993

2.2 Wanneer denkt u dat de opstelling bedrijfsklaar is?

Op het moment dat de bronhouder geleverd wordt, wil ik direct kunnen starten met de metingen. Ik verwacht de levering omstreeks 15 november 1993.

2.3 Hoelang gaat u met de opstelling werken?

3 weken

2.4 Blijft de opstelling bestaan na afloop van uw werkzaamheden?
Vermeld, indien mogelijk, hoelang de opstelling zal blijven bestaan.

Nee, deze opstelling wordt daarna afgebroken. De stralings apparatuur gaat dan terug naar het IRI.

2.5 Schema, uitleg van de gebruikte symbolen en een duidelijke verklaring van de apparatuur en experimenten.
Geef steeds aan welke chemische reacties kunnen optreden (met $\Delta H°_R$) en vermeldt bij de uitleg de maximale temperatuur en maximale druk (eventueel vacuüm) waarmee wordt gewerkt.
Op deze bladzijde en bladzijde -4- gaarne de uitleg.
Bladzijde -5- is gereserveerd voor uw schema. Eventueel kunt u die bladzijde vervangen door een kopie van een reeds bestaand schema van uw apparatuur. Vermeld dan wel op deze kopie het veiligheidsrapportnummer.
Op bladzijde -6- moet de symbolenlijst, behorende bij het schema op bladzijde -5-, staan. Ook bladzijde -6- kan vervangen worden door een kopie van een reeds bestaande symbolenlijst. (Ook hier weer het veiligheidsrapportnr. vermelden).

Veiligheidsrapportnummer:662

Uitleg voor de werking van de apparatuur:

De bronhouder bestaat uit lood, gevat in een RVS huis. In het centrum van de bron houder kan een RVS as op en neer bewegen tussen twee standen; stralings positie en afgeschermde positie. In de as zitten twee ingekapselde bronnen op een afstand van 12 cm van elkaar, elke ingekapselde bron is een cilindertje van 6 mm diameter en 8 mm hoogte. Door middel van perslucht kan de as in de bovenste positie gebracht worden; de stralingspositie. In stralings positie treden er twee smalle bundels gamma straling uit de (bron)collimatoren en gaan door de kolom heen. De twee smalle bundels vallen op de detector collimatoren en vervolgens op de detectoren. De signalen van de twee detectoren worden daarna naar de verwerkingsapparatuur verstuurd. Zowel de bronhouder als de detectoren kunnen met behulp van een pallet-wagen (wagen om pallets uit te laden en te verplaatsen) op de gewenste hoogte gezet worden.
Het ontwerp van het geheel is goedgekeurd door de Stralings Beschermings Dienst (SBD) van het IRI, en voldoet aan de stralingstechnische vergunningseisen (zie bijlage).

De kolom is gemaakt van perspex en wordt gevuld met polystyreen deeltjes tot een hoogte van 1 m boven de lucht-verdeelplaat, waarna via vier inlaten lucht in de kolom wordt gebracht. De luchtkamer van de kolom is gemaakt van PVC. Het luchtdebiet kan ingesteld worden met behulp van een rotameter. De leiding waarmee de lucht wordt aangevoerd is van koper met uitzondering van het laatste stuk, wanneer de luchtleiding wordt gesplitst in vier slangen, die de luchtkamer van vier verschillende kanten beluchten. Deze slangen zijn van PVC. De luchttoevoer is beveiligd d.m.v. een overdrukbeveiliging.

Veiligheidsrapportnummer:662

Schema:

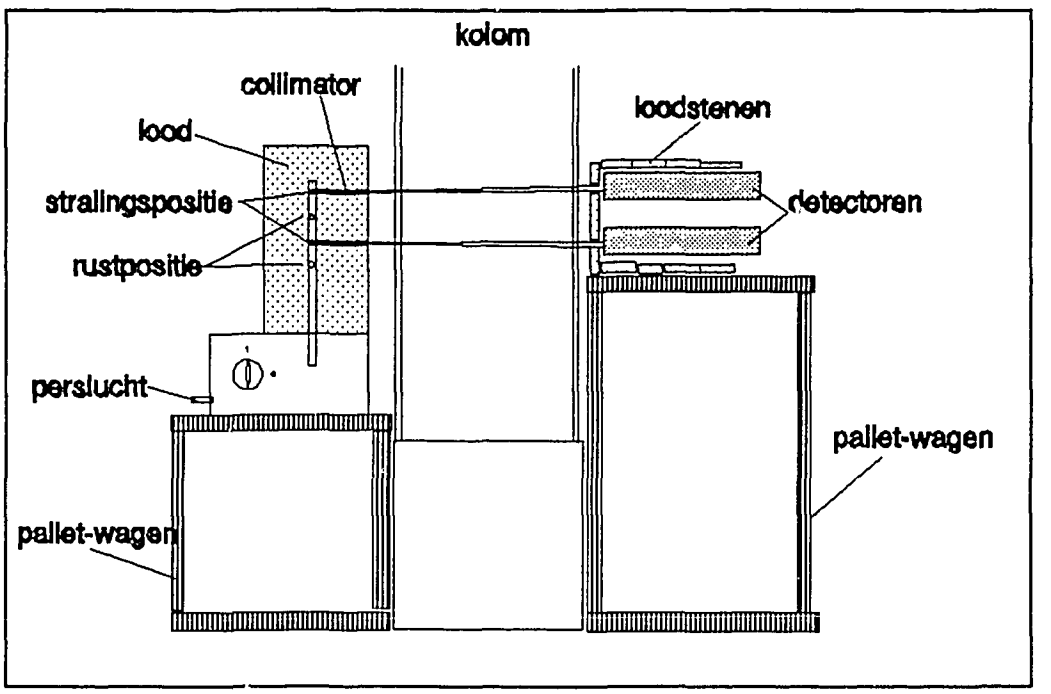

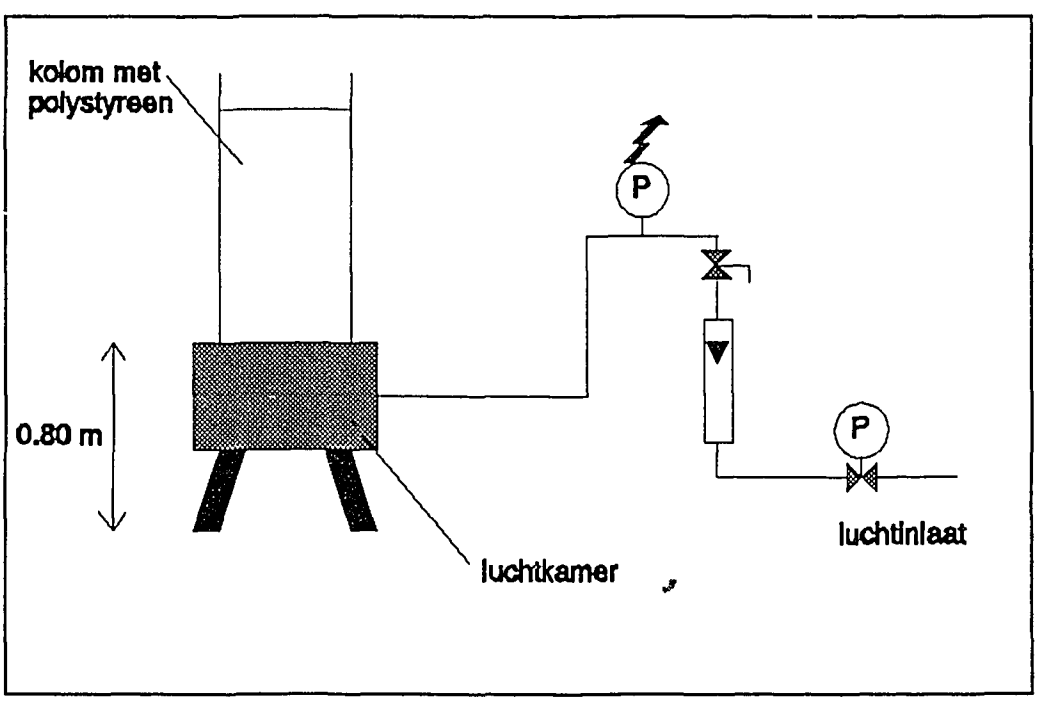

Veiligheidsrapportnummer:662

Symbolenlijst:
voor de te gebruiken symbolen wordt verwezen naar de "Handleiding voor het maken van een fabrieksvoorontwerp" van prof. ir. A.G. Montfoort.

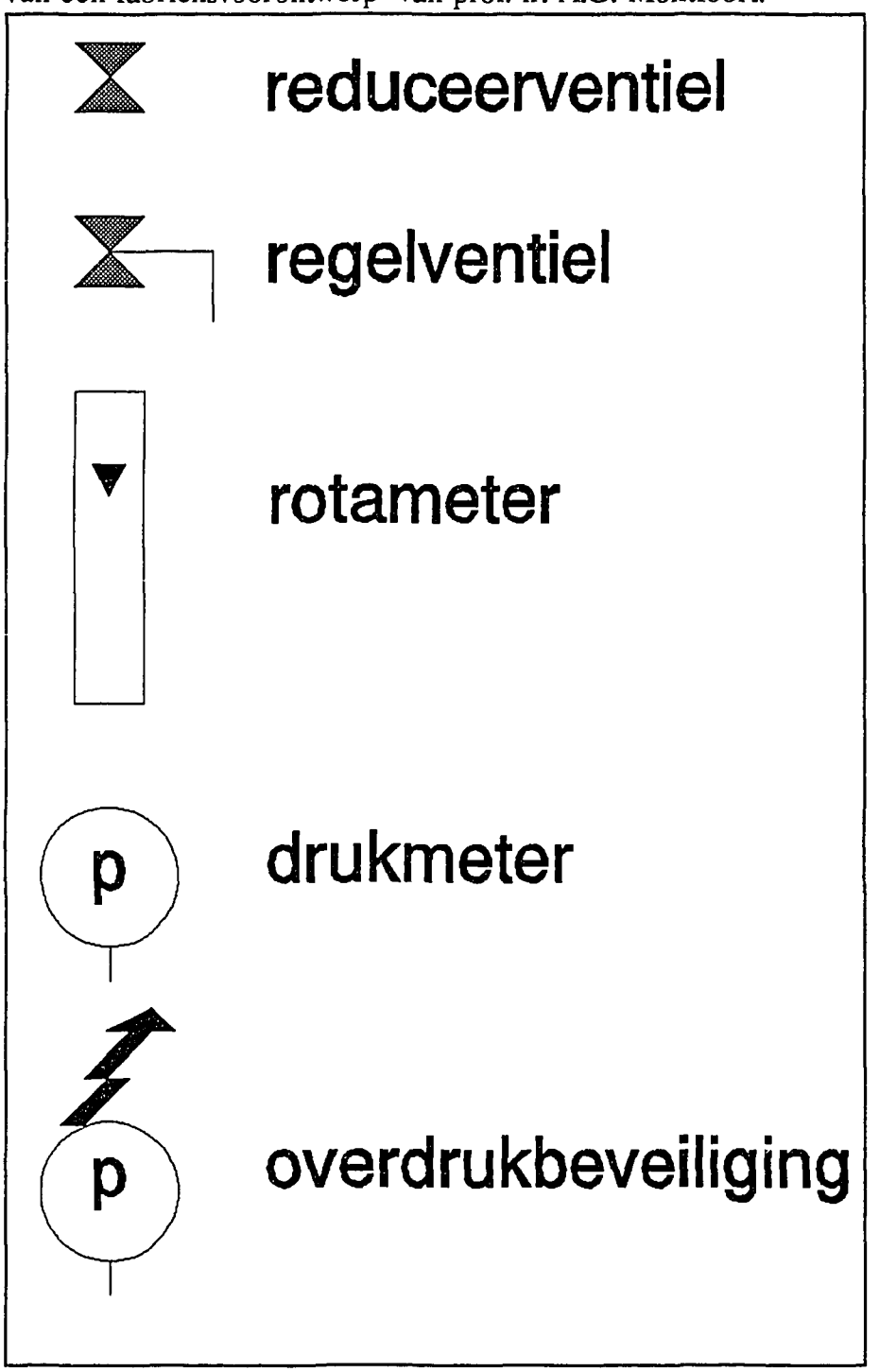

Veiligheidsrapportnummer:662

3. SITUERING VAN DE TOEGEPASTE EXPERIMENTELE APPARATUUR.

Zaalplattegrond met situering van:
- de opstelling, - brandblussers, - branddouches,
- brandslangen, - branddekens, - oogdouches,
- spoelbak, - vluchtwegen(min. 0,8m), -noodschakelaars.

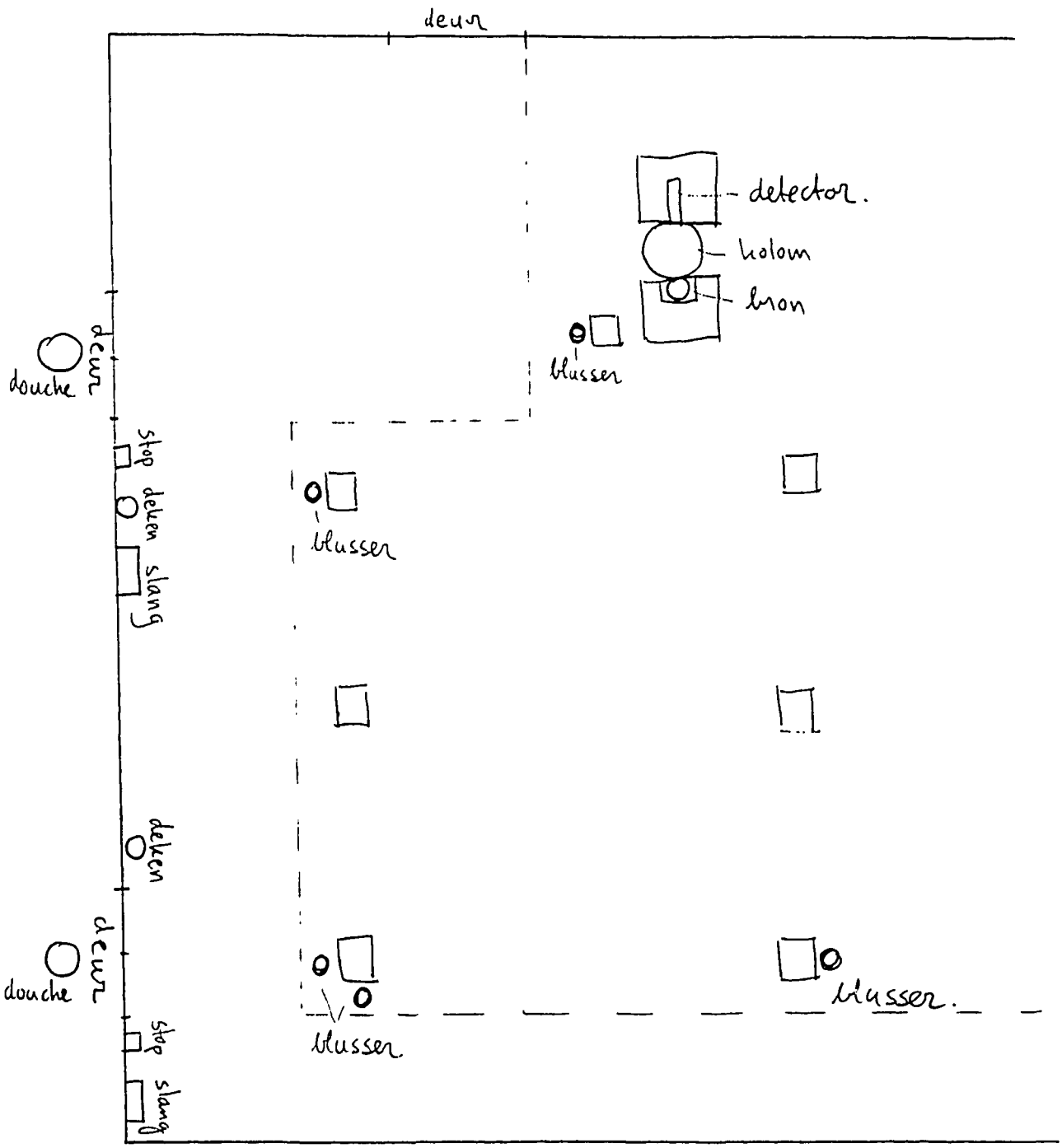

Veiligheidsrapportnummer:662

4. WERKEN ONDER DRUK OF VACUÜM IN GLASWERK.
(Zie ook III.b Veiligheidsreglement CPT)

4.1 Bij welke absolute druk of (vacuüm) wordt er gewerkt?

atmosfersiche druk.

4.2 Bij welke temperatuur wordt gewerkt?

kamertemperatuur

4.3 Gebruikt u daarbij gevaarlijke gassen of vloeistoffen?
(bijvoorbeeld H_2, CO of Hg)

Nee.

5. WERKEN ONDER HOGE DRUK.
(Zie ook III.c Veiligheidsreglement CPT)

Onder 2.5 heeft u vermeld onder welke maximale absolute druk wordt gewerkt.
Indien u bij een druk > 2 bara drukvaten gebruikt, dan dient u 5.1 in te vullen.

Er wordt perslucht gebruikt om een RVS as van ongeveer 30 cm
lang omhoog te bewegen.

Veiligheidsrapportnummer:662

6. HET GEBRUIK VAN CHEMICALIëN EN GASSEN.

6.1 Geef de specificaties van de chemicaliën en gassen, waarmee gewerkt wordt, in onderstaande tabel weer. (Zie ook de literatuurlijst in het Veiligheidsreglement)

100 mCi Cs-137 bron (2 stuks).

- 100 mCi = 3.7 10^9 becquerel (Bq). 1 Becquerel komt overeen met 1 desintegratie per seconde.

- Cs-137 zendt een gamma energie uit: 662 keV. Cs-137 heeft een halfwaarde tijd van 30 jaar.

Veiligheidsrapportnummer:662

6.2 Omschrijf de fysiologische uitwerking van de te gebruiken giftige/schadelijke chemicaliën en geef aan hoe eerste hulp verleend kan worden. Indien van de te gebruiken gevaarlijke chemicaliën chemiekaarten bestaan, moet een kopie hiervan bij de opstelling aanwezig zijn en dient ook een kopie bij dit rapport gevoegd te worden. Maak onderscheid tussen korte- en lange termijn effecten. (Zie literatuurlijst in het Veiligheidsreglement)

7. AANLATEN VAN APPARATUUR EN BEVEILIGINGEN.

7.1 Wordt verwacht dat de apparatuur in werking is buiten de normale werktijd? Zo ja, vermelden welke apparatuur dit is.

Nee, dit wordt niet verwacht

Opmerking: Indien deze vraag met ja is beantwoord, dit na goedkeuring van dit rapport door de Veiligheidscommissie, melden aan de Laboratoriumbeheerder i.v.m. wekelijks cq maandelijks vereiste goedkeuring van continue draaiende apparatuur door het beheer. Het beheer kan aan kortlopende continue experimenten een dagelijkse goedkeuring verbinden.

7.2 Zijn duidelijke instructies aangebracht hoe te handelen bij storing of gevaar? (Aangeven in 3. Situering)

Deze worden aangebracht op bronhouder. Bij het opbouwen van de kolom zullen aanwijzingen bij de opstelling worden aangebracht.

7.3 Op welke wijze is de glazen apparatuur beschermd tegen wegspringen bij breuk (b.v. kleefband, veiligheidsscherm)?

Geen glazen apparatuur gebruikt.

7.4 Heeft u een veiligheidsbril of een gelaatsscherm? Gebruikt u hem?

Ja, de veiligheidsbril zal gedragen worden.

Veiligheidsrapportnummer:662

7.5 Welke brandblusmiddelen zijn aanwezig?
Zijn deze geschikt voor uw systeem?
Zo nee, welke veranderingen moeten aangebracht worden?

Er zijn zowel dekens, CO_2 blussers als brandslangen aanwezig, wat voldoende is.

7.6 Geldt een rookverbod?

Ja, er geldt een rookverbod.

7.7 Is de ventilatie zodanig dat de MAC-waarde niet wordt overschreden?

niet van toepassing.

N.B.: Capaciteit zuurkast is ca. 600 m^3/h per meter breedte.

7.8 Omschrijf het beveiligingssysteem. Denk hierbij aan beveiligingen tegen lekkages of leidingbreuk, te hoge druk, te hoge temperatuur, uitvallen van voedingsstromen b.v. gas, water, elektriciteit (op juiste plaatsen stroomloos open of dichte kleppen). In H_2-leidingen contactmanometers met magneetspringkontakten gebruiken (geen sleepkontakten i.v.m. vonkvorming).

Zie bijlage met de vergunning voor het gebruik van ingekapselde bronnen, onder IV werkzaamheden.
Verder is de straling naar de muur toegericht, en staan bron en detector zo dicht mogelijk tegen de kolom aan, dit om te voorkomen dat de bundel straling op iemand valt.
Verder zijn de (collimatie)pluggen beveiligd tegen het uit de bronhouder vallen.
Een slot is aanwezig om de aan/uit knop heen.
Een rood licht signaleert het in gebruik zijn van het systeem; dat de bronnen in stralingspositie zijn.
Er is een noodstop knop, deze zorgt voor het wegvallen van de perslucht, waardoor de bronnen terugvallen in afgeschermde positie. Tevens geldt dat als de spanning uitvalt, de bronnen ook terug vallen naar afgeschermde positie.
Bij ingebruikstelling van het systeem zal door de stralingsdeskundige van de TU Delft of diens vertegenwoordiger het niveau van de verstrooide straling gemeten worden, en eventueel wordt er nog voor extra afscherming gezorgd.
Er is een overdrukbeveiliging op de luchttoevoer.
Er is een noodstop knop voor de spanning.

Veiligheidsrapportnummer:662

7.9 Hoe is het plan om de beveiligingen te controleren en met welke frequentie?

Voor en na mijn metingen met dit systeem.

Bij veel van deze beveiligingen is een beveiligingskast vereist. Hieronder volgt een beschrijving van één bepaald type beveiligingskast; vele andere typen zijn echter denkbaar. Het is daarom zeer gewenst al in het ontwerpstadium contact op te nemen met medewerkers van de elektrotechnische ondersteuningsgroep.
Voorbeeld beveiligingskast: op de kast kunnen een aantal verbreekkontakten worden aangesloten (deze staan in serie). De output van de kast is 380 of 220 Volt, waarop de te beveiligen apparatuur is aangesloten. Bij het verbreken van één kontakt wordt de output spanningsloos gemaakt (een speciale startprocedure is nu nodig om de apparatuur weer in werking te zetten).
Praktijkvoorbeeld: kontaktmanometer en kontaktthermometer in verwarmde pompleiding; bij te hoge druk òf te hoge temperatuur wordt het kontakt verbroken en de pomp en de leidingverwarming, die beide aangesloten zijn op de output van de kast, zijn dan spanningsloos.

7.10 Kan met één schakelaar (liefst rode noodknop) de voedingsgassen, de spanning en eventueel het water uitgeschakeld worden?

Voedingsgassen : Ja

Spanning : Ja

Water :

Houdt rekening met eventuele noodzaak van koelwater als het systeem down gaat!

Veiligheisrapportnummer:662

8. AFVOER EN/OF VERNIETIGING VAN OVERTOLLIGE CHEMICALIëN.

8.1 Welke chemicaliën-resten zullen ontstaan?
Hoe worden ze vernietigd of afgevoerd?
Denk aan de regeling van de Commissie Afvoer Afvalchemicaliën (CAAC/DAAS)!

Na afloop van de experimenten zal de bronhouder met daarin de 2 100 mCi Cs-137 bronnen terug naar het IRI gebracht worden. (t.a.v. de Stralings Beschermings Dienst)

9. LITERATUURSTUDIE EN OPMERKINGEN.

9.1 Welke literatuur heeft u bestudeerd i.v.m. veiligheidsaspekten?
(zie ook literatuurlijst in het Veiligheidsreglement)

Cursus stralingsveiligheid niveau 5B is gevolgd, en met succes afgerond.

9.2 Heeft u wensen of opmerkingen betreffende de veiligheid in uw werkruimte?

Bij ingebruikstelling zal het niveau van de verstrooide straling gemeten worden, dit kan eventueel leiden tot aanvullende maatregelen. Hierbij kan gedacht worden aan extra loodafscherming, of het verminderen van de bereikbaarheid van de opstelling indien deze in bedrijf is.